Deliverable D3.42
First assessment of performance indicators of Superconducting direct drive and Pseudo magnetic direct drive generators

Dong Liu, Asger B. Abrahamsen,

Alasdair McDonald, Andreas Penzkofer, Andrew Myers, Arnaud Dolacinski , Arwyn Thomas, Axel Mertens, Ben Hendriks, Chris Kirby, Constanze Goedeckemeyer, David Black, Dennis Karwatzki, Ewoud Stehouwer, Fujin Deng, Kais Atallah, Kenneth Thomsen, Max Parker, Niklas Magnusson, Per Hessellund Lauritsen, Steve Finney, Stuart Calverley, Zhe Chen and

Henk Polinder

Document Name:	First assessment of performance indicators of SC and PDD generators
Confidentiality Class	PU
Document Number:	Deliverable D3.42
Author:	Dong Lui, Asger B. Abrahamsen & Henk Polinder
Review:	WP3
Date:	13 September 2013
WP:	WP3
Task:	Task 3.1-3.4

TABLE OF CONTENTS

CHAPTER 1 INTRODUCTION

1.1   Background

This report is the documentation of the deliverable D3.42 "First assessment of performance indicators of superconducting and Pseudo magnetic direct drive generators" of work package 3 electro mechanical conversion.

The superconducting and pseudo magnetic direct drive generator technologies are investigated because they have the potential to reduce the tower top mass of the INNWIND turbines.

1.2   Objective: performance indicators

The performance indicators used in this report are the following.
- Weight, size and cost of the generator system (CAPEX)
- Efficiency of the generator system.

In this first assessment of performance indicators, we do not discuss operational cost because the technology is not mature enough for a good assessment.

This report discusses both 10 and 20 MW generator systems. Probably the numbers of the 10 MW systems are more accurate than for the 20 MW system because in the 20 MW system there are more unknowns.

1.3   Starting points

The INNWIND reference turbines at 10 and 20 MW are used to determine the torque and rotation speed specification of the direct drive generator systems. The size of the machines are found from the torque, whereas the mass and cost are found from the mass density and cost of the used materials.

1.4   Structure of the report

The structure of this report is organized by an introduction to current trends of wind turbine drive trains in chapter 2, an investigation of the possible nacelle layouts to hold the superconducting and pseudo magnetic direct drive, a chapter on KPI of the superconducting generators based on NbTi, MgB_2 and YBCO coated conductors, a chapter on the Pseudo magnetic direct drive generator, a chapter on power electronics suited for the two direct drive generators and finally a comparison chapter.

CHAPTER 2 OVERVIEW OF STATE OF THE ART GENERATOR SYSTEMS

2.1 Introduction

In present days, variable-speed generators are dominant over constant-speed generators in wind turbine applications. The most commonly used generators nowadays for wind turbine applications are doubly-fed induction generator (DFIG), brushless generator with gear and full converter (BGGFC) and direct-drive generator (DD). Each of them has advantages and disadvantages against the others but it is not clear yet which one is the best.

Aiming at addressing the disadvantages of these popular generator systems, several future generator systems have been presented. Analyses have shown that they would be suitable for wind turbine applications and that some of them are promising for 10-20 MW wind turbines.

This chapter at the beginning discusses the requirements and basic relations of a wind turbine generator, then overviews the state-of-the-art generators for wind turbine applications and introduces the possible future generator systems. From several future generator systems, magnetic pseudo direct-drive generators and superconducting direct-drive generators are chosen to be investigated in the INNWIND.EU project.

2.2 Requirements and basic relations

1. Requirements

The key objective of the development in wind turbines is to minimize the cost of energy delivered to the power system. Some implications are related to the cost of energy.

1) Capital expenditures (such as manufacturing, transportation and installation) are important but not decisive. Because operational expenditures (such as repair and maintenance) also have to be considered.
2) The cost varies over time due to price variation.
3) The energy yield depends on the location where the wind turbine is installed because wind conditions are different between locations.
4) The efficiency of the generator system is important but not decisive, because low efficiency with low cost of energy is better.

Besides fulfilling this key objective, wind turbine generator systems must meet a number of other requirements:
1) Grid connection
A wind turbine generator must meet the requirements of grid codes, such as grid-fault ride-through. Similar to conventional power plants, wind farms must supply qualified active and reactive power for frequency and voltage control.
2) Reliability and availability
Especially for offshore wind turbines, operational expenditures may form a significant part (in the order of 30%) of the cost of energy. Therefore requirements related to reliability, availability and maintainability are getting more attention and more research in this field is

necessary [1]-[7]. Proper protection against the aggressive humid and salty offshore environment is extremely important.

3) Variable speed

To enable optimal match between the generator and the aerodynamic of the rotor, the generator is required to have a variable speed. The power that can be captured from the wind with a wind turbine is given by

$$P = \frac{1}{2}\rho_{air}C_p(\lambda,\theta)\pi r_b^2 v_w^3 \tag{2.1}$$

where ρ_{air} is the air mass density, v_w is the wind speed, r_b is the turbine rotor radius (or the blade length) and C_p is the power coefficient, which depends on the specific design of the blade, the blade pitch angle θ and the tip speed ratio λ. The power coefficient is maximum for a constant tip speed ratio.

2. Basis scaling functions

The cost of a generator depends on the size and the material used. The size of a radial flux generator is in first approximation given by

$$P = \omega_m T = 2\pi\omega_m r_s^2 l_s F_d = 2\omega_m F_d V_r \tag{2.2}$$

where ω_m is the mechanical angular speed, r_s is the air-gap radius, l_s is the axial stack length, F_d is the shear stress and V_r is the rotor volume of the generator.

The shear stress F_d means the force per square meter of active air gap surface area and is given by

$$F_d = \frac{1}{2}\hat{A}_s\hat{B}_g cos\gamma \tag{2.3}$$

where $\hat{A}_s$ and $\hat{B}_g$ are the amplitudes of the fundamentals of the stator current loading and the air-gap flux density, and γ is the angle between them.

This shear stress is rather constant over a wide range of generator types and power levels, because it is the product of the flux density, which is limited because of iron saturation, and the current loading, which is limited because of thermal dissipation.

The torque level of the generator increases more than proportional to the power level. This is because the blade tip speed must be limited to avoid excessive mechanical forces, wear and audible noise. If the rated blade tip v_{trated} is assumed independent of the size of the rotor, then the mechanical rotational speed of the rotor ω_m is inversely proportional to radius of the rotor. The rated torque can then be written as

$$T_{rated} = \frac{P_{rated}}{\omega_{mrated}} = \frac{r_b P_{rated}}{v_{trated}} \propto r_b^3 \propto P_{rated}^{3/2} \tag{2.4}$$

3. Ways to increase power

(INNWIND.EU, WP3 internal report, First assessment of performance indicators of SC and PDD generators)

At power levels below 5 MW, geared doubly fed induction generators (DFIG) and direct-drive generators (DD) are widely used. With the increase of power to 10 MW and higher, geared DFIGs face the problem mainly from the significant loads on the mechanical gearbox and DDs encounter the problem of large size, big mass and high cost. It is necessary to design new generators to handle 10-20 MW while keeping low costs of energy.

As seen from (2.2) there are three ways to realize the increase of power:
1) To increase the volume V_r of the generator rotor. This leads to big size and higher weight and cost.
2) To increase the rotational speed of the rotor ω_m. This is achieved mainly by employing gearbox. Mechanical gearboxes are not promising because of their low reliability and the very high loading imposed. Magnetic gearboxes can be applied so that the mechanical contact between gear teeth is eliminated and the reliability goes higher.
3) To increase the shear stress F_d

The stator current loading $\hat{A}_s$ is mainly limited by the stator heat dissipation. Forced liquid cooling instead of forced air cooling can increase $\hat{A}_s$ but at the expenses of efficiency reduction.

The air-gap flux density $\hat{B}_g$ is mainly limited by the saturation of ferromagnetic cores. Using non-ferromagnetic cores can increase $\hat{B}_g$ but the reluctance of magnetic circuit will become very large and the distribution of flux density will get much more complicated.

It can be seen from the above that four variables (V_r, ω_m, $\hat{A}_s$, $\hat{B}_g$) determine the increase of power from current 5 MW to future 10-20 MW. As seen from (2), if a power rating is given, the best way to reduce the size of the generator is to enhance the shear force or increase the speed, which is the challenge of designing generators for 10-20 MW wind turbines.

2.3   State-of-the-art generator systems

As constant-speed generators are hardly used nowadays at high power levels, there are three most commonly used generator systems for wind turbines (depicted in Fig. 2-1).
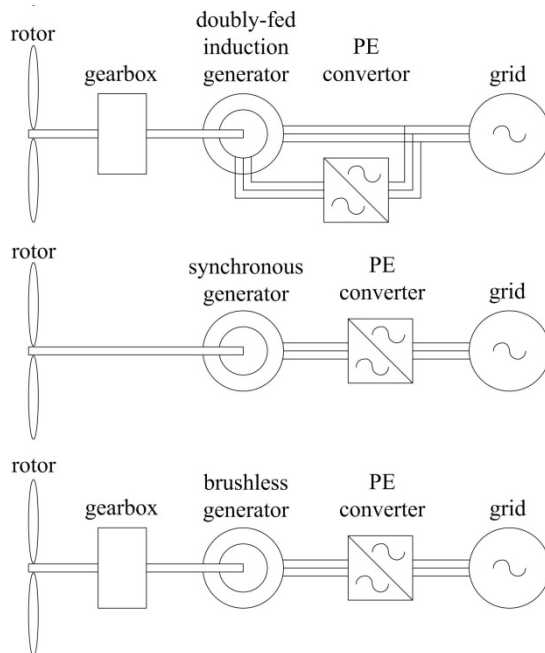
Fig. 2-1. The three commonly used generator systems

1. Doubly-fed induction generator (DFIG)

A doubly-fed induction generator systems consists of a multi-stage gearbox, a relatively low-cost standard doubly-fed induction generator and a partly rated (approximately 25% of the rated power) power electronic converter feeding the rotor winding. Pitch control limits the output power to rated power at wind speeds above rated. The power electronic converter enables a speed range from roughly 60% to 110% of the rated speed and this is sufficient for a good energy yield.

This system has a flexible match with audible noise, mechanical loads, power quality and energy yield, compared with constant-speed generator systems. But at the beginning it was not possible to fulfil the grid-fault ride-through capabilities in standard DFIG systems. After developments, however, enabling grid-fault ride-through has been successful in DFIG systems [8]-[14]. The failure rate of the multi-stage gearbox is high and therefore the use of gearbox limits the application of DFIG systems.

2. Brushless generator with gear and full converter (BGGFC)

Several large manufactures have developed variable speed wind turbine generator systems with a gearbox, a brushless generator and a converter for the full rated power. Pitch control limits the output power to rated power at wind speeds above rated. This system is mainly used to
1) obtain better grid-fault ride-though characteristics than a DFIG system
2) avoid the maintenance and the failures of the brushes of the DFIG.

However, a fully rated converter introduces more losses than a partly rated converter as in a DFIG.

There are several variants of BGGFC systems because different generator types and different gearboxes are combined. Several manufactures use permanent-magnet (PM) generators (Fig. 2-2) while squirrel cage induction generators are also used. The number of gear stages in this system may vary from one to three. The low number of gear stages results in larger generators but the elimination of high speed stages makes this system more efficient and more reliable [15], [16].
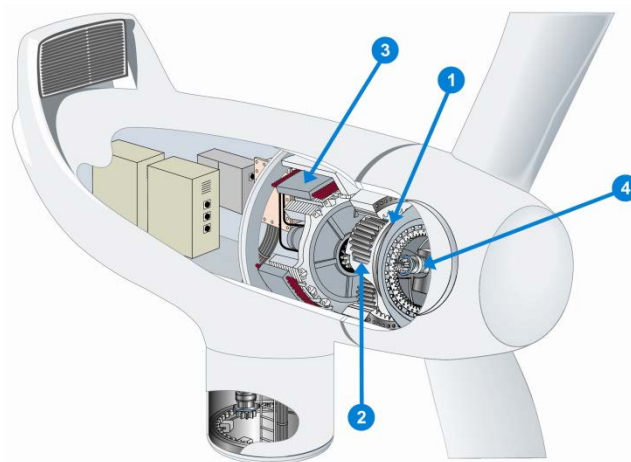
The rotor is combined to the power unit using a custom-made three-row roller bearing (1).
The roller bearing transfers the rotor loads directly to the main casing past the planetary gear and generator.
The single-stage planetary gear (2) increases the rotating speed from 8-25 rpm to 44-146 rpm.
The low speed permanent magnet generator (3) produces the electricity.
The rotational speed of rotor is controlled by three independent electric pitches (4).

Fig. 2-2. Sketch of the Multibrid® system. Source: Winwind.

3. Direct-drive generator (DD)

Gearless generator systems with direct-drive synchronous generators have been developed since 1992. A fully rated power electronic converter is necessary for the grid connection.

Electrical excitation was used when permanent magnets were very expensive. Now the price of permanent magnets is not very high so the focus has shifted to permanent-magnet generators, but Enercon is still successfully applying electrical excitation to their DD generators (Fig. 2-3).
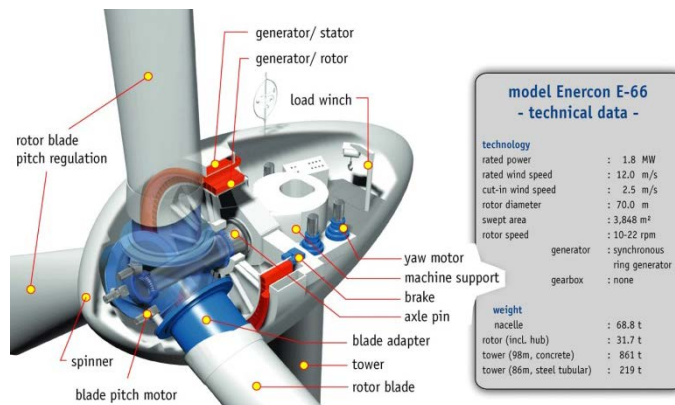
Fig. 2-3. Sketch of a gearless nacelle, in this case of an Enercon E-66 direct-drive wind turbine. Source: Bundesverband WindEnergie e.V.

The main reason for using DD systems is to increase reliability by avoiding the maintenance and the failures of the gearbox and by reducing the number of turbine components. However it has yet to be proven that the reliability of DD is really better than that of gear systems [17].

The main disadvantages of DD generator are:

1) The low-speed high-torque generator is large, heavy and expensive.
2) Low speed generators are less efficient than high speed ones.

A lot of work has been done to optimize these generators. The electromagnetic and thermal limitations of the iron cored radial flux generators as applied in the industry are described in [18]-[23]. Tooth wound concentrated winding generators have been presented to reduce the manufacture cost of DD generators but additional losses due to additional space harmonics are a point of concern [24]-[26].

2.4   Future generator systems

This section describes proposed future generator elements and systems for wind turbines and lists the critical advantages and disadvantages compared to the currently used generator systems. For most of the proposed future systems, we are not yet able to predict if they will lead to a cost of energy lower than that of the currently used generator systems. It is needed to investigate their cost of energy.

1.   Mechanical continuously variable transmission (CVT)

The CVT is a mechanical transmission which can change the speed steplessly through an infinite number of effective gear ratios between maximum and minimum values. A basis CVT is usually constituted by a planetary gear stage, where the power from the high speed end of the first-stage step-up gear is supplied to the carrier, the output power delivered to the generator is taken from the annulus shaft and the sun is driven by a variable speed electric drive. The speed control of the driver machine determines the capability to regulate the speed of the turbine across a wide range, by maximizing the power extraction from the wind for wind speed below the rated speed [27].

The advantage of mechanical CVT is that it enables the generator to rotate at a constant speed no matter how fast the wind turbine rotor rotates [27]-[29]. This makes it possible to use directly grid-connected synchronous generators with electrical excitation, thus avoiding power electronic converters.

The issues of mechanical CVT to be emphasized are:
1) To obtain a reasonable speed variation, the power level of the variable speed system must be considerable, comparable to DFIG systems.
2) This system increases the complexity of gearbox.

Therefore convincing advantages of mechanical CVT over DFIG systems have not been seen yet.

2. Hydraulic transmission systems

Hydraulic transmission systems can be divided into hydrodynamic and hydrostatic transmissions [30]-[32]:
1) The WinDrive (of Voith) is based on a hydrodynamic transmission or a torque converter, where turbines give energy to and take energy from an oil flow. This only works for high speeds, so this system is combined with a gearbox.
2) The drive trains of Wikov, ChapDrive and Artemis (of Mitsubishi) are based on hydrostatic transmissions or positive displacement pumps, where cylinders displace pressurized oil. The Wikov system consists of a combination of a gearbox and a hydraulic system, while the gearbox is omitted in the systems of ChapDrive and Artemis.

Hydraulic transmissions have the big advantages:
1) They are significantly lighter and cheaper than gearboxes.
2) Hydraulic transmission systems are normally used as continuously variable transmissions (CVT), so a directly grid-connected synchronous generator can be used, thus avoiding power electronic converters.

However, hydraulic transmissions have not yet become commercially successful in wind turbines. The reasons are:
1) The efficiency is lower than that of a gearbox.
2) There is a risk of pollution with oil
3) There is no data on the reliability of hydraulic transmission systems in wind turbines, because these systems have not yet been used on a reasonable scale in wind turbines.

However the fact that they are used in many other applications with low speeds and high torques, such as excavators and aeroplanes, can indicate that the reliability can probably be made acceptable.

3. Alternative direct-drive generators

Direct-drive generators for wind turbines need reduction of cost, size and weight especially at high power levels, because according to (4) the torque level increases more

than proportional to the power level. Several alternative direct-drive generators are presented to meet this requirement.

1) Transverse-flux permanent-magnet generators have been proposed in [33]-[38] to increase the shear stress. However, until now the resulting shear stress in this application has not exceeded the of normal radial-flux generators because of the relatively large air gap. Other disadvantages of these machines are the low power factor and the complicated construction due to the three-dimensional flux paths.

2) Structural mass is the heaviest part in a direct-drive generator. Different methods have been proposed to reduce the amount of structural material:

a) The idea to use large diameter generators with an air core removes the attractive force between stator and rotor [39]-[41] has been adopted by Sway Turbine (Fig. 2-4) and Boulder Wind Power. Along comparable lines, Goliath uses a large diameter generator, but this generator seems to have an air gap winding between the stator and rotor iron as described in [42]. Such constructions make it possible to use less electromagnetically active and structural material. However, protection of the windings and the magnets against the aggressive environment with humidity and salt is an issue.

b) In [39], [43]-[45], it is proposed to reduce the distance between the bearings and the location of the electromagnetic forces by using hybrid magnetic bearing or fluid bearings. This enables the use of lighter constructions, but the bearings become more complicated.

Fig. 2-4. Picture of the large diameter direct drive generator of Sway Turbine. Source: Sway Turbine.

4. Brushless doubly-fed induction generator

In [46]-[52] it has been proposed to use a brushless doubly-fed induction generator (BDFIG) for wind turbines. A BDFIG has two stator windings, one of which is connected to the grid (the so-called power winding) and the other (the so-called control winding) is supplied via a power electronic converter, in the same manner as a DFIG. The machine has two principle fields, associated with the two stator windings, of different pole numbers which cross-couple via the rotor. The rotor has a short-circuited winding consisting of so-called nested loops (Fig. 2-5). The machine operates in a synchronous mode with a fixed ratio between shaft speed and the two stator frequencies, again like DFIG.
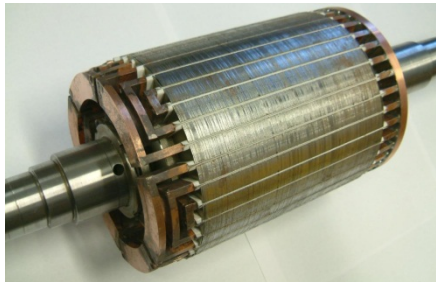
Fig. 2-5. The rotor of a brushless DFIG with 6 nested loops, as used in a machine with a stator with a 4-pole and an 8-pole winding.

The BDFIG is not easy to analyse despite its simple construction and only recently more straightforward design procedures have emerged. Following the description of relatively small experimental machines, several larger machines have recently been built, including a 70 kW machine from Brazil [53], a Chinese machine rated at 200 kW and a 250 kW machine built in UK (believed to be the largest one to date) [54].

These larger machines demonstrate that the BDFIG can be built in larger sizes but a machine with a MW rating remains to be demonstrated. There are restrictions on the allowable pole numbers of the two principle fields, with the highest available natural speed (corresponding to the synchronous speed of DFIG) with a 2-pole/6-pole combination being 750 rpm on a 50 Hz system. Therefore the BDFIG is seen as a natural part of a medium speed drive with a natural speed in the order of 300 rpm. Research is in progress to develop this approach.

The BDFIG shares the following benefits with the DFIG:
1) The cost of construction is low because no permanent magnet is used.
2) Only a fractionally rated power electronic converter need be employed.

The BDFIG has its advantage over DFIG:
1) The absence of brush-gear obviates one of the main failure modes of the DFIG. The reliability increases.
2) Grid-fault ride-through performance is significantly improved.
3) High speed gear stage of the gearbox is avoided because BDFIG is a medium speed generator, increasing the efficiency and the reliability.

Compared with a DFIG of the same speed, BDFIG is probably larger because of the additional winding.

5. Magnetic pseudo direct-drive generator

A magnetic gear is combined with an electrical machine to realize a magnetically geared drive of high torque density in various ways. The magnetic pseudo direct-drive (PDD) generator is realizing the possibility of applying magnetic gears in wind turbines. In a PDD generator, the magnetic gear and the electrical generator are mechanically as well as magnetically integrated [55], [56].

When compared to the basic arrangement of magnetic-gear machines, the PDD
1) facilitates access and cooling of the stator winding and
2) simplifies manufacturing significantly,
especially for large machines since it only has two air gaps.

Prototypes of PDD machines have been designed and tested for various applications. A PDD machine with a continuous torque output of 4 kNm has been tested, and a prototype with a torque output of ~20 kNm is currently going through the initial testing phase.

Development is in progress to increase torque to magnitudes required for wind turbines. Fig. 2-6 shows a design of a PDD generator for a 3 MW wind turbine. This design has the following advantages:
1) Because of the inherently low electric loading, the rated efficiency of this design is more than 98%.
2) The total mass of generator, including the structural components, is only 35 tons. The overall diameter is 3.8 m. Therefore, it is anticipated that the size/mass of PDD generators would be less than 50% of that of permanent-magnet direct-drive generators.
3) Although the quantity of permanent magnets in a PDD machine may be higher, this can be significantly reduced by appropriate optimization. Another idea to reduce the use of permanent magnets is to use electrical excitation to replace some of the permanent magnets.
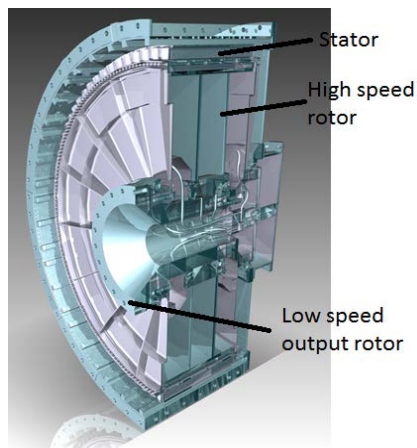
Fig. 2-6. 3MW, 15rpm pseudo direct drive generator for a wind turbine (Courtesy of Magnomatics Limited)

Summarizing, the most important advantages of the PDD are
1) the anticipated reduction of weight compared to direct-drive generators and
2) the significant reduction of maintenance compared to mechanical gearboxes.

The most important disadvantage is the large amount of permanent magnet material.

6. Superconducting direct-drive generator

Superconducting machines have been proposed for wind turbines by both industry [57]-[59] and academia [60]-[65], due to their potential for high torque density and efficiency. Superconductors have the following features:

1) Superconductors exhibit almost zero DC resistance and therefore are commonly proposed for field windings in wound field synchronous generators.

2) With a vanishing DC resistance, the resistive losses will be suppressed and the field current can be increased such that air gap flux density can achieve 2-3 T. Therefore machines using superconductors have very high torque density. Using (2), the volume of a superconducting machine can be reduced by a factor of 2-3 compared to a traditional machine with an air gap flux density just below 1 T.

3) Machines with superconductors have better efficiency compared to traditional machines including permanent magnet machines and electrically excited machines according to

$$P_{Cu} \propto J_{Cu}^2 V_{Cu} \qquad (2.5)$$

If the current density J_{Cu} on the stator is kept constant as the machine is reduced in size, the copper losses P_{Cu} will be proportional to the volume of copper V_{Cu} and hence will reduce as the machine becomes smaller in size.

4) Superconductors only remain superconductive as long as their operating point is kept within three interdependent limits:
- Critical current density
- Critical flux density
- Critical temperature

These limits bring substantial uncertainties and challenges to the employment of superconductors in wind turbine generators.

There are three categories of superconducting wires:
- Low temperature superconductors (LTS) with critical temperatures below 18 K
- High temperature superconductors (HTS) with critical temperatures below 110 K
- MgB$_2$ discovered in 2001 with critical temperature below 39 K intertwined between LTS and HTS.

LTS has been proposed by General Electric (GE) for a 10 MW direct-drive wind turbine [58], where the LTS field winding is stationary and the armature winding rotates with slip rings. LTS is commercially available at relatively low cost for the MRI devices and GE suggests to transfer the MRI technology to the wind turbine. However, as the operating temperature needs to be kept at 4 K, the machine would require a complex cooling system and thermal insulation, which to date has deterred all LTS machines' development.

HTS has been proposed by American Superconductor (AMSC) for a 10 MW direct-drive wind turbine [59]. HTS has the advantage that the cooling system and thermal insulation can be relatively simple, where the cryocoolers can be purchased off the shelf. On the downside, HTS is expensive and is currently not available in sufficient lengths for commercial roll-out.

MgB$_2$ has been proposed by Advanced Magnet Lab (AML) in a fully-superconducting 10 MW direct-drive wind turbine [60], where both armature and field windings are superconducting. This concept has the following problems:

1) The superconductor carries alternating current, resulting in large losses in the superconductor and consequently higher requirements for cooling power. These losses could be limited by further development of MgB$_2$ wires with very small filaments, but currently no MgB$_2$ wire is commercially available at a relatively high magnetic field.

2) MgB$_2$ wire is commercially available at a relatively low price if the flux density is kept at 1 T. However, if the magnetic field is increased to 3 T, the price becomes comparable to HTS at similar flux densities and temperatures [61].

3) MgB$_2$ requires an operating temperature of 15-20 K and would therefore also require sophisticated cooling systems and thermal insulation.

Summarizing, there are three different types of superconductors and all the three have been proposed for future 10 MW wind turbines. None of these have been built or demonstrated yet. For other applications, such as ship propulsion, superconducting machines have been built and tested [63]-[65], but they have not yet become a commercial success. This shows that the area of superconducting wind turbine generators is very far from standardization and all paths are still open to be explored.

2.5 Power electronic converters

In variable speed wind turbine generator systems with partly or fully rated power electronic converter, mostly the standard back-to-back voltage source inverter is used, for both DFIG and full converter systems. This power conversion needs more than one stage to convert the frequency and the voltage level to fit the grid as illustrated in Fig. 2-7. The growing power rating needs the increase of the voltage on the DC link. A typical value would be 5 kV for a 3.3 kV primary side grid voltage. To handle these voltages, multilevel converters are needed.
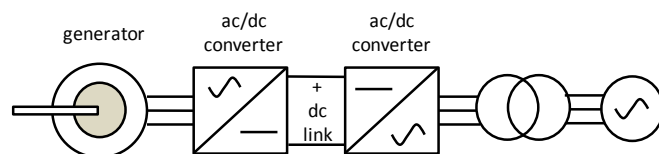
Fig. 2-7. Overview of the power conversion components.

The further evolution of wind power systems will be largely driven by reliability considerations, which implies that mature multilevel converters such as the 3-level Neutral Point Clamped topology would be favoured. The choice of suitable converter topologies and further development of power electronic devices and device packages will be largely driven by a better understanding of failure mechanisms and thermal cycling considerations. Especially the generator side converter is badly affected by the temperature cycle behaviour and non-linear factors of the wind loading such as turbulences and gusts. In DFIG and superconducting direct-drive systems, the situation is aggravated because the converters have to handle AC frequencies which can be in the order of or below 2 Hz, which is comparable to the thermal time constants of the device packages.

As a result, modular fault tolerant conversion system [66]-[70] and DC link transformerless generator system [71]-[74] are the two trends of the development of power electronic converters for wind turbines.

2.4   Conclusion

There is no convergence towards a single best wind turbine generator system, but instead the variety of wind turbine generator systems is increasing. At power levels below 10 MW, the three currently used variable speed systems (with gearbox and DFIG, with gearbox and full converter and direct drive) are expected to remain for the coming years.

Hydraulic transmissions enables continuously variable transmission and are significantly lighter than mechanical gearboxes, but their efficiency is lower.

A brushless DFIG is a medium speed generator without brushes and with improved grid-fault ride-through characteristics compared to DFIGs. But its use of mechanical gearbox leaves challenges to reliability and cost.

The superconducting generator system and the pseudo direct drive generator system have the potential to beat the cubic law. Magnetic pseudo direct drives are smaller and lighter than direct-drive generators, but need a sufficiently low and stable magnet price to be successful. Also superconducting generators can be smaller and lighter than normal direct-drive generators, but both cost and reliability need experimental demonstration. These two generator systems are promising for 10-20 MW wind turbine applications and are therefore to be investigated further.

Power electronic converters are developed towards reliable modular multilevel topologies and these topologies are to be investigated for 10-20 MW wind turbines.

References

[1] P. Tavner, Offshore wind turbines: reliability, availability and maintenance, Stevenage: IET, 2012.
[2] F. Spinato, The reliability of wind turbines, PhD thesis Durham University, 2008.
[3] P.J. Tavner, F. Spinato, G.J.W. van Bussel, E. Koutoulakos, "Reliability of wind turbine subassemblies," IET Proceedings – Renewable Power Generation, 2009, vol. 3, pp. 387-401.
[4] H. Arabian-Hoseynabadi, P.J. Tavner, H. Oraee, "Reliability comparison of direct-drive and geared drive wind turbine concepts" Wind Energy, 2010 (vol. 13), pp. 62-73.
[5] E. Echavarria, B. Hahn, G.J.W. van Bussel, T. Tomiyama, "Reliability of wind turbine technology through time", Journal of Solar Energy Engineering, 2008 (vol. 130), pp. 031005-1-8.
[6] P.J. Tavner, S. Faulstich, B. Hahn, G.J.W. van Bussel, "Reliability and availability of wind turbine electrical and electronic components", EPE Journal, 2011 (vol. 20).
[7] H. Polinder, H. Lendenmann, R. Chin, W.M. Arshad, "Fault tolerant generator systems for wind turbines", IEEE International Electric Machines and Drives Conference (IEMDC), 2009, pp. 675-681.

[8] Z. Chen, J.M. Guerrero, F. Blaabjerg, "A review of the state of the art of power electronics for wind turbines" IEEE Trans. on Power Electronics, 2009 (vol. 24), pp. 1859-1975.

[9] R. Cardenas, R. Pena, S. Alepuz, G. Asher, "Overview of Control Systems for the Operation of DFIGs in Wind Energy Applications",
IEEE Trans. on Industrial Electronics, 2013 (vol. 60), pp. 2776-2798.

[10] J. Morren, S.W.H. de Haan, "Ridethrough of wind turbines with doubly-fed induction generator during a voltage dip," IEEE Trans. on Energy Conversion, 2005 (vol. 20), pp. 435–441.

[11] C. Wessels, F. Gebhart, R.W. Fuchs, "Fault ride-through of a DFIG wind turbine using a dynamic voltage restorer during symmetrical and asymmetrical grid faults", IEEE Trans. on Power Electronics, 2011 (vol. 26), pp. 807-815.

[12] A.D. Hansen, G. Michalke, "Fault ride-through capability of DFIG wind turbines", Renewable Energy, 2007 (vol. 32), pp. 1594-1610.

[13] G. Pannell, D.J. Atkinson, B. Zahawi, "Minimum-threshold crowbar for a fault-ride-through grid-code-compliant DFIG wind turbine", IEEE Trans. on Energy Conversion, 2010 (vol. 25), pp. 750-759.

[14] L.G. Meegahapola, T. Littler, D. Flynn, "Decoupled-DFIG fault ride-through strategy for enhanced stability performance during grid faults", IEEE Trans. on Sustainable Energy, 2010 (vol. 1), pp. 152-162.

[15] H. Polinder, F.F.A. van der Pijl, G.J. de Vilder, P. Tavner, "Comparison of direct-drive and geared generator concepts for wind turbines", IEEE Trans. on Energy Conversion, 2006 (vol. 21), pp. 725-733.

[16] H. Li, Z. Chen, H. Polinder, "Optimization of Multibrid Permanent Magnet Wind Generator Systems", IEEE Trans. on Energy Conversion, 2009 (vol. 24), pp. 82-92.

[17] H. Arabian-Hoseynabadi, P.J. Tavner, H. Oraee, "Reliability comparison of direct-drive and geared drive wind turbine concepts" Wind Energy, 2010 (vol. 13), pp. 62-73.

[18] R. Scott Semken, M. Polikarpova, P. Röyttä, J. Alexandrova, J. Pyrhönen, J. Nerg, A. Mikkola, J. Backman, "Direct-drive permanent magnet generators for high power wind turbines: benefits and limiting factors", IET Renewable Power Generation, 2012, pp. 1-8.

[19] M. Mueller, A. Zavvos, "Electrical generators for direct drive systems: a technology overview", Electrical drives for direct drive renewable energy systems, M. Mueller, H. Polinder, Editors, Oxford: Woodhead Publishing, 2013, pp. 1-29.

[20] H. Polinder, "Principles of electrical design of permanent magnet generators for direct drive renewable energy systems", Electrical drives for direct drive renewable energy systems, M. Mueller, H. Polinder, Editors, Oxford: Woodhead Publishing, 2013, pp. 30-50.

[21] A. McDonald, M. Mueller, A. Zavvos, "Electrical, thermal and structural generator design and systems integration for direct drive renewable energy systems", Electrical drives for direct drive renewable energy systems, M. Mueller, H. Polinder, Editors, Oxford: Woodhead Publishing, 2013, pp. 51-79.

[22] A. Jassal, K. Versteegh, H. Polinder, "Case study of the permanent magnet direct drive generator in the Zephyros wind turbine", Electrical drives for direct drive renewable energy systems, M. Mueller, H. Polinder, Editors, Oxford: Woodhead Publishing, 2013, pp. 158-174.

[23] V. Ruuskanen, J. Nerg, M. Niemela, J. Pyrhonen, H. Polinder, 'Effect of Radial cooling ducts on the Electromagnetic Performance of the Permanent Magnet Synchronous Generators with Double Radial Forced Air Cooling for Direct-Driven Wind Turbines' IEEE Trans. on Magnetics, 2013.

[24]   S. Brisset, D. Vizireanu, P. Brochet, "Design and Optimization of a Nine-Phase Axial-Flux PM Synchronous Generator With Concentrated Winding for Direct-Drive Wind Turbine", IEEE Trans. on Industry Applications, 2008 (vol. 44). pp. 707-715.

[25]   H. Polinder, M.J. Hoeijmakers, M. Scuotto, "Eddy-current losses in the solid back-iron of permanent-magnet machines with different concentrated fractional pitch windings", IEEE International Electrical Machines and Drives Conf. (IEMDC), Antalya, 2007, pp. 652-657.

[26]   A.K. Jassal, H. Polinder, D. Lahaye, J.A. Ferreira, "Analytical and FE calculation of eddy-current losses in PM concentrated winding machines for wind turbines", IEEE International Electric Machines and Drives Conf (IEMDC), Niagara Falls, 2011, pp. 727-732.

[27]   C. Rossi, P. Corbelli, G. Grandi, "W-CVT continuously variable transmission for wind energy conversion system", in Proc. of the IEEE conference on power electronics and machines in wind applications, 2009, pp. 1-10.

[28]   B.-R. Höhn, "Future transmissions for wind turbines", Applied Mechanics and Materials, 2011 (vol. 86), pp.18-25.

[29]   V. Miltenović, M. Velimirović, M. Banić, A. Miltenović, "Design of wind turbines drive train based on CVT", Balkan Journal of Mechanical Transmissions, Volume 1 (2011), Issue 1, pp. 46-56, ISSN 2069–5497.

[30]   N. Diepeveen, "On Fluid Power Transmission for Offshore Wind Turbines", PhD thesis Delft University of Technology, 2013.

[31]   A. Ragheb, M. Ragheb, "Wind turbine gearbox technologies", First international nuclear & renewable energy conference (INREC), 2010, pp. 1-8.

[32]   B. Skaare, B. Hörnsten, F.G. Nielsen, "Modeling, simulation and control of a wind turbine with a hydraulic transmission system", Wind Energy, October 2012.

[33]   H. Weh, H. May, "Achievable force densities for permanent magnet machines in new configurations", Proc. International Conference on Electrical Machines, Munich, 1986, pp. 1107-1111.

[34]   J. Hystad, "Transverse flux generators in direct-driven wind energy converters," PhD-thesis Norwegian University of Science and Technology, Trondheim, 2000.

[35]   M. Dubois, "Optimized permanent magnet generator topologies for direct drive wind turbines", PhD-thesis Delft University of Technology, 2004.

[36]   D. Bang, "Design of transverse flux permanent magnet machines for large direct-drive wind turbines", PhD-thesis Delft University of Technology, 2010.

[37]   D. Svechkarenko, A. Cosic, J. Soulard, C. Sadarangani, "Transverse Flux Machines for Sustainable Development - Road Transportation and Power Generation", Proc. 7th International Conference on Power Electronics and Drive Systems, 2007, pp. 1108-1114.

[38]   A. Zavvos, D.J. Bang, A. Mcdonald, H. Polinder, M. Mueller, 'Structural analysis and optimisation of transverse flux permanent magnet machines for 5MW and 10 MW direct drive wind turbines', Wind Energy, 2012, pp. 19-43.

[39]   M. Mueller, A. Zavvos, "Electrical generators for direct drive systems: a technology overview", Electrical drives for direct drive renewable energy systems, M. Mueller, H. Polinder, Editors, Oxford: Woodhead Publishing, 2013, pp. 1-29.

[40]   A. McDonald, M. Mueller, A. Zavvos, "Electrical, thermal and structural generator design and systems integration for direct drive renewable energy systems", Electrical drives for direct drive renewable energy systems, M. Mueller, H. Polinder, Editors, Oxford: Woodhead Publishing, 2013, pp. 51-79.

(INNWIND.EU, WP3 internal report, First assessment of performance indicators of SC and PDD generators*)*

[41]   M.J. Kamper, J.H.J. Potgieter, J.A. Stegman, P. Bouwer, "Comparison of air-cored and iron-cored non-overlap winding radial flux permanent magnet direct drive wind generators", Energy Conversion Congress and Exposition (ECCE), 2011, pp. 1620-1627.

[42]   E. Spooner, P. Gordon, J.R. Bumby, C.D. French, "Lightweight ironless-stator PM generators for direct-drive wind turbines", IEE Proceedings - Electric Power Applications, 2005 (vol. 152), pp. 17-26.

[43]   G. Shrestha, H. Polinder, D. Bang, J.A. Ferreira, 'Structural Flexibility: A Solution for Weight Reduction of Large Direct Drive Wind Turbine Generators', IEEE Trans. on Energy Conversion, 2010, pp. 732-740.

[44]   G. Shrestha, "Structural Flexibility of LargeDirect Drive Generators for Wind Turbines", PhD thesis Delft University of Technology, 2013.

[45]   D. Bang, H. Polinder, J.A. Ferreira, Seung-soo Hong, "Structural mass minimization of large direct-drive wind generators using a buoyant rotor structure", in Proc of the IEEE energy conversion congress and exposition, 2010, pp. 3561-3568.

[46]   R.A. McMahon, P.C. Roberts, X. Wang, P.J. Tavner, "Performance of BDFM as generator and motor", IEE Proceedings - Electrical Power Applications, 2006 (vol. 153), pp. 289-299.

[47]   T. Long, S. Shao, E. Abdi, P. Malliband, M.E. Mathekga, R.A. McMahon, P.J. Tavner, "Symmetrical low voltage ride-through of a 250 kW Brushless DFIG", 6th IET Int. Conf. on Power Electronics, Machines and Drives (PEMD), Bristol, UK, 2012, pp. 1-6.

[48]   C.S. Brune, R. Spee, A.K. Wallace. "Experimental evaluation of a variable speed, doubly-fed wind-power generation system", IEEE Trans. on Industry Applications, 1994 (vol. 30), pp. 648 – 655.

[49]   E. Abdi, Xiaoyan Wang, Shiyi Shao Shao, R. McMahon, P. Tavner, "Performance characterisation of brushless doubly-fed generator", IEEE Industry Applications Society Annual Meeting, 2008.

[50]   R. Carlson, H. Voltolini, F. Runcos, P. Kuo-Peng, N.J. Batistela, "Performance analysis with power factor compensation of a 75 kw brushless doubly fed induction generator prototype", IEEE International Electric Machines & Drives Conference, IEMDC '07, 2007.

[51]   "Industrialization of a 3 MW Medium-Speed Brushless DFIG Drivetrain for Wind Turbine Applications", Windrive 315485, EU FP7 Project, www.bdfig.com.

[52]   P.C. Robert, R.A. McMahon, P.J. Tavner, J.M. Maciejowski, T.J. Flack, "Equivalent circuit for the brushless doubly fed machine (BDFM) including parameter estimation and experimental verification", IEE Proceedings – Electric Power Applications, 2005, pp. 933-942.

[53]   R. Carlson, H. Voltolini, F. Runcos, P. Kuo-Peng, N.J. Batistela, "Performance analysis with power factor compensation of a 75 kw brushless doubly fed induction generator prototype", IEEE International Electric Machines & Drives Conference, IEMDC '07, 2007.

[54]   T. Long, S. Shao, E. Abdi, P. Malliband, M.E. Mathekga, R.A. McMahon, P.J. Tavner, "Symmetrical low voltage ride-through of a 250 kW Brushless DFIG", 6th IET Int. Conf. on Power Electronics, Machines and Drives (PEMD), Bristol, UK, 2012, pp. 1-6.

[55]   K. Atallah, J. Rens, S. Mezani, D. Howe, "A novel "pseudo" direct-drive brushless permanent magnet machine", IEEE Trans. on Magnetics, 2008 (vol. 44), pp. 4349-4352.

[56]   Linni Jian, K.T. Chau, J.Z. Jiang, "A magnetic-geared outer-rotor permanent-magnet brushless machine for wind power generation", IEEE Trans. on Industry Applications, 2009 (vol. 45), pp. 954-962.

(INNWIND.EU, WP3 internal report, First assessment of performance indicators of SC and PDD generators)

[57]   C. Lewis, J. Muller, "A direct drive wind turbine HTS generator", IEEE Power Engineering Society General Meeting, June 2007, pp. 1-8.

[58]   R. Fair, "Superconductivity for large scale wind turbines", Final Scientific Report - DE-EE0005143, General Electric – Global Research, Niskayuna/DUNS No. 086188401, 2012.

[59]   G. Snitchler, B. Gamble, C. King, P. Winn, "10 MW class superconductor wind turbine generators", IEEE Trans. on Applied Superconductivity, 2011 (vol. 21), pp. 1089-1092.

[60]   A.B. Abrahamsen, B.B. Jensen, E. Seiler, N. Mijatovic, V.M. Rodriguez-Zermeno, N.H. Andersen, J. Østergård, "Feasibility study of 5 MW superconducting wind turbine generator", Physica C: Superconductivity, 2011, (vol. 471), pp. 1464-1469.

[61]   B. B. Jensen, N. Mijatovic, A. B. Abrahamsen, "Development of superconducting wind turbine generators", Journal of Renewable Sustainable and Energy, 2013 (vol. 5), pp. 023137.

[62]   Ronghai Qu, Yingzhen Liu, Jin Wang, "Review of Superconducting Generator Topologies for Direct-Drive Wind Turbines", IEEE Trans. on Applied Superconductivity, 2013 (vol 23).

[63]   O. Keysan, "Application of high-temperature superconducting machines to direct drive renewable energy systems", Electrical drives for direct drive renewable energy systems, M. Mueller, H. Polinder, Editors, Oxford: Woodhead Publishing, 2013, pp. 219-252.

[64]   S.S. Kalsi, Applications of high temperature superconductors to electric power equipment, Hoboken: Wiley-IEEE Press, 2011.

[65]   D. Kostopoulos, H. Polinder, A. van den Brink, "High temperature superconducting generators for direct drive wind turbines: a review", Proc. of European Wind Energy Association Conf., 2012, pp. 1-10.

[66]   C.H. Ng, M.A. Parker, L. Ran, P.J. Tavner, J.R. Bumby, E. Spooner, "A multilevel modular converter for a large, light weight wind turbine generator", IEEE Trans. on Power Electronics, 2008 (vol. 23), pp. 1062-1074.

[67]   Fujin Deng, Z. Chen, "A new structure based on cascaded multilevel converter for variable speed wind turbine", Annual Conference on IEEE Industrial Electronics Society (IECON), 2010, pp. 3167-3172.

[68]   S.S. Gjerde, T.M. Undeland, "Fault tolerance of a 10 MW, 100 kV transformerless offshore wind turbine concept with a modular converter system", Power Electronics and Motion Control Conference (EPE/PEMC), 2012, pp. LS7c.3-1 - LS7c.3-8

[69]   N.R. Brown, T.M. Jahns, R.D. Lorenz, "Power Converter Design for an Integrated Modular Motor Drive", Conf. Record of the 42nd IEEE IAS Annual Meeting, pp. 1322-1328.

[70]   J.J. Wolmarans, M.B. Gerber, H. Polinder, S.W.H. de Haan, J.A. Ferreira, "A 50kW Integrated Fault Tolerant Permanent Magnet Machine and Motor Drive", IEEE Power Electronics Specialists Conference (PESC 2008), 2008, pp. 345-351.

[71]   M. Sztykiel, "Overview of power converter designs feasible for high voltage transformer-less wind turbine", IEEE International Symposium on Industrial Electronics (ISIE), 2011, pp. 1420.1425.

[72]   P.K. Olsen, S. Gjerde, R.M. Nilssen, J. Hoelto, S. Hvidsten, "A transformerless generator-converter concept making feasible a 100 kV light weight offshore wind turbine: Part I - The generator", IEEE Energy Conversion Congress and Exposition (ECCE), 2012, pp. 247-252.

[73]   S. Kouro, J. Rodriguez, Bin Wu,S. Bernet, M Perez, "Powering the future of industry: high-power adjustable speed drive topologies", IEEE Industry Applications Magazine, 2012, (vol. 18, no. 4), pp. 26 - 39.

[74]   J.A. Ferreira, "The multilevel modular DC converter", IEEE Trans. on Power Electronics, 2013 (vol. 28), 2013, pp. 4460-4465.

(INNWIND.EU, WP3 internal report, First assessment of performance indicators of SC and PDD generators*)*

CHAPTER 3 PROPOSED NACELLE STRUCTURES

3.1 Introduction

The objective of this chapter is to discuss possible nacelle structures for the INNWIND.EU turbines.

3.2 Description of proposed nacelle structures

There are several structural challenges for wind turbines of the 10 and 20 MW class, this is mainly caused by the very large rotor diameter (178m and 252m) required for these turbines. These very large rotors are very heavy and introduce very high bending moments which need to be transferred from the rotor into the tower. The main bearing system is the key component responsible for transferring these loads from the rotor into the support structure.

In general the following three types of main bearing system topologies can be identified:

- Single main bearing
- One or multiple main bearings on a revolving main shaft
- One or multiple main bearings on a stationary main shaft

Although single main bearing solutions are increasingly popular, it is possible to use this topology for the Super Conducting Direct Drive (SC-DD) and the Pseudo Direct Drive (PDD). Siemens is using this main bearing topology in their SWT-6.0 wind turbines. But the currently available bearing capacity is insufficient for the Innwind requirements, and the only solution to increase the capacity is increasing the bearing diameter and width. For the 10MW using this type of bearing might be possible in the near future, but it is very uncertain if a single main bearing solution for the 20MW will ever be feasible and cost effective.
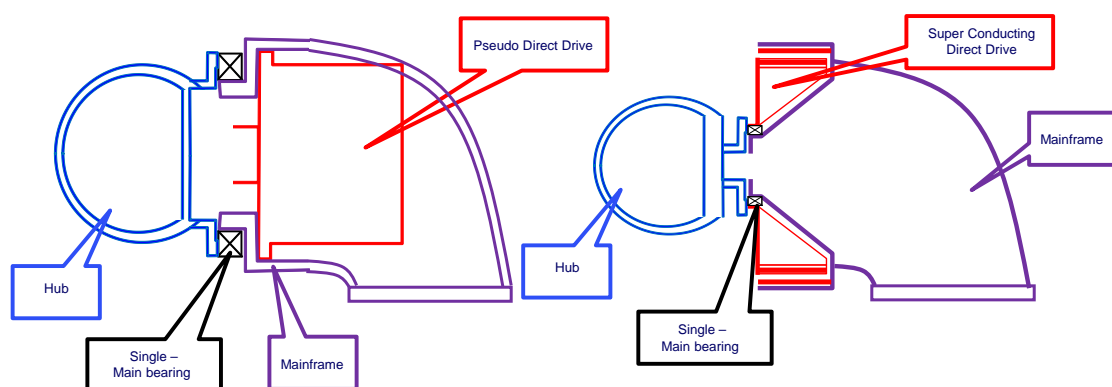

Figure 3-1: Single main bearing in combination with a PDD (left) and a SC-DD (right)

The main bearing system on a revolving main shaft is a well-known solution used in many wind turbine designs. This main bearing topology can be used for the SC-DD and the PDD. In case of the PDD, the PDD drive will be connected at the non-rotor side of the revolving main shaft. Some turbine designs using this topology are GE 4.0, Repower 6m and Vestas V164. The main disadvantage of this topology is the distance between the rotor hub centre and the upwind main bearing. This results in a high loading on the upwind main bearing. At this moment it is very difficult if not impossible to find a suitable upwind main bearing for the 20 MW. It might be that this will change in the future. Another disadvantage is that such a very high capacity upwind main bearing will have a significant effect on the main shaft, main bearing housing and mainframe design. This will result in a costly and uncompetitive wind turbine design.
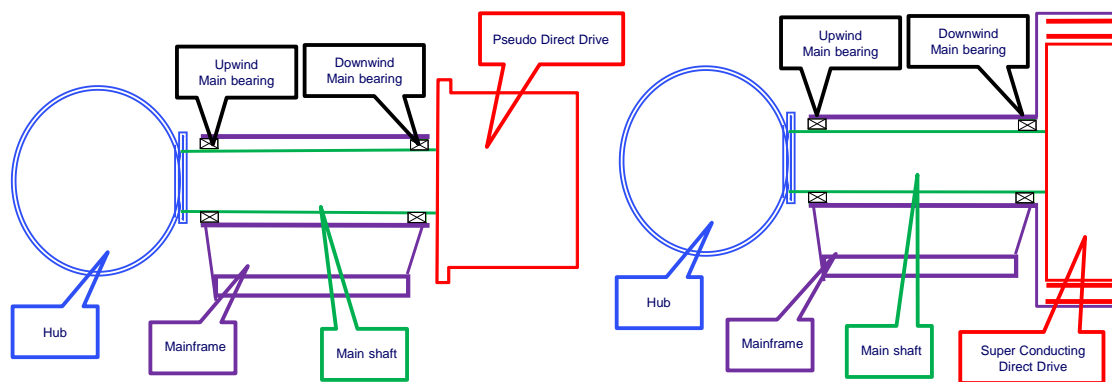

Figure 3-2: Two main bearings on a revolving shaft in combination with a PDD (left) and a SC-DD (right)

The third option is the main bearings on a stationary main shaft. This stationary shaft is also known as a kingpin. The main advantage of this design is that the main bearings can be located in the rotor, where the rotor loads are introduced into the support structure. From a main bearing system point-of view this is the preferred solution. It is even likely that available main bearings have sufficient capacity to handle the loads of the 20 MW. This main bearing topology is a very common design in direct drive wind turbine, but uncommon in a geared wind turbines. This is because it is difficult to find a suitable location for the gearbox. Some wind turbines using this topology are the Alstom Haliade, Alstom (Ecotecnia) ECO-80/100 and the Enercon E-126.
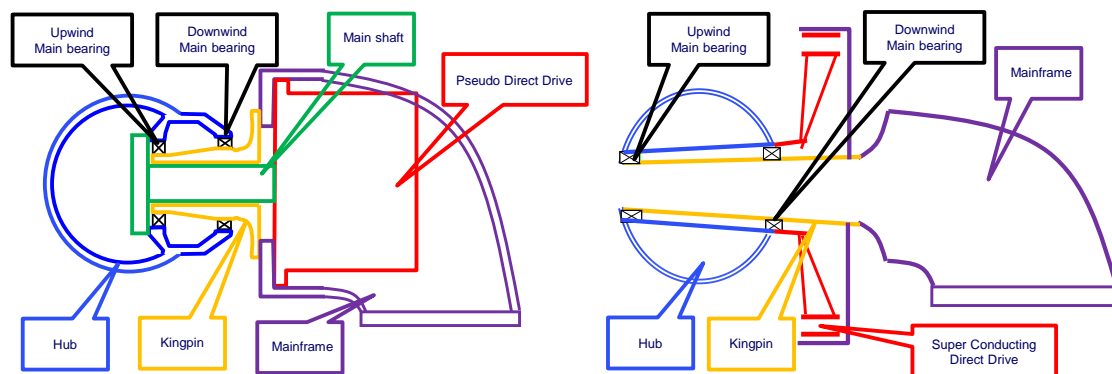

Figure 3-3: Two main bearings on a kingpin in combination with a PDD (left) and a SC-DD (right)

GL-Garrad Hassan has developed an alternative layout of the stationary shaft in combination with a gearbox. This layout has the gearbox mounted on the upwind side of the rotor. This layout has several advantages over all the previous layouts. It has the advantages of the main bearing loading of the kingpin. In case of the PDD it does not require a main shaft and the PDD don't have to fit within the mainframe which is better for the PDD and the mainframe. For the SC-DD there is a reduced distance for cooling lines which need to have a revolving coupling from the center of the kingpin at the upwind side of the rotor. The added mass of the PDD or SC-DD in front of the rotor has no significant effect on the yaw bearing, because the rotor can be moved closer to the tower. It does require a revolving casing PDD instead of a stationary PDD.
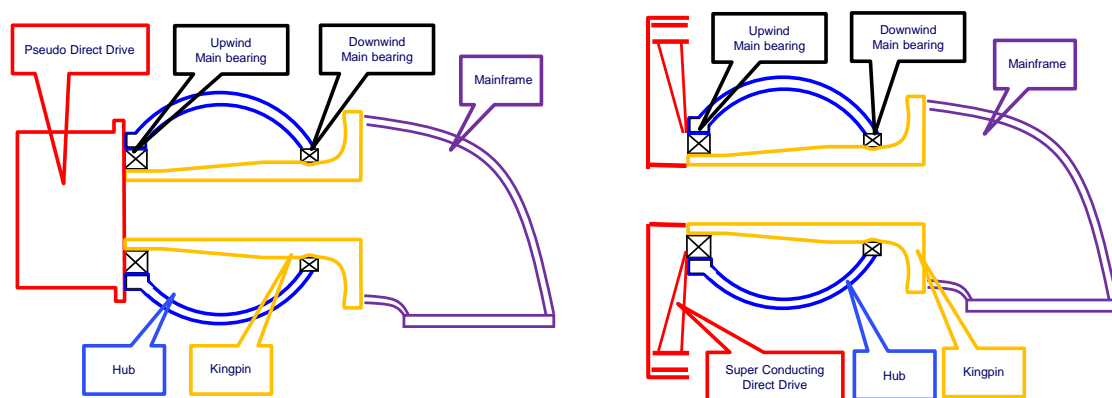

Figure 3-4: Selected kingpin layout with a PDD (left) and a SC-DD (right)

Some key points of the selected kingpin layout are:

- Nearly identical structure for the PDD and the SC-DD, resulting in a better comparison between the PDD and SC-DD
- Most realistic layout for a 20MW 252m rotor wind turbine (using existing components and manufacturing limitations)
- Very efficient structure (structural components sized for transferring loads, not for secondary requirements)
- Lowest impact on the design of the SC-DD cooling system
- (Almost) no restriction on generator dimensions
- Requires inverted (rotating housing) design of PDD
- Limited bearing deflections are expected which allow to use the main bearings as generator bearings

- To correctly determine performance indicators like the size, weight and cost of the nacelle require the knowledge of the loading from the rotor. At this moment the work package group 2 is working on the light weight rotor design. The current best estimate of the nacelle mass is based on 3D modelling and simplified strength calculations. The mass is between 350 and 450 tonne which does not include the rotor and the tower structure. It does include the PDD or SC-DD system with an estimated mass of between 125 and 175 tonne.

3.3   Conclusion: performance indicators

The rotor loading has a very large effect on the final size, mass and cost of the nacelle. To do a final estimate on these performance indicators, a more final version of the rotor loads should be available. This is expected within the next few months.

Another requested performance indicator is the bearing losses in the main bearing system. Based on calculations, the bearing losses were calculated between 5 and 7 kW.

The interface dimensions for the PDD and the SC-DD are shown in the figures shown below.
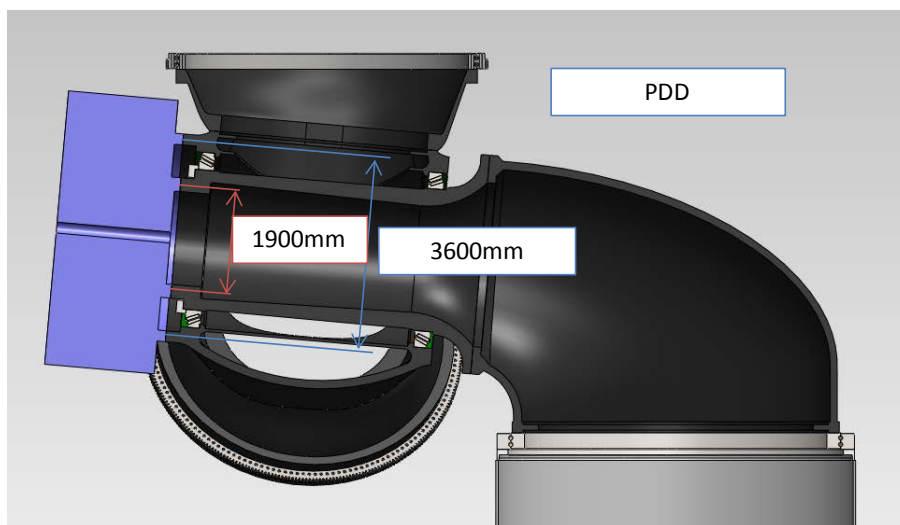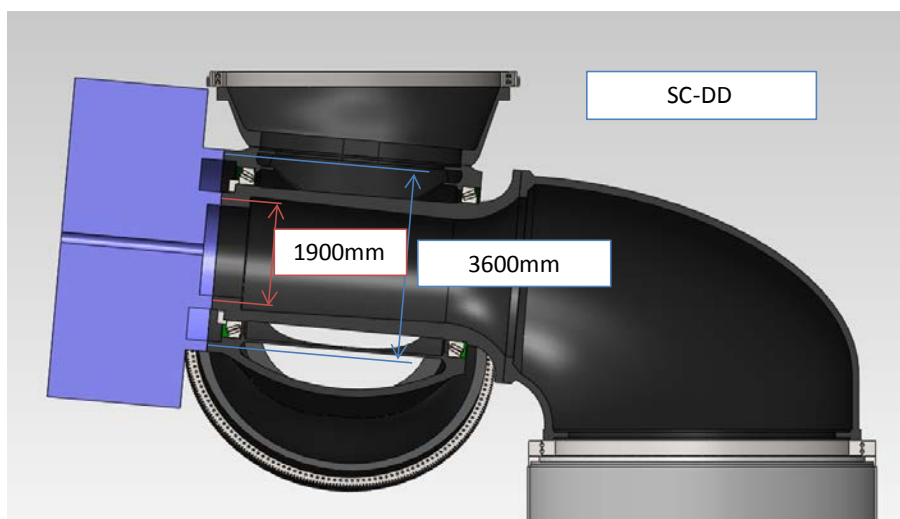

Figure 3-5: Main PDD interface dimensions

Figure 3-6: Main SC-DD interface dimensions

CHAPTER 4 SUPERCONDUCTING GENERATORS

4.1 Introduction

The objective of this chapter is to outline the basic principle of superconducting direct drive generators for wind turbines and to present the argument used to estimate the performance indicators in terms of size, mass, efficiency and cost of selected generators designs based on the main types of superconducting wires commercially available today: $NbTi/Cu$, MgB_2/Ni and coated conductor of the $YBa_2Cu_3O_{6+x}$ high temperature superconductor.

This chapter is structured with a generator introduction, state-of-the-art superconducting wind turbine generator proposals, discussion of the selection of target design's of INNWIND.EU, an estimation of the performance indicators of selected designs and finally a discussion of the advantages and challenges of the deigns as well as a recommendation of how to further improve the performance.

4.1.1 Superconductivity

Superconductivity in materials is caused by a pairing of a fraction of the conduction electrons into a quantum fluid of Cooper pairs, which consist of two electrons with opposite direction of movement. All the electron pairs are quantum mechanically entangled and will therefore behave collectively as a condensate of super-electrons instead of individually as the initial conduction electrons. Usually two electrons would repel one another, since both have a negative charge, and would therefore never join in a pair. However in metals one negative moving electron can attract the positive ions of the crystal lattice in a track behind the electron. Thus a region slightly more positive than the rest of the crystal lattice is formed and can attract another electron, whereby the pair is formed by an intermediate interaction through the a local crystal lattice distortion. This local lattice distortion is the pairing mechanism of metals as formulated in the Bardeen, Cooper & Schrieffer (BCS) theory from 1957[1]. A new class of superconductors called the High Temperature Superconductors (HTS) were discovered in insulating ceramic materials in 1987, but the pairing mechanism is not the local lattice distortion and is still unexplained constituting one of the grand challenges of physics [2]. However a condensate of Cooper pairs is formed in the HTS and many of the fundamental properties are the same as for the metal superconductors, but specific values can be quite different.

In the following the characteristic quantities of superconductors is outlined and shortly explained:

Critical temperature T_C: The temperature at which the first electron pair turns into the superconducting condensate. More and more conduction electrons are paired up and enter the superconducting condensate as the temperature is decreased below T_C. A maximum density of the condensate is reached at $T = 0$ K far below T_C.

The consequence of the electron pair condensate is that internal currents can be created inside a piece of material and these currents will be completely loss free with $R = 0 \ \Omega$, hence the name superconductor. One way to create a loss free current is to apply an

external magnetic field to a sample, which is then cooled below the critical temperature T_C. The superconductor will create a super-current at the surface of the sample and expel the magnetic field from the interior of the superconductor causing B = 0 Tesla. This effect is known as the Meissner effect [3]. Increasing the applied field in the Meissner state will cause a higher screening supercurrent, which is limited by the pairing strength of the electron pairs. They will break up and the sample is turned into the normal state above a certain critical applied field B_C.

In some types of superconductors a second phenomenon will take place as an applied field is increased and that is the inclusion of magnetic vortex lines in the interior of the sample. A vortex line contains one quantum of magnetic flux Φ_0= h/2e, where h is Planck's constant and 2e is the charge of the Cooper pair. This flux is confined by supercurrents circulating around the vortex line, which have a centre that is not superconducting. The vortex lines repel one another and order into a hexagonal lattice. The average magnetic flux density B_{av} inside the superconductor is directly related to the distance a between the flux lines in the lattice, since there is one flux quantum per unit cell with an opening angle of β = 60⁰

$$a = \sqrt{\frac{\Phi_0}{B_{av}.sin\beta}}$$ (4.1)

There are two important length scales related to the vortex line. The first is the **penetration depth** λ, which is the decay exponent of the magnetic flux density away from the vortex line centre. The second is the **coherence length** ξ, which describes the size of the non-superconducting core of the vortex line. The vortex line can exist when $\frac{\lambda}{\xi} > \frac{1}{\sqrt{2}}$, which is called a type-II superconductor. All practical superconductors are of this type and vortex lines will be present.

Upper critical field B_{c2}: The presence of the vortex lines imposes a limit to how close they can be packed, since superconductivity will disappear if the distance between them is reaching the size of the non-superconducting core. Thus if $a \sim \xi$ in eq. 4.1 one will obtain the upper critical field, which more correctly is

$$B_{C2} = \frac{\Phi_0}{2\pi\xi^2}$$ (4.2)

Superconductors got their name due to the fact that loss-free internal currents could be established, but this is not true for external transport currents in superconductors containing vortex lines as is the case in field coils of magnets or generators. The problem is that an external transport current density J will interact with the vortex line and create a force per length of the vortex line

$$F_{vortex} = \Phi_0 z \times J$$ (4.3)

If a vortex line starts to move an electric field is generated in the vortex core causing a resistance different from zero related to the transport current. The vortex line can however be prevented from moving if non-superconducting regions of a size similar to the coherence length ξ are incorporated in the material by adding nano-particles and nano engineering of the micro structure. This is called pinning of vortex lines and a pinning force f_{pin} will result. In a very simple picture one can say that as long as the force acting on the vortex is smaller than the pinning force ($F_{vortex} < F_{pin}$) then loss free current transport is possible, but losses

will increase abruptly as the current interaction force exceeds the pinning force ($F_{vortex} > F_{pin}$).

Critical current density J_c: The current density imposed by an external transport current J where the vortex lines will start to be pulled out of the pinning sites incorporated in a specific superconducting material and losses will arise. In the simple model of eq. (4.3) one would obtain J_C when $F_{vortex} = F_{pin}$ giving

$$J_C = \frac{F_{pin}}{\Phi_0} \tag{4.4}$$

Thus a very clean superconducting material is basically useless in an application where high magnetic field is to be produced, because there are no pinning sites to trap the vortex lines. Practical superconductors need both a basic chemical composition and also a nano-engineered micro structure providing pinning of the vortex lines. The effectiveness of the pinning sites will depend heavily on the original chemical composition of the superconductor and also on the operation temperature T compared to the critical temperature T_C as well as the applied field B_a compared to the upper critical field B_{C2}. Secondly the pinning mechanism involves a strong interaction between all the vortex lines and the critical current is a result of the collective deformation of the vortex line system with respect to the distribution of pinning sites in a sample. The voltage drop U along a superconducting sample of length L and carrying a DC current I is often observed to be given by a power law

$$U = LE_0 \left(\frac{I}{I_C(B,T)}\right)^{n(B,T)} \tag{4.5}$$

Where E_0 is a reference electric field often defined as 1 µV/cm, $I_C(B,T)$ is the critical current being a function of the local field and temperature and the *n*-value indicates how abrupt the voltage will increase in case $I > I_C$. The physical meaning of the *n*-value is the ratio of the "collective" pinning energy scale and the thermal energy scale $K_B T$, where K_B is the Boltzmann constant. By considering the F_{pin} in eq 4.4. is the collective response of the vortex lines then a simple argument would be that it should scale by the ratio between the density of pinning sites n_{pin} and the density of vortex lines $n_{vortex} \sim 1/a^2 \sim B_{av}$ from eq. 4.3, because if there are more vortex lines than pinning sites then the vortex lines are more easily displaces in the vortex lattice system. Thus the magnetic field scaling of the critical current is expected to be

$$J_C = \frac{F_{pin}}{\Phi_0} \sim \frac{n_{pin}}{n_{vortex}} \sim \frac{1}{B_{av}} \tag{4.6}$$

where B_{av} is the local magnetic flux density inside the superconductor.

Irreversibility field B_{irr}: The applied field at which the critical current density of a specific practical superconducting material is becoming zero. Thus one must be sufficient below B_{irr} in applications in order to sustain almost loss free transport currents. The material is still superconducting above B_{irr}, which is much lower than the upper critical field B_{c2}, but the vortex lines are flowing around just by the thermal excitations in the material. The vortex line system is said to be melted and behaves as a liquid.

The pinning of the vortex lines will result in a hysteretic response of a superconductor if the applied magnetic field is cycled whereby vortex lines are moved in and out of a sample. Thus superconductor will experience an AC loss if exposed to either AC magnetic fields or AC currents creating AC magnetic fields. Secondly a piece of bulk superconductor can act as a "permanent" magnet is vortex lines are pushed into the sample and the external field is removed.

4.1.2 Practical superconductors

The practical superconductors used in large scale application such as magnets for magneto resonance imaging (MRI), fusion energy and accelerators are mostly based on the metal alloys: NbTi and Nb_3Sn. They are produced by the Powder-In-Tube (PIT) method, where rods of the superconducting material is packed in a billet of copper or other support metals and drawn to wires of several kilometer of length. This allows the creation of multi-filament wires with up to several thousands of filaments in wires of diameter of 1 mm.

The PIT method has also been applied to more recently discovered superconductors like the MgB_2 metal alloy by using a support matrix of iron (Fe) or nickel (Ni). It has also been applied to the ceramic high temperature superconductor $Bi_2Sr_2Ca_2Cu_3O_{10+x}$ (Bi-2223), but here the support metal must be silver and the wires are often rolled flat into tapes, because the ceramic grows as plates, which must be aligned in order to support a supercurrent. These tapes are often called the first generation (1G) of high temperature superconducting tapes, since they were developed and commercialized in the 1990'ties. The usage of silver as the support metal and a complicated pinning at high temperature was found to impose a limitation on lowering the price of the tape and an alternative was investigated.

The ceramic high temperature superconductor $YBa_2Cu_3O_{6+x}$ (YBCO) have pinning properties much better than the Bi-2223 superconductor, but the powder-in-tube method does not work for tape production, because the alignment of the ceramic grains must be better than a few degrees. A new tape architecture was developed and called coated conductors or the second generation (2G) of high temperature superconducting tapes. This is based on a flat metal substrate onto which a series of thin ceramic layers are deposited. The alignment of YCBO grains is transferred from either aligning a nickel metal substrate by rolling or by growing a layer of aligned CeO on a poly crystalline substrate like Hasteloy. The substrate and ceramic layers are enclosed by support metal by either electroplating silver/copper onto the substrate or by laminating with metal strips such as
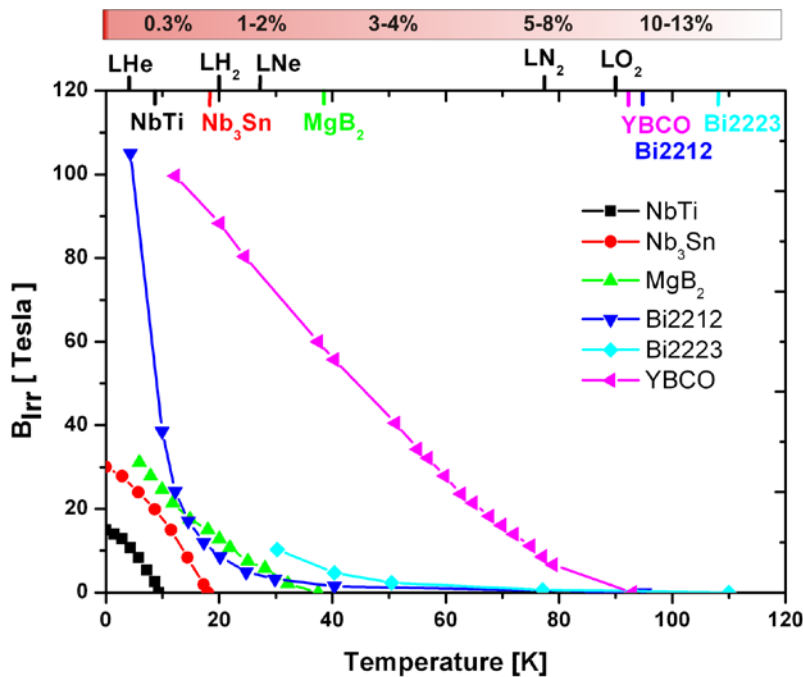
copper or steel.

Figure 4-1. Phase diagram showing the irreversibility magnetic field B_{irr}, where the critical current that can be supported by the major commercial superconductors, is going to zero. Thus choosing a superconductor for a wind generator operating with magnetic field in the range B = 3-5 Tesla is limited to temperatures below T = 30 K for most of the superconductor except for the YBCO type which has a large potential. The lower tick-marks on the top axis are showing the critical temperature T_C at which the superconducting state is formed and the top tick-marks indicate the boiling point of several cryogenic liquids (helium, hydrogen, neon, nitrogen and oxygen). The figures in the top bar are typical efficiencies of cryogenic cooling devices, where 1% at T = 25 K indicate that removing 1 W of heat in the cold takes 100 W of electricity going into the compressors of the cooling system. Reproduced from [4].

Figure 4-1 shows the field and temperature phase diagram of the major practical superconductor materials available as commercial wires or tapes [4]. The critical temperatures T_C of the different superconductors are marked on the top axis and are ranging from 9.8 K for NbTi and all the way up to 110 K for Bi-2223. The vertical axis is showing the irreversibility field B_{irr} as function of temperature and indicates the maximum operation magnetic flux density of the different superconductors. Starting from the lowest temperature NbTi is found to be useful in magnetic fields up to $B \sim 10$ Tesla at the boiling point of liquid helium (LHe) T = 4.2 K as indicated on the top axis. This is the workhorse superconductor of the Magneto-Resonance-Imaging (MRI) industry and about 20000 MRI systems have been installed world wide [5]. The Nb3Sn can operate in magnetic fields up to $B \sim 30$ Tesla and the T_C = 18 K. This is also often used in combination with liquid helium at T = 4.2 K in superconducting magnets or superfluid helium cooled down to T = 2 K resulting in improved cooling capacity in large accelerators (CERN) or fusion magnets (ITER). NbTi and Nb3Sn wires constitute the major fraction of the commercial superconductivity business today.

MgB$_2$ can operate in magnetic flux densities up to $B \sim 40$ Tesla and the T_C = 39 K. The superconductivity of MgB$_2$ was first discovered in 2001 and commercial wires have been offered for some years. MgB$_2$ can be used with liquid helium as cooling media, but it offers the possibility to operate at T = 20 K using close cycle cryocoolers instead of using liquid helium. This is currently investigated by the MRI industry, since the possibility of shortages of helium has been suggested[5]. The alternative cryogenic fluids are liquid hydrogen (LH$_2$) with a boiling point of T = 18 K and liquid neon (LNe) with a boiling point at T = 27 K. Hydrogen is available both cheaply and in plenty of amounts, but the challenges of the safety issues such as the risk of explosions, hydrogen embrittlement of structural metal parts and diffusion trough cryostat parts are considerable. Liquid neon is completely safe and a better coolant than LHe, but the price is higher than hydrogen and helium.

The high temperature superconductors YBCO with T_C = 93 K and Bi-2223 with T_C = 110 K can be cooled by immersing them into liquid nitrogen(LN$_2$) boiling at T = 77 K. LN$_2$ is commercially available in large and cheap quantities. It should be noted that B_{irr} of Bi-2223 remains limited to rather low temperatures in the order of $T \sim 20$-30 K, whereas the B_{irr} of YBCO is orders of magnitude higher showing the potential of the YBCO coated conductors.

Superconducting wires and tapes are composite structures and attention should be paid that stress applied during manufacturing or during operation in high magnetic field is not breaking the filaments or the thin-film inside the conductors. Several quantities are defined to secure no degradation of the superconducting properties. The critical bending diameter D_{bend} is indicating the smallest diameter that the conductor can be wound around without degradation. The critical strain ε_c indicates how much elongation the conductor can tolerate without introducing cracking of the filament or films.

A central quantity for the design of superconducting wind turbine generators is the engineering current density J_e as function of magnetic flux density and operation temperature of the different conductors, because that determines the dimensions of the field generating coils. From this the usage of conductor and hence the price of the superconductor coils can be determined for the analysis of the cost of a device. The engineering current density J_e is defined as the critical current I_C of a specific wire divided by the cross sectional area including support metals (and also the insulation of the wire if it is known)

$$J_e = \frac{I_C}{A_{conductor} + A_{insulation}} \tag{4.7}$$

Figure 4-2 is showing the engineering current density of several wires relevant for superconducting wind generators as function of temperature and magnetic flux density. The plot is indicating a comparison between then typical performance of the low temperature superconductor NbTi operated at liquid helium temperature and then alternatives MgB$_2$ and the YBCO coated conductor operated around 20 K. It is clear that NbTi at T = 4.2 K is outperforming both MgB$_2$ and YBCO operated at T = 20 K, but it illustrates that lifting the operation temperature of the superconductor is reducing the performance of the wire quite a bit. Secondly the magnetic field suppression of the critical current as formulated in eq. 4.4 is observed and in order to obtain current densities J_e in the order of 100-200 A/mm^2 in a field of 3-4 Tesla both the MgB$_2$ and the coated conductors must be operated at temperatures in the order of T = 10-20 K.

In the following sections the trade-off between a high J_e at a low operation temperature and thereby a lower usage of conductor is discussed in comparison to a simpler cryostat design using a higher operation temperature giving a better efficiency of the cooling system.
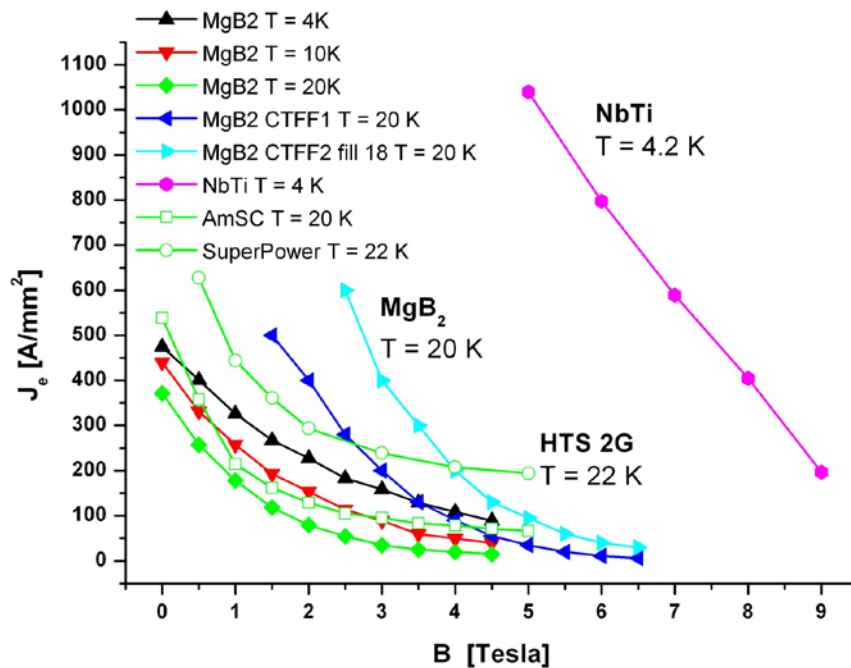

Figure 4-2. Plot of engineering current density J_e of NbTi, MgB$_2$ and 2G YBa$_2$Cu$_3$O$_{6+x}$ coated conductors as function of applied field and different temperatures. With a target of the magnetic flux density in the order of B = 4 Tesla a J_e ~ 200 A/mm^2 should be possible with an operation temperature of T = 20 K for both the MgB$_2$ and for the 2G coated conductor. The NbTi wire technology is very mature and the low temperature performance is an order of magnitude better than MgB$_2$ and the HTS at T = 20 K, but it should be remembered that both NbTi and the Nb$_3$Sn are not superconducting anymore at that temperature. The properties of the both MgB$_2$ and the 2G-HTS are expected to improve over the next few year, since the conductor technology still undergoes rapid development.

4.2   Description of a possible generator topology

Superconductors can be introduced in generators both as bulk pieces being the equivalent of "stronger" permanent magnet or as "almost zero resistance" wires in coils used either to generate magnetic field or in armature windings collecting the power of the generator.

Bulk superconducting machines

Bulk superconductors can trap flux lines as explained in section 4.1 and can act like a permanent magnet with a remanence flux density of several Tesla and higher than an equivalent Nd$_2$Fe$_{14}$B magnet. The challenge of bulk superconducting machines is however to first magnetise the bulk superconductors while they are mounted on the rotor. This will either call for an additionally superconducting magnet or for an advanced flux pumping

method, which is still being investigated [6]. Since this magnetization procedure will have to be repeated after a loss of cooling or grid loss in an offshore wind farm it is not considered further in the INNWIND.Eu project.

Superconducting field windings

Superconducting wires are an advantage in coils for the production of the DC magnetic field in synchronous generators, because the higher engineering current density allows more compact coils producing the same magneto motive force mmf and offer more compact machines. Thus one can replace copper of the rotor of a synchronous generator by superconducting coils with a much smaller cross section area.

A second advantage is that the usual Joule heating $P = UI = RI^2$ of a copper coil with resistance R is replaced by the power law relation of eq. 4.5. giving $P = ILE_0(I/I_C)^n$, where the n-value is typically in the order of 10-40. The magnetic flux produced by a copper coil holding a current of I will scale like $\Phi = LI$, where L is the self-inductance of the coil, but the heat dissipation scales faster as, $P = RI^2$. This challenge is solved in usual electrical machines by introducing laminated steel of soft ferromagnetic material, which contain magnetic domain that are easily aligned by the applied field from the coil. However once the laminates are saturated around $B_{laminate} \sim 1.5$ Tesla the dissipation of the coil will increase fast compared to the flux with further increase of the current. Thus in any conventional electrical machine the magnetic flux density in the airgap will most likely not exceeds about 1 Tesla. With superconducting field coil one can surpass the saturation limit of the laminates and use this to create a magnetic flux density in the airgap, which is considerably higher than for conventional generators based on copper windings or permanent magnets.

The armature of such a superconducting synchronous generator is most likely made of copper operated at room temperature and allowing conventional forced air or liquid cooling of the windings.

A cryostat must be constructed around the superconducting coils in order to provide sufficient thermal insulation to keep the superconductors cold at the operation temperatures $T = 4\text{-}40\ K$. This will cause a considerable larger air-gap compared to conventional generators, but make the mechanical air gap between the cryostat wall and the armature small compared to the magnetic air gap. Thus increasing the mechanical air gap of the generator to secure no contact under all load conditions of the turbine is not changing the properties of the generator very much. An additional challenge is to construct a torque transfer element capable of transferring the torque of the turbine blades and into the cold support of the coils, without causing an unacceptable heat load to the coils.

Finally a cryogenic cooling system must be constructed in order to remove the heat flow into the superconducting coils caused by heat conduction through the torque transfer element as well as the residual gas of the vacuum chamber and by radiation. The heat dissipated in the superconducting coils due to DC and AC losses as well as the heat from the current leads to the coils will also have to be removed by the cooling system.

Fully superconducting generators

There are several proposals of fully superconducting machines, where both the field as well as the armature windings are made of superconducting coils. The advantage of a

superconducting armature is the high current density and thereby the compactness of the machine. Secondly both the field and armature coils can be at the cold operation temperature without the need of a cryostat wall in between, whereby the air gap can be made smaller than for the generator with only superconducting field windings.

The challenge is however that the superconductors of the armature will be exposed to both AC magnetic fields and currents, which will impose AC losses that are orders of magnitudes larger than the DC losses imposed by the power law of eq 4.5. These losses will be dissipated as heat in the windings of the coils and have to be removed by the cryogenic cooling system. The efficiency of typical cryogenic cooling system is only in the order of 1 % at $T = 10 K$ as shown in the top bar of figure 4.1. Currently most studies have shown that the AC losses imposed in NbTi, MgB2 and the HTc conductors result in un-acceptable losses in fully superconducting machines. Multifilament MgB2 wires might become suitable for superconducting armature windings if the AC losses can be reduced by reducing the filament size to a few micro-meters[7].

A second challenge of the fully superconducting generator with field and armature windings in a shared insulation vacuum is that a rotating vacuum seal will be needed. A leak through this rotating seal will cause a build-up of ice inside the generator and the removal of this ice will need a heating of the entire generator to room temperature before the water vapour can be pumped away. Since conductors with sufficiently small AC losses are not available commercially and due to cryogenic challenges the fully superconducting generator is not considered further in the INNWIND.EU project.

4.2.1 Introduces which generator topology is chosen

The focus of the INNWIND.EU task on superconducting generators will be on direct drive radial flux synchronous generators with superconducting field windings and a copper armature at ambient temperature. This topology is chosen because all major sub components such as superconductors, cryostat, cryogenic cooling devices and direct drive armatures are readily commercially available. The investigation of the feasibility of the subsystems combined into a superconducting wind turbine generator is therefore much easier to evaluate than if technologies depending on major breakthroughs were chosen (Such as bulk or fully superconducting generators). Secondly this topology have allready been proposed by major industrial players such as the 10 MW SeaTitan of American Superconductors[8], a 8 MW direct drive wind generator of the former Converteam (now GE uk) [9] and finally the 10 MW direct drive wind generator of GE Global research [10]. Several large superconducting machines have been demonstrated for the marine propulsion application by the companies listed above as well as Siemens Coorporate Technology [11].

4.2.2 Explains why this generator topology is chosen

A major argument for the choice of the radial flux direct drive generator is that it must be incorporated into the king-pin nacelle design as proposed by GH in section 3. This nacelle design based on a king-pin and two main bearings supporting the turbine rotor is the current best suggestion to a design that will survive the turbines loads in the power range approaching P = 20 MW. There are two possible positions of the generator in the kin-pin design:

1. Two rings between the turbine rotor and the tower

2. Two rings in front of the turbine rotor.

The first generator position option is quite similar to the current design of the permanent magnet direct drive generators of the partner Siemens Wind Power. This design will be further investigated by Siemens Wind Power and DTU as part of the task 3.1.2 "Demonstration of superconducting pole pair", where the idea is to investigate how to introduce the superconducting rotor with the least changes of the current direct drive design of Siemens Wind Power. The demonstration of Siemens Wind Power will be conducted in the following phases in order to investigate the feasibility of the concept illustrated in figure 4-3b.

Phase A: Design and test of down scaled race track coil
Phase B: Extrapolation of performance indicators to P = 10-20 MW generators
Phase C: Design and test of downsized, segmented cryostat
Phase D: Rotation test of segmented cryostat and test of cryosystem reliability

There are GO/NO GO criteria formulated between each phases. Especially Phase C and D will only be executed if the analysis of Siemens Wind Power shows that the Cost Of Energy (CoE) of the superconducting technology is lower than the CoE of the Siemens Wind Power Direct Drive Permanent Magnet technology in 2020. The INNWIND.EU budget for task 3.1.2. only covers phase A and B, whereas the funding for Phase C and D will be found from other sources.

The second generator position option is quite novel and will be investigated by DTU, TUD and SINTEF in the tasks 3.1.1. "Superconducting generators" as well as the task 3.1.3 "Demonstration of MgB_2 coil".
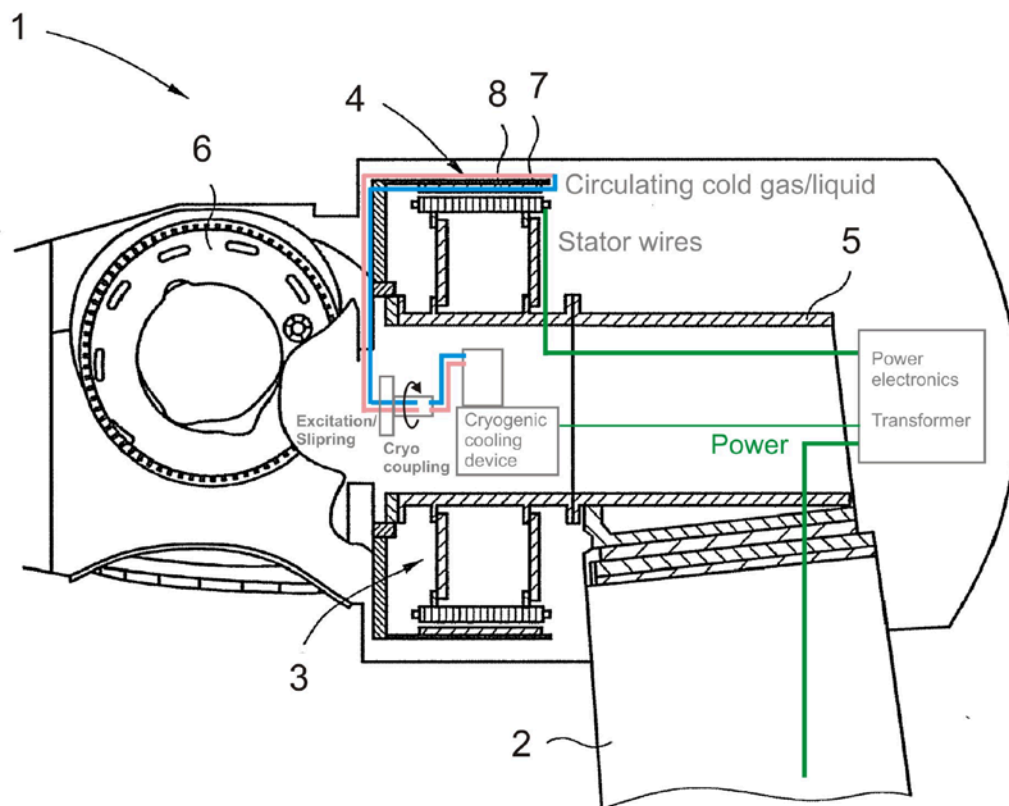
Figure 4-3. Illustration of the Siemens Wind Power concept of changing the current permanent magnet direct drive generator into a superconducting version, where the permanent magnets are replaced by superconducting race track coils. The philosophy of the concept is to have no machinery (cold heads and compressors) in the rotating frame and to use high temperature superconductors in order to obtain the simplest cryogenic system and thereby increase the reliability. The nacelle drawing is reproduced from J. K. Booth, U. Eriksen, J. B. Nielsen and H. Stiesdal, "Wind turbine with a generator", US 2012/0217752 A1.

The front mounted kin-pin generator opens for two different generator configurations as shown on figure 4-4:

1. Rotating outer superconducting field windings and a fixed inner armature

    This configuration has the advantage that the power from the armature can be easily connected to the power electronics in the nacelle, whereas the superconducting coils must be supported and cooled in the rotating frame.
    The cooling of the superconducting coils can be done by inserting cryocooler coldheads through the cryostat wall and supplying the cold heads with a pulsating helium gas from a compressor placed in the nacelle. A rotating helium gas pressure coupling will be needed for this and has been proposed by American Superconductors for the Sea Titan [12].
    A second option is to have a cryogenic cooling device in the nacelle providing a cold gas flow, which is transferred through a rotating cryo-coupling and out to the superconducting coils. This method has been demonstrated by the former Converteam [13].

2. Fixed inner superconducting field windings and an outer rotating armature

The advantage is that the superconducting coils and cryocooler cold heads are fixed inside the nacelle and there is no need for a rotating gas or cryogenic liquid coupling. Secondly heat pipes based in liquid Helium can be used to ensure an equal temperature distribution in the support structure of the superconducting coils. This method has been proposed by GE Global Research and is a transfer of the cooling technology from the MRI business of GE [14].

The disadvantage is however that the full power of the armature must be transferred to the nacelle trough slip-rings before it enters the power electronics in the turbine.
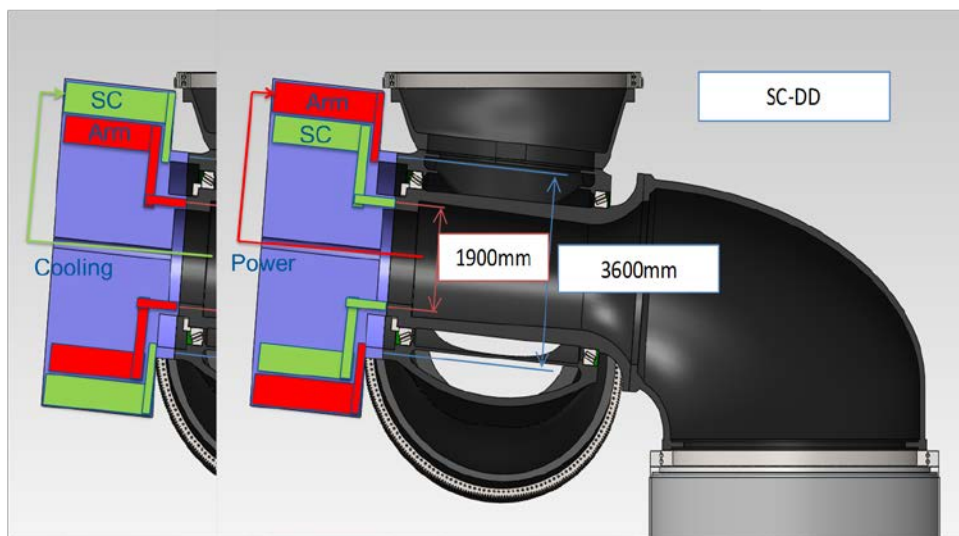
Figure 4-4. Illustration of outer rotating superconducting field coil (left) and inner fixed superconducting coils (right). The green line in the center indicates a transfer of cryogenic coolant to the superconducting coils, whereas the red line indicates the need to transfer the full power from the rotating armature.

4.2.3 Methodology for estimation of performance indicators

The methodology used for the first estimate of the performance indicators of the superconducting generators is focused on the active generator materials being superconductor wire, copper in the armature and the laminates used to confine the magnetic flux in the generator. The air gap distance is estimated from a simple model of the cryostat and the torque transfer element.

The target size of the superconducting generators are based on the reference direct drive generator size as determined from the INNWIND.EU reference turbine specified in the power range P = 10-20 MW. The torque τ of the generator is related to the shear stress F_d by

$$\tau = 2\pi r^2 L F_d \qquad\qquad (4.8)$$

where r is the radius of the air gap, L is the active length.

The dimensions of the reference generator is estimated by assuming a shear stress in the order $F_{d,\ Ref}$ = 45 KN/m² representing a basic permanent magnet generator [15] and by using the torque and speed specifications of the INNWIND.EU reference turbine as outlined in chapter 1 and shown in table 4-1. The first target size of the superconducting generators is simply found by assuming that the shear stress can be increased up to a factor of 4 giving $F_{d,\ Ref}$ ~ 180 KN/m² by increasing the air gap magnetic flux density. This is utilized to reduce the radius of the reference machine by a factor of two as illustrated in table 4-1.

Power (kW)	2500	3000	5000	6000	10000	15000	20000
Rotor diameter (m)	89	98	126	138	178	218	252
Max Tip Speed (m/s)	90	90	90	90	90	90	90
Hub height (m)	70	74	88	94	114	134	151
Max Specific Power (W/m2)	401	401	401	401	401	401	401
Omega (rad/s)	2,02	1,84	1,43	1,30	1,01	0,82	0,71
RPM	19,29	17,61	13,64	12,45	9,65	7,88	6,82
Torque (kNm)	1336	1757	3780	4969	10691	19641	30240
Rotor swept area (m2)	6234	7481	12469	14963	24938	37407	49876
Generator diameter [fraction of blade] (m)	4,01	4,39	5,67	6,21	8,02	9,82	11,34
Generator length (m)	1,18	1,29	1,66	1,82	2,35	2,88	3,33
Generator aspect ratio Lgen/Dgen	0,29	0,29	0,29	0,29	0,29	0,29	0,29
Airgap [fraction of blade] (mm)	4,01	4,39	5,67	6,21	8,02	9,82	11,34
SC generator diameter (m)	2,00	2,20	2,84	3,11	4,01	4,91	5,67

Table 4-1. The specifications of the INNWIND.EU reference turbine including 8 % loss in the drive train to obtain the torque requirement. The diameter and length of the reference direct drive generator is obtained by assuming a shear stress of $F_{d,Ref}$ = 45 KN/m² corresponding to a permanent magnet machine. The upper target of the superconducting direct drive is found by assuming an increase of the shear force up to a factor 4 resulting in $F_{d,SC}$ ~ 180 KN/m² and half the diameter.

The electromagnetic torque τ_{EM} of a radial flux generator with p poles is related the peak flux density in the air-gap $B_{g,p}$, the peak current loading of the armature $A_{S,p}$ and the radius r of the air gap as well as the active length L of the machine

$$\tau = \pi B_{g,p} A_{S,p} r^2 L \cos(p\psi) \qquad (4.9)$$

where the airgap flux density distribution is assumed

$$B(\theta) = B_{g,p} \cos(p\theta) \qquad (4.10)$$

and the sheet current distribution is assumed sinusoidal and displaced by the angle ψ

$$I_S = A_{S,p} \cos\big(p(\theta - \psi)\big) \qquad (4.11)$$

The armature current loading is assumed to be in the order of $A_{S,p}$ ~100 kA/m with a current density in the order of $J_{S,rms}$ ~ 2-3 A/mm². This should be obtainable using current generator technology and should ensure a reasonable efficiency of the generator. By equating eq. 4.8 and 4.9 it is seen that

$$F_d = \frac{1}{2} B_{g,p} A_{S,p} \cos(p\psi) \qquad (4.12)$$

By inserting the target shear stress F_d = 180 kN/m² and the current loading it is seen that the peak flux density in the air gap of such a superconducting machine should be

$$B_{g,p} = \frac{2F_d}{A_{S,p}} = \frac{2 \cdot 180 \; kN/m2}{100 \; kA/m} = 3.6 \; Tesla \qquad (4.13)$$

This design idea is the main driver for the first evaluation of the performance indicators of the superconducting generator and it should be investigated if the more compact generator is feasible from an overall offshore turbine point of view.

There is another design approach which will be investigated as future work and that is to utilize the higher air gap flux density to decrease the current loading and thereby improve the generator efficiency at the cost of a larger generator. The specification of the reference turbine in table 4-1 includes a drive train loss of 8 % similar to gearbox based drive trains. PM direct drive trains are expected to have a similar loss due to the copper armature and the power electronics. Once the input wind speed distribution of the INNWIND.EU reference turbine has been determined by work package 1 then the extra income by a 1% more efficient drive train should be determined. A compromise between the above two philosophies will be part of analysis of task 3.1.1. A rough estimate of the value of a 1% increased efficiency can be done by assuming a 40 % capacity factor of an 10 MW offshore turbine with 25 year life time. The produced energy will be E = 10 MW x 25 years x 8760 hours/year x 40 % = 876000 MWh and 1% corresponds to 8760 MWh. If this can be sold at 50 €/MWh then then saving is 438 k€.

(INNWIND.EU, WP3 internal report, First assessment of performance indicators of SC and PDD generators)

A method to estimate the active mass of 2.5 tesla class superconducting generator have previous been applied to a 5 MW direct drive generator [16]. A reluctance model of the active parts of the generator is used to estimate the amount of superconductor needed by varying the number of poles in the generators. Two dimensional Finite element modelling is used to confirm the magnetic flux density inside the machine. It is then checked if the magnetic flux density in any of the superconductors is lower than the critical engineering current density J_e. The following issues needs to be considered:

1) Thickness of stator region
2) Thickness of cryostat
3) Thickness of back iron

The thickness of the stator conductor section t_S is specified according to the current loading $A_{S,p}$, the current density J_S and finally the conductor filling factor f_S, which is assumed to be 50% in order to allow for non-magnetic and non-conducting teeth of an air cored stator type.

$$t_S \sim \frac{A_{S,p}}{\sqrt{2} J_{S,rms} f_S} = \frac{100\frac{kA}{m}}{\sqrt{2}\cdot 2-3\frac{A}{mm^2}\cdot 0.5} = 5-7\ cm \qquad (4.14)$$

The cryostat and the torque transfer element must be investigated in a joint effort to secure a thermal isolation of the superconductors. Figure 4-5 illustrates the basic construction of the cryostat. An outer container ensures that vacuum can be established in order to remove the gas heat conduction. The torque of the turbine must however be transferred all the way to the cold superconductor coils and a torque tube is needed for that. This tube should be made as thin and as long as possible *L1* in order to minimize the heat flow, but at the same time it should comply with the structural forces. The preferred material should have a low thermal conductivity and high strength. Thus stainless steel 304 or titanium alloys are candidates. If the superconductors are to operate at low temperatures around 4 K then a radiation shield made of high thermal conducting material (copper or aluminium) is often inserted and thermalized at T = 40-80 K. The torque tube extends further down the length *L2* to the coil support holding the coils in a material of high strength and thermal conductivity, such as high strength aluminium. The radiation heat inflow to the cold parts can be reduced by inserting sheets of Multi Layer Insulation (MLI) in-between the wall at ambient temperature and cold parts. MLI consists of N = 10-30 thin plastic foils covered by a reflecting layer of metal. Each layer will reflect half of the heat radiation, whereby a huge reduction factor of the heat inflow of can be obtained. On-going work on the cryostat and the torque tube indicates that *L1* and *L2* should of the same order of magnitude as the generators and one can imagine a fold back configuration as recently proposed by GE [17]. Figure 4-6 illustrates the fold-back torque tube cryostat where all the cryogenics is contained in a tube like cryostat which can have the Kin-pin going through the centre. Having the torque tube folded up behind the superconductor coils is giving extra distance to the cryostat wall. A preliminary estimate of the cryostat wall thickness if operating around 30 K is roughly 10 mm space for the MLI and vacuum insulation, a steel tube of approximately 10 mm thick as cryostat wall and another steel tube of 10 mm thickness facing the superconducting coils. For lower temperature the radiation shield is probably needed and extra distance is added. If this cannot be realised by the foldback torque tube design then cryogenic torque arms as well as alternative end sections for the cryostat must be investigated for the front mounted king-pin generators.
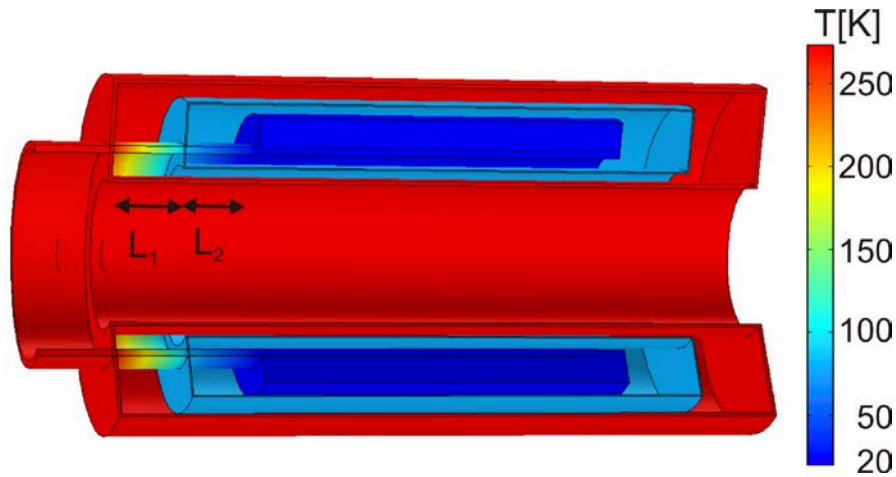
Figure 4-5 Illustration of cryostat with a torque tube for transferring the turbine torque to a radiation shield after L_1 and then to the cold support of the superconducting coils after L_2.
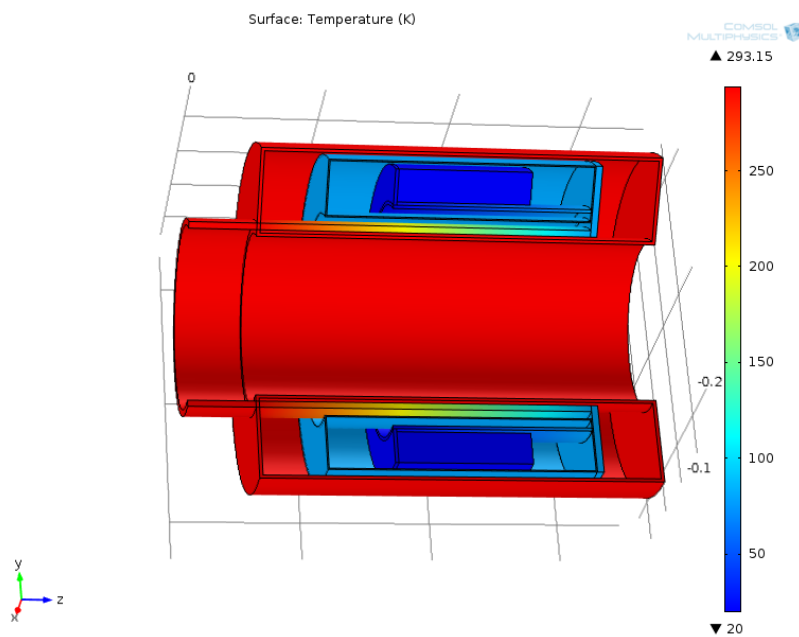

Figure 4-6 Fold-back torque tube as suggested by GE global research for the 10 MW NbTi generator [17]. This configuration allows for a long torque tube inside the cryostat.

The cooling of the cold parts can be done by several methods

1) Installation of metal tubes containing a flow of cold gas or cryogenic liquid injected to the radiation shield and cold parts and cooling the torque tube on the way out. The gas is circulated in a closed loop and brought to a cryogenic cooling machine for recooling. Thus there is a need for a cryogenic rotating coupling, which is not a trivial part [18].

2) Mounting of two stage cryocooler cold-head going through the vacuum wall and through the radiation shield. The first stage of a cold head is usually at T = 80 K and then second stage is a T = 4-20 K as shown on figure 4-7. The coldhead is operated using a pulsating helium gas flow at ambient temperature and is created by a close cycle helium compressor. A second one stage cold head providing T = 80 K can be mounted on the radiation shield and will remove most of the heat coming from the ambient heat side. A central question is if cold heads can be rotated and if the compressor can be rotated. If only cold heads are rotating then the helium gas must go through a rotating seal. If the compressors can be rotated then only electricity for the compressors must be transferred through a slip ring.

Figure 4-7 Cryo-cooler cold heads and corresponding helium compressor units. **Left:** RDK-415D two stage cold head for T_2 = 4 K & T_1 = 30 K from Sumitomo Heavy Industries (SHI) and the F-70 Helium compressor unit as recommended by GE Global Research for the 10 MW NbTi generator using 4 units [17]. **Middle:** CTI-1020 two-stage cold head for T_2 = 20 K & T_1 = 80 K from Helix Technologies and model 9600 compressor recommended by American Superconductor for the 10 MW SeaTitan generator [12]. Typical weight of the cold-head and compressor is 20 kg and 100 kg respectively. **Right:** AL600 one-stage cold head from Cryomech and recommended by GE Global Reseach for precooling of the 10 MW generator to T ~ 100 K [17]. Low: Helium gas line connection between SHI cold head and compressor (two per unit and up to 20 m length).

Finally the thickness of the back iron of such a machine can become quite thick because large pole openings can be made with superconducting race track coils. The bigger the

opening the less wire is used and therefore the price of the machine goes down. However if 2.5 Tesla is in half of the pole width then it will take a similar thickness of fully saturated iron to contain that flux. Thus back-iron thickness in the order of 10-15 cm can easily be imagined. This is however heavy and a compromise between price and weight must be searched for the different types of machines.

4.2.4   NbTi base line (GE-global research)

The 10 MW NbTi direct drive generator as proposed by GE global Research [17] will be used as the base line performance indicators in INNWIND. The generator is based on an inner stationary cryostat holding race track coils made of NbTi and an outer rotating armature equipped with slip-rings. The advantage of the stationary superconductor is used to mount cryo-cooler cold heads directly onto a cold ring holding the superconductors and to install a liquid helium heat pipe system in the cold ring to equalize the temperature distribution of the superconducting coils. This cryogenic technology system solution is a direct transfer from the MRI business of GE as described in [14].

GE Global Research has published a detail design report [17] on the design and a cost of energy model has also been done. Table 4-2 summarizes the properties published by GE as well as extrapolations of these properties if the length of the machine is increased in proportion to the increased torque τ demand, which will scale like

$$\frac{\tau_2}{\tau_1} = \left(\frac{P_2}{P_1}\right)^{\frac{3}{2}} \tag{4.14}$$

where P is the turbine rated power. This factor is 1.84 and 2.83 going from 10 MW to 15 MW and from 10 MW to 20 MW respectively, which is indicating that putting 2 and 3 of these machines in a row should comply with the turbine demand. A rough estimate of the properties up to 20 MW can be done by a similar mass scaling as shown in table 4-2. The scaling of the usage of superconductor is done using the generator active length as the straight section of the race track coils and the inner race track radius $R_{racetrack}$ = 124 mm [17]. This gives that 232 km is used in the end section and 488 km in straight sections for the 10 MW. The costs of the extrapolated generators are found by assuming that the superconductor wire still constitutes 33 % of the generator cost. Thus additional cryo-coolers will be included by doing this, but there might be a need for additional cooling of both superconductor and armature, because the cooling path is longer. Secondly the torque tube must be increased in order to support an almost 3 times higher torque, but this has not been included in the analysis.

Finally it should be stressed that the up-scaling of the GE generator is done in the most simple manner and a more feasible generator can most likely be obtained by optimizing the dimensions of the generator by making the diameter larger. However it should be said that the GE design is based on a one-piece cryostat and a connected heat pipe structure. Thus it is not trivial to increase the diameter of such a cryostat to say 6 or 9 meters. Additionally the GE generator is intended mounted in the nacelle behind the hub of a nacelle being the equivalent of the kin-pin. Thus a question is if a 6 meter added length to the 20 MW kin-pin makes sense in order to make room for the generator. The GE concept can however easily be mounted in-front of the king pin rotor as illustrated on figure 4-4. For such a mount it will be recommended to investigate a larger diameter generator.

KPI GE NbTi SCDD	6 MW	10 MW (36 poles)	15 MW	20 MW
Diameter[m]	4.83	4.83	4.83	4.83
Diameter airgap [m]		4.29		
Length [m]	0.813	1.88	2.54# (3.46)	5.32
Mass [tons]		145 (135)	267	410
Length SC [km]		720	1130	1613
Mass SC [kg]		3840		
Cost SC [k€]		546 (33 % of total)	857	1223
Efficiency [%]		95-96		
Generator cost [k€]		1644	2597 (3288)+	3706 (4932)
Gen cost / capacity [€/kW]		164.4	173.2 (219)	185.3 (247)
COE [€/MWh]*		57.3		

Table 4-2. Key performance indicators for the GE Global Research NbTi 10 MW direct drive proposal reproduced from [17] . The size scaling at 6 and 15 MW is taken from [14]. It is interesting to note that the price per kilo of the NbTi superconducting coil is 142 €/kg, which is close to the price of the permanent magnets for direct drive wind turbines. *The COE estimate is based on a 250 MW offshore wind farm at 30 meter water depth (see Fair for details). #Length scaling seems too small to provide enough torque unless air-gap field strength is increased. Additional scaling of the 10 MW generator properties to 20 MW is done by increasing the length according to the torque demand . This approach is the equivalent of putting 2 and 3 generators in a row and does not represent an optimized solution, but a simple extrapolation. The parenthesis shown for the generator cost is determined by the 2 and 3 machine extrapolation+.

4.2.5   MgB$_2$ direct drive generator (DTU)

The first estimate of the properties of MgB$_2$ direct drive generators have been obtained by choosing a generator diameter in between the reference scenario and the most compact superconducting scenario, because the MgB$_2$ superconductors are not as powerfull as the NbTi in high field (see fig 4-2). Secondly the dimension of the coils of the generator was chosen such that the cross section of the coil could be realised in the test cryostat, but with a reduced length compared to the full size generator. Figure 4-8 is showing the test cryostat and table 4-3 is summarizing the demonstration race track coil layout consisting of 10 double pancake coils based on a 3 mm wide MgB$_2$ tape stabilized by a Cu strip. The resulting cross section of the race track coil is approximately 8 cm x 8 cm and with an opening between them of 30 cm. The straight section of the demonstrator coil is 0.5 m, but will be expanded up to 3 meters in the 10 MW generator model.
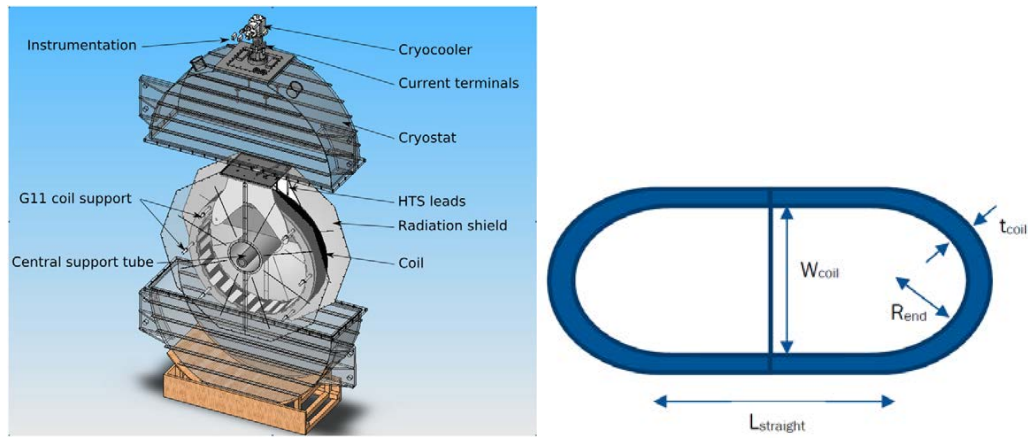
Figure 4-8. **Left:** Cryostat for the test of the MgB$_2$ coil holding a circular coil tested in the ALUHEAT project [20]. The cryostat can hold a coil with diameter of 1.2 m and the inner support tube imposes an opening larger than 0.25 m. **Right:** Illustration of a race track coil with a straight section $L_{straight}$ and opening W_{coil}. The thickness of the coil is t_{coil} and the height H_{coil} is in the direction into the paper. The end section is formed as a half circle with a radius of R_{end}. The demonstration is chosen with W_{coil} = 0.3 m and $L_{straight}$ = 0.5 m and a cross section of 8 cm x 8 cm.

Length strait section: L_{strait} [m]	0.5
Opening inside pancake: W_{coil} [m]	0.3
Radius of end winding: R_{end} [m]	0.15
Number of turns in pancake layer	100
Thickness of MgB$_2$ tape: $T_{SC, tape}$ [mm]	0.7
Width of MgB$_2$ tape: $W_{SC, tape}$ [mm]	3.0
Thickness of insulation: $T_{insulation}$ [mm]	2*0.07 = 0.14
Width of insulation: $W_{insulation}$ [mm]	~ $T_{insulation}$ + T_{spacer} ~ 1.0
Thickness of pan cake (windings)T_{coil} [mm]	N * (t_{tape} + $t_{insulation}$) ~100 * (0.7 mm + 0.14) = 84 mm
Height of pan cake coil: H_{coil} [mm]	2*w_{tape} + $w_{insulation}$ ~2*3 mm + 1.0 mm = 7 mm
Length of tape in single pan cake: $L_{singlepancake}$ [m]	$L_{singlepancake}$ = N·[2·L_{strait} + 2πR_{end}]+ 2π·t_{wire}·N(N+1)/2 = 100· [2·0.5 m + 2π·0.15 m] + 2π·0.84 mm*100*101/2 = 100 m + 94.2 m + 26.6 m = 220.8 m
Length of tape in double pan cake: L_{DP} [m]	441.6 m
Spacer between double pancakes: $L_{coilspace}$ [mm]	1
Number of double pancakes $N_{pancakes}$	10
Coil assembly height [mm]	$N_{pancakes}$ ·[H_{coil} + $L_{coilspace}$] = 10·8 mm = 80 mm
Total tape usage $L_{tapetotal}$[m]	10·441.6 m = 4416 m
Field coil width [m]	84
Field coil height [m]	80
Race track filling factor A_{SC}/A_{coil} [%]	62.5

Table 4-3. Dimensions of the MgB$_2$ race track demonstration coil based on a 3.0 mm x 0.7 mm MgB$_2$ tape from Columbus superconductor.

The sizing of a series of MgB$_2$ direct drive generators were determined using analytical expression of the field distribution [21] and by assuming an outer Cu-armature supported by back iron, inner superconducting coils supported by a non-magnetic material and a cryostat wall in between the rotor and the armature. There is presently no back iron behind the rotor in order to save weight, but further studies must be done to determine if it should be included to boost the magnetic flux density and shield any cryogenic equipment placed in the hub. Adding iron will also drive down the price of the generator, since less tape is needed. The opening of the race track coils were kept constant by increasing the pole number and diameter, while reducing the length of the generator in order to obtain the target torque.

R00 Fe	M	2,70	4,00	5,00	6,00
R0	M	2,60	3,90	4,90	5,90
R4 Armature	M	2,60	3,90	4,90	5,90
R3	M	2,54	3,84	4,84	5,84
R2 Superc.	M	2,50	3,80	4,80	5,80
R1	M	2,42	3,72	4,72	5,72
Lgen	M	3,10	1,26	0,80	0,54
p Polepair	--	18,00	25,00	32,00	38,00
I	--	1,00	1,00	1,00	1,00
Jf SC J	A/m^2	7,00E+07	7,00E+07	7,00E+07	7,00E+07
Alpha	rad	0,06	0,04	0,03	0,03
Beta	rad	0,09	0,06	0,05	0,04
As_armature	A/m	100000,00	100000,00	100000,00	100000,00
Br	Tesla	1,64	1,80	1,79	1,82
Torque	Nm	1,06E+07	1,07E+07	1,07E+07	1,06E+07
P_armature_end	W	210014,02	155631,93	143338,17	138595,95
P_efficiency_end	%	0,98	0,98	0,99	0,99
freq_gen	Hz	2,90	4,02	5,15	6,11
Msctot	Kg	10486,69	6904,03	5826,02	5080,43
MCutot	Kg	17272,06	14527,64	14380,51	14909,04
MFetot	Kg	23277,03	14246,70	11382,87	9261,14
Mtot active	Kg	51036,00	35679,00	31590,00	29250,00
Lsctot	Km	627,61	413,20	348,68	304,06
PriceSCtot	€	2,51E+06	1,65E+06	1,39E+06	1,22E+06
PriceCutot	€	259080,84	217914,60	215707,71	223635,64
PriceFeTot	€	69831,10	42740,11	34148,61	27783,43
Price active Mat.	€	2,84E+06	1,91E+06	1,64E+06	1,47E+06
Price / kW	€/kw	284,00	191,00	164,00	147,00

Table 4-4. Sizing of 10 MW MgB$_2$ direct drive generators based analytical approximations and keeping the cross section of the race track coils similar to the MgB$_2$ demonstration coil.

As seen from table 4-4 then the MgB$_2$ demonstration coil could be used directly to build a 12 meter diameter generator with an active length of 0.5 m. This is however considered as large and smaller diameter machines can be realized at the expense of using more superconductors.

Finite element analysis has been applied to the 5.8 meter diameter generator using the cross section dimensions of the demonstration coil instead of ideal arches as used in the analytical analysis. This results in a slight adjustment of the diameter as well as the number of pole pairs. Figure 4-9 is showing the magnetic flux distribution in cross sections thought one of the 32 poles of the generator, when assuming a race track coil current density of J$_{coil}$ = 70 A/mm^2.
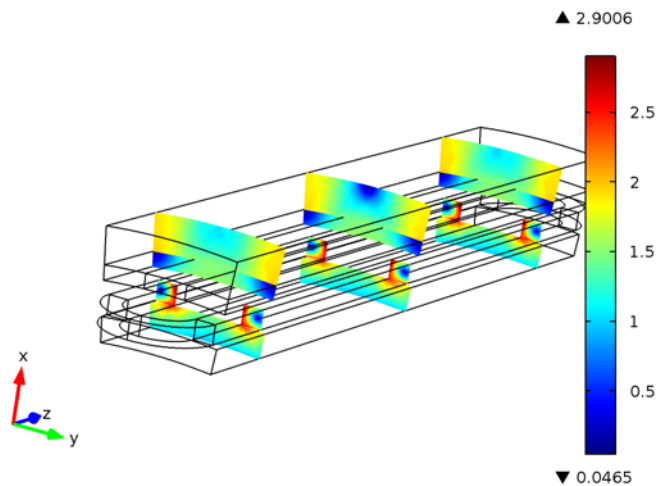
Figure 4-9. Finite element calculation of the magnetic flux density distribution in one of the poles of a 32 pole MgB$_2$ direct drive generator when using a coil current density of J$_{coil}$ = 70 A/mm^2.

A central part of the generator design is to make sure that the superconducting tapes remain superconducting when then current in the race track coil is ramped up to the operation point. Figure 4-10 is showing the flux in the centre cross section and it can be seen that the resulting magnetic flux density in the armature is approximately 1.5 Tesla, but the magnetic flux density at the inner surface of the race track coils is about 2.7 Tesla.
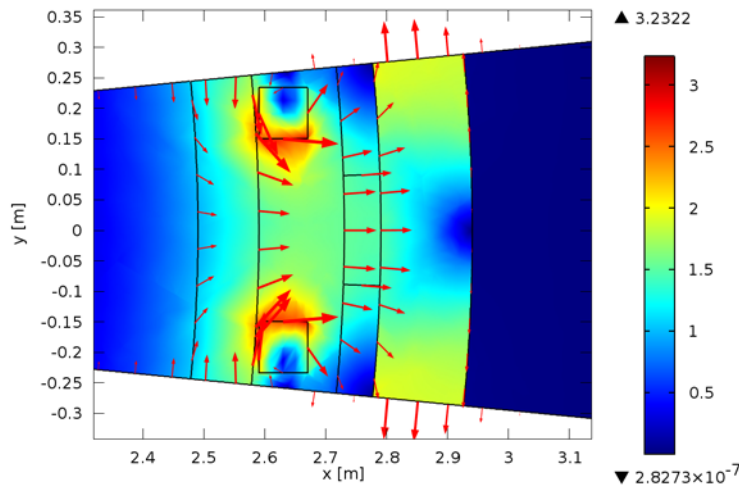
Figure 4-10. Magnetic flux density in centre cross section of the generator when the coil current density is 70 A/mm². The flux density at the edge of the race track coil in the straight section is approximately 2.7 Tesla.

Secondly the end-winding of the race track coil will experience an even higher field of 2.9 Tesla as shown on figure 4-11 and figure 4-12. Thus in order to determine the proper loading of a superconducting generator then the load line is determined by evaluating the maximum flux density on the inner sides (straight and end section) of the race track coil as function of the current density in in the coil.
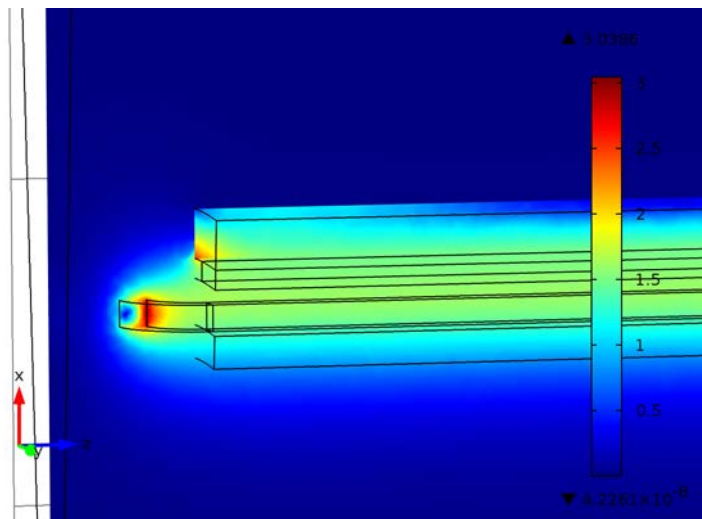
Figure 4-11. Magnetic flux density distribution at end-section of the pole. It should be noted that the flux is in the order to 2.9 Tesla as the end section of the race track coil.
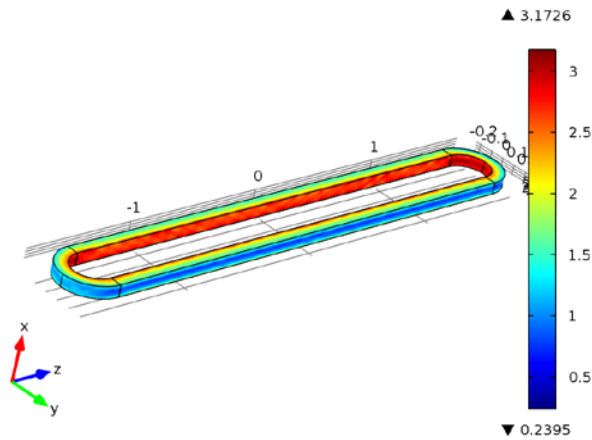
Figure 4-12. Illustration of magnetic field distribution of race track coil when placed in a 10 MW 32 pole direct drive generator. It should be noted that the flux density is higher on the inside of the end-sections compared to the straight sections.

The load line can then be plotted on top of the magnetic field dependence of the engineering critical current density of the used superconductor as shown on figure 4-13.
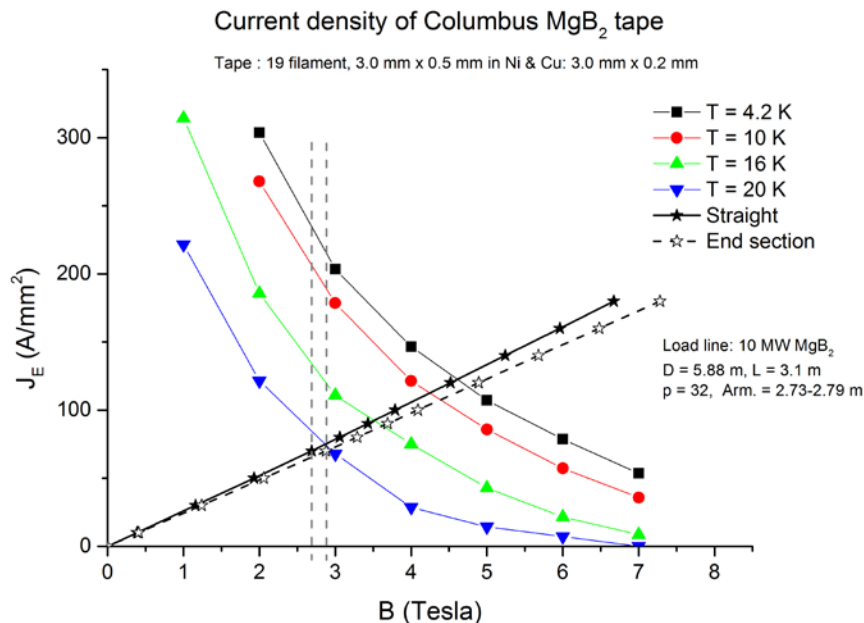
Figure 4.13. Load line of 10 MW MgB$_2$ direct drive generator and the corresponding engineering critical current of the MgB$_2$ tape of Columbus superconductors. A target coil current density of J$_{coil}$ = 70 A/mm² will result in about 2.7 and 2.9 Tesla in the straight and end-section respectively. The flux density in the airgap will be around 1.5 Tesla. One will have to reduce the tape engineering current density of the plot by the 62 % filling factor of the race track coil, whereby an operation temperature between T = 10-16 K will be needed to have sufficient margin from the operation point and to the critical current.

The engineering current density plotted is the critical current of the tape divided by the tape cross section including the Cu stabilizer strip, but the insulation of the wires and the pancake coil spacers must also be included as shown in table 4.3. The resulting filling factor of the coil is only 62 %, whereby the coil current density is only 62% of the tape current density. A certain margin of 25-50 % to the critical current density should be reserved at the operation point and from figure 4-13 it is seen that the J_{coil} = 70 A/mm² will not be possible at T = 20 K using the present wire. Decreasing the temperature between T = 10-15 K will give an operation point between 55 % and 84 % of the engineering critical current density of the tape. This margin is sufficient to proceed with stability analysis in case the superconductor is pushed out of the superconducting condition and a quench is imposed. Thus it must be investigated that the subsequent energy release will not destroy the tape in the race track coil. Passive and active measures to protect the coil from the quench must also be considered.

The properties of the 10 MW MgB₂ direct drive generator are collected in table 4.5

$R_{Fe\ out}$ [m]	2.94	Torque [MNm]	10.6
$R_{Armature\ out}$ [m]	2.79	Speed [rpm]	9.65
$R_{Armature\ in}$ [m]	2.73	Poles [2p]	32
$R_{Supercond\ out}$ [m]	2.69	Frequency [Hz]	2.57
$R_{Supercond\ in}$ [m]	2.59	$B_{air\ gap}$ [T]	1.5
$L_{generator}$ [m]	3.1	Arm. loading [A/m]	10^5
R_{End} [m]	0.15	Arm. Fill [%]	50
W_{coil} [mm]	84	Shear stress [kN/m²]	75
H_{coil} [mm]	80	Efficiency [%]	97.7
$L_{SC\ single\ pancake}$ [m]	740.9	J_{coil} [A/mm²]	70 @ 3 Tesla
$L_{SC\ double\ pancake}$ [m]	1481.7	J_{tape} [A/mm²]	113 @ 3 Tesla
$L_{SC\ Race\ track\ coil}$ [km]	14.82	M_{Cu} [kg]	19415
$L_{SC\ total}$ [km]	474.2	M_{Fe} [kg]	24998
Tape unit cost [€]	4 (→ 1)	M_{active} [kg]	52331
SC cost [k€]	1897 (→ 474)	Cost Cu [€]	291234
$M_{Superconductor}$ [kg]	7918.1	Cost Fe [€]	74994
$M_{cryostat+cooler}$ [kg]	TBD	Cost total [k€]	2263 (→ 840)
Cost cryostat	TBD	Cost / cap. [€/kW]	226 (→ 84)

Table 4-5. Summary of 10 MW MgB₂ generator properties. Cost in parenthesis indicates the expected cost of the conductor including up-scaling and learning.

The conclusion on the first assessment of the MgB₂ direct drive generator is that a 1.5 Tesla class machine can be realized now based on the cross section dimensions of the MgB₂ demonstration coil. The first performance indicators of this machine are summarized in table 4-5 and further work must be done to determine the price of the cooling system.

4.2.6 Coated conductor (AmSC + DTU 10 MW design)

Coated conductors have been proposed for the 10 MW SeaTitan turbine by American Superconductors and a feasibility study has been conducted by NREL [22]. The nacelle configuration is based on a double bearing between the hub and the superconducting generator. The generator is based on rotating inner superconducting field coils cooled with cryocooler cold heads mounted into the cryostat. The compressors for the cold-heads are positioned inside the nacelle and the high pressure Helium lines are transferred through a rotating gas coupling. The armature is based on copper windings and is at ambient temperature [23].

Table 4.6 is summarising the properties of the 10 MW SeaTitan generator and also the extrapolated values to 20 MW. It is seen that the shear stress is not as high at the GE NbTi generator and also that the estimated price is higher than for the GE machine.

KPI AmSC 2G SCDD	10 MW (24 pole)	15 MW	20 MW
Diameter[m]	4.5 – 5		
Length [m]	3.3	~ 2 x 10 MW ~ 6.6	~ 3 x 10 MW ~ 9.9
Mass [tons]	150-180	~ 2 x 10 MW ~ 300	~ 3 x 10 MW ~ 450
Shear stress [kN/m²]	~ 120	~ 120	~ 120
Efficiency [%]	96		
Generator cost [k€]	2380	~ 2 x 10 MW ~ 4760	~ 3 x 10 MW ~ 7140
Gen cost / capacity [€/kW]	238	~ 317	~ 357
COE [€/MWh]*			

Table 4.6. KPI of 10 MW 2G generator of the SeaTitan turbine of American Superconductor [8] & [22]. Note: Costs stated in 2010 US$ and converted by 2013 €/$ = 1.3 of today.

Table 4.7 is showing a proposal of a high shear stress generator based on 2G tape from Superpower Inc as done by Jensen et al. [24]. The magnetic flux density at the superconducting field coils is reaching up to 5 Tesla in order to make the generator compact, but this clearly comes at the price of an increased conductor usage. The design is based on a tape with a width of 4 mm and an assumed unit price length of 24 Euro/m. The critical current used in the design was measured in 2011 [16] and an operation temperature in around T = 40 K was assumed. From the analysis below it is clearly seen that the current price of the generator is about a factor of 10 too high in order to become feasible.

Thus in order decrease the usage of 2G tape we will work on designs running at lower temperature say T = 10-30 K. Secondly we will monitor the development of the 2G tapes, since a current ARPA-E REACT program by University of Houston, Teco-Westinghouse,

Superpower and co. workers have a goal to improve the T = 30 K , B =2.5 Tesla properties by a factor of 4. This will be done by

1) Increase the tape width from 4 to 12 mm.
2) Double the thickness of the superconductor layer.
3) Double the pinning properties of the tape at T = 30 K and B = 2.5 T by targeted optimization of the nano-engineering of the pinning sites in the superconductor.

The expected impact of the tape improvements on a 10 MW superconducting wind turbine generator has been predicted by Teco-Westinghouse and is shown in table 4.8 [25]. It is seen that a considerable price reduction is expected due to the targeted development at T = 30 K and B = 2.5 Tesla.

KPI Jensen 2G SCDD	10 MW (24 pole)	15 MW	20 MW
Diameter[m]	5.5	5.5	5.5
Length [m]	1.5	2.76	4.24
Active mass [tons]	69*	~ 2 x 10 MW ~ 138	~ 3 x 10 MW ~ 207
Shear stress [kN/m²]	168.1		
Efficiency [%]	97.8 – 1¤		
Tape length [km]	351	563	815
Tape price [€]#	8417	13522	19567
Generator cost [k€]	8740	~ 2 x 10 MW ~ 17480	~ 3 x 10 MW ~ 26220
Gen cost / capacity [€/kW]	874	1165	1311
COE [€/MWh]			

Table 4.7. KPI of 10 MW 2G High field generator of Jensen at. al. [24] and extrapolated to P = 20 MW by only extending the length of the generator. This generator is based on second generation (2G) high temperature superconducting 4 mm wide tape from Superpower Inc. The unit length price is assumed to be 24 Euro/meter for a tape with properties measured in 2011# [16]. The active mass includes the mass of the armature and field winding back iron, the armature copper and the superconductors*. The cooling system is allowed to only reduce the overall efficiency by 1 %¤.

KPI ARPA-E UH SCDD	10 MW Now	10 MW 2015	15 MW 2015	20 MW 2015
Tape length [km] 12 mm width (Superpower)	65	16.25	~ 2 x 10 MW ~ 33	~ 3 x 10 MW ~ 49
Tape price [€]#	5400	1350	2742	4070
Generator cost [k€]	6500	2450	4900	7350
Gen. cost / capacity [€/kW]	650	245	326	368
COE [€/MWh]				

Table 4.8. Expected usage of 12 mm 2G tape if based on the current Superpower technology and on the development target of the ARPA-E REACT program of University of Houston & Superpower on improving the wind turbine specific tape (T = 30 K, B = 2.5 Tesla) by a factor of 4 [25]. It should be noted that the unit price length is 83 Euro/m in both scenarios and the feasibility improvement is expected in the better properties of the tapes. An additional price of 1.1 MEuro for the remaining generator system at 10 MW has been added to the superconductor price in order to obtain an estimate of the total generator system. This price is estimated from the GE NbTi generator and needs verification.

4.2.8 Discussion of performance indicators

The most important performance indicator of the superconducting direct drive generators is the price normalized by the capacity of the turbine, since this can be compared to the overall INNWIND.EU targets. Initial studies of work package 1 indicates that an offshore capacity cost of 1.5 M€/MW for the turbine seems acceptable in the range P = 10-20 MW. Secondly by using the cost break down of current gearbox based offshore turbines one can get an estimate of the combined cost fraction covered by the gearbox and the generator. This fraction is often found to be approximately 20% of the capacity cost giving 300 k€/MW. Thus if the capacity price of the superconducting generators exceeds this limit then it indicated that the drive trains will be more expensive than the current gearbox solution and cost savings related to the properties of the direct drive will be necessary to the make the entire turbine more feasible.

Figure 4-14 is showing the capacity cost of the superconducting drive trains considered in work package 3 as well as the 300 €/kW threshold indicating a feasible solution. First of all the GE NbTi generator performance is looking very promising from a cost point of view and will be considered the base-line scenario for the superconductor direct drive wind generator. The cost of capacity of the "Jensen 2G" generator represents a high flux density machine, which is quite compact as shown on figure 4-15, and is almost an order of magnitude too high compared to the threshold, because the 4 mm wide 2G tape from Superpower is so expensive. The 10 MW proposal from the University of Houston & Teco-Westinghouse is giving a somewhat smaller cost of capacity, which is likely to be related to a smaller magnetic flux density and an optimized machine, but it is still too high compared to the threshold. This is however reached by using target properties of the 12 mm superpower tape tailored for wind generators operating at T = 30 K and B = 2.5 Tesla, which is being developed for 2015 in an on-going ARPA-E REACT program by University of

Houston and partners. Thus the 2G tape technology will have to improve considerably in order to become feasible, but development target have been formulated to meet these.

Finally the mass estimates of the generators are shown in figure 4-16 and the partial load efficiencies of the GE and AmSC 10 MW generators are shown in figure 4-17 together with typical estimated of a permanent magnet direct drive and a gearbox drive train [22].
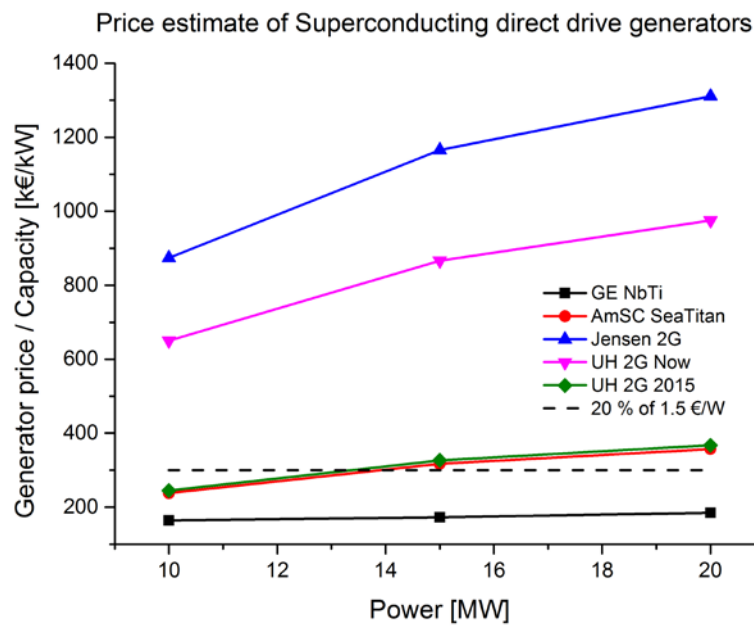

Figure 4-14. Cost of capacity of superconducting direct drive generators as extrapolated by a simple scaling, where the length was increased to fulfill the torque demand of the INNWIND.EU reference turbines.
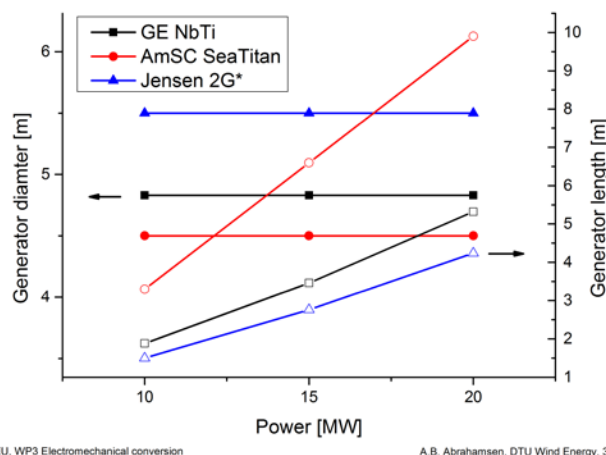
Figure 4-15. Sizes of the superconducting direct drive generators extrapolated by scaling the length of the 10 MW generators according to torque demand of INNWIND.EU reference turbines.
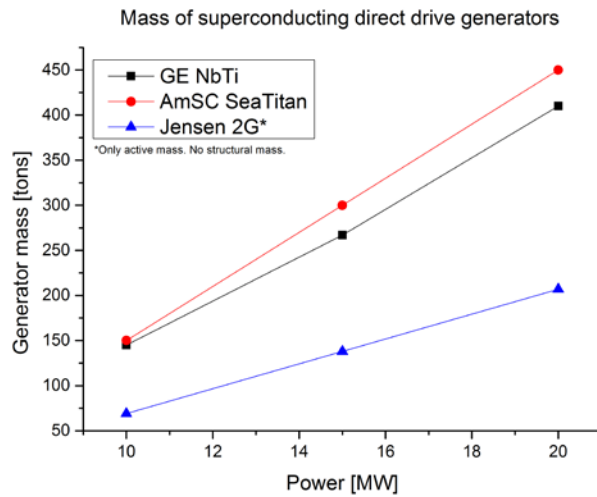
(INNWIND.EU, WP3 internal report, First assessment of performance indicators of SC and PDD *generators)*

Figure 4.16. Weight of superconducting direct drive generators extrapolated by scaling the length of the 10 MW generator by the torque demand of the INNWIND.EU reference turbines. * The Jensen 2G generator mass only contains the active mass.
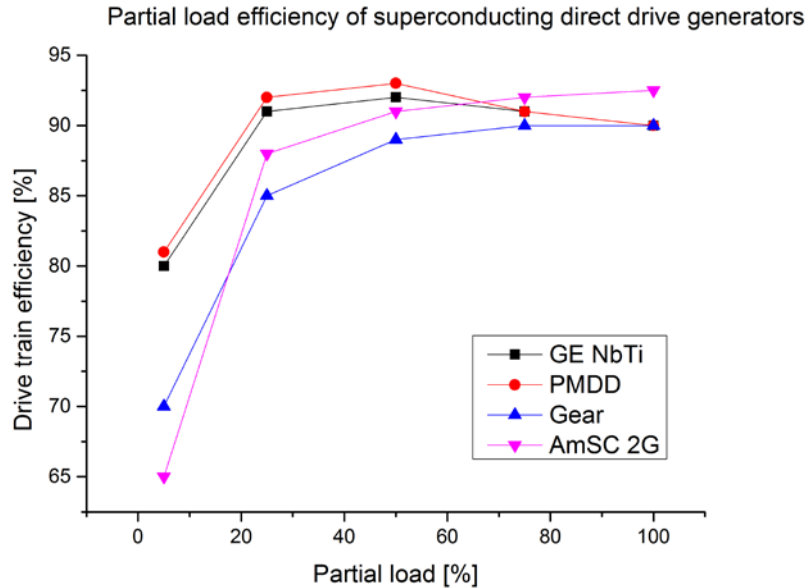
Figure 4.17. Partial load efficiency of 10 MW GE NbTi and 10 MW AmSC direct drive generators as reproduced from [17] and [22].

4.3   Conclusion: Performance indicators

The first estimate of the performance indicators of the superconducting direct drive generators have been extrapolated from the two main industrial 10 MW proposals given by GE Global Research (NbTi at T = 4.2 K) and American Superconductors (2G YBCO at T= 30 K). The NbTi machine of GE offers some very attractive performance indicators and it will be considered as the baseline of the further INNWIND work. The American Superconductor machine is falling below the threshold at 10 MW and it should be investigated if a better feasibility at 20 MW can be obtained by increasing the machine diameter.

A first estimate of a 10 MW MgB_2 generator has been obtained and the price performance indicator are higher than for the NbTi, but the MgB_2 tape is not as mature as the NbTi and a considerable learning should be expected. Initial work on applying a fold-back torque tube as illustrated on figure 4-6 is indicating that using stainless steel instead of high strength Ti-alloys as proposed by GE might be a possibility due to the higher operation temperature. Secondly the advantage of having an operating temperature of 10 K is investigated, but further work is needed to confirm the design and also the price.

A proposal on a 10 MW generator based on 4 mm wide YBCO 2G tape from Superpower has been investigated by DTU in order to obtain a current price estimate based on current tape properties and tape unit prices as obtained by a university like DTU ordering some 100 meters of tape. This study indicates that the 2G tape is about an order of magnitude too expensive today, but the cost of capacity threshold of the direct drive generators could be reached if the 2015 target properties of the 12 mm wide 2G tape from Superpower was used. An optimization study of this machine must be done in order to search for an optimum of the feasibility. Siemens wind power will also investigate the 2G technology and evaluate the feasibility based on the demonstration of the technology.

4.3.1   Future work

The current estimates give an overview of expected properties of the superconducting generators in terms of the active material, but the structural material will now also have to be included in order to search for better prize optima. Secondly the integration of the torque tube / cooling systems to the structural support must be investigated in details in order to quantify the generator price. Also the integration with the power electronics should be investigated in details. It is proposed that a lumped parameter model of the 10 MW MgB_2 generator of this report is provided to the power electronics task and that such a model will be incorporated into the integrated design platform of the HAWC-II model of the 10 MW INNWIND reference turbine. That will allow investigation of the performance of the superconducting generator under the load conditions of the INNWIND reference turbine.

Finally we need to get feedback from work package 1 of the INNWIND project in order to learn if it pays off to provide a smaller and more light weight generator. What is the total system price saving by having a 100 tons lighter generator? If it is neglect able then the future optimization of the generators should focus more on driving the price down taking into account not getting too big or too heavy.

(INNWIND.EU, WP3 internal report, First assessment of performance indicators of SC and PDD generators*)*

4.4   References

[1]   J. Bardeen, L. N. Cooper and J.R. Schrieffer, "Theory of Superconductivity", Phys. Rev. 108 (1957) 1175.

[2]   H. Rogalla and P. Kes, "100 years of superconductivity", CRC press 2012, ISBN 978-1-4398-4398-4946-0.

[3]   W. Meissner and R. Ochsenfeld, "Ein neuer Effekt bei Eintritt der Supraleitfähigkeit", Naturwissenshaften 21, (1933) 787

[4]   B.B. Jensen, N. Mijatovic and A.B. Abrahamsen, "Development of superconducting wind turbine generators", J. Renewable Sustainable Energy 5, 023137 (2013).

[5]   Y. Lvovsky, E.W. Stautner and T. Zhang, "Novel technologies and configurations of superconducting magnets for MRI", Supercond. Sci. Technol. 26 (2013) 093001.

[6]   M. Zhang, W. Wang, Y. R. Chen and T. Coombs, "Design Methodology of HTS Bulk Machine for Direct-Driven Wind Generation", IEEE TRANSACTIONS ON APPLIED SUPERCONDUCTIVITY, VOL. 22, NO. 3, JUNE 2012, p. 5201804.

[7]   H. Taxt, N. Magnusson, M. Runde and Silvia Brisigotti, "AC Loss Measurements on Multi-Filamentary MgB2 Wires With Non-Magnetic Sheath Materials", IEEE TRANSACTIONS ON APPLIED SUPERCONDUCTIVITY, VOL. 23, NO. 3, JUNE 2013, p. 8200204.

[8]   G. Snitchler, B. Gamble, C. King and P. Winn, "10 MW Class Superconductor Wind Turbine Generators", IEEE TRANSACTIONS ON APPLIED SUPER-CONDUCTIVITY, VOL. 21, NO. 3, JUNE 2011, p. 1089.

[9]   C. Lewis and J. Müller, "A direct drive wind turbine HTS generator", 2007 IEEE POWER ENGINEERING SOCIETY GENERAL MEETING, VOLS 1-10 — 2007, p. 3638

[10]   R. Fair et. al., "Superconductivity for Large Scale Wind Turbines", General Electric – Global Research, DOE report DE-EE0005143, 2012.

[11]   W. Nick, J. Grundmann and J. Frauenhofer, "Test results from Siemens low-speed, high-torque HTS machine and description of further steps towards commercialisation of HTS machines", Physica C 482 (2012) 105–110.

[12]   G. Snitchler, "Progress on high temperature superconductor propulsion motors and direct drive wind generators" International Power Electronics Conference (IPEC), 2010, p. 5 – 10, 10.1109/IPEC.2010.5542327.

[13]   GE news centre, "GE Successfully Trials Breakthrough High-Temperature Superconducting Technology for Next-Generation Power Generation", April 4 2013.

[14]   W. Stautner, R. Fair, K. Sivasubramaniam, K. Amm, J. Bray, E. T. Laskaris, K. Weeber, M. Douglass, L. Fulton, S. Hou, J. Kim, R. Longtin, M. Moscinski, J. Rochford, R. Rajput-Ghoshal, P. Riley, D. Wagner and R. Duckworth, "Large Scale Superconducting Wind Turbine Cooling", IEEE TRANSACTIONS ON APPLIED SUPERCONDUCTIVITY, VOL. 23, NO. 3, JUNE 2013, p. 5200804.

[15]   Henk Polinder, Member, IEEE, Frank F. A. van der Pijl, Gert-Jan de Vilder and Peter J. Tavner, " Comparison of Direct-Drive and Geared Generator Concepts for Wind Turbines", IEEE TRANSACTIONS ON ENERGY CONVERSION, VOL. 21, NO. 3, SEPTEMBER 2006, p. 725.

[16]   A.B. Abrahamsen, B.B. Jensen, E. Seiler, N. Mijatovic, V.M. Rodriguez-Zermeno, N.H. Andersen, J. Østergård, "Feasibility study of 5 MW superconducting wind turbine generator", Physica C 471 (2011) 1464–1469.

[17]   R. Fair et. al., "Superconductivity for Large Scale Wind Turbines", General Electric – Global Research, DOE report DE-EE0005143, 2012.

(INNWIND.EU, WP3 internal report, First assessment of performance indicators of SC and PDD generators*)*

[18]   R. Sato, B. Felder, M. Miki, K. Tsuzuki, H. Hayakawa and M. Izumi, "Helium-Neon Gas Mixture Thermosyphon Cooling and Stability for Large Scale HTS Synchronous Motors", IEEE TRANSACTIONS ON APPLIED SUPERCONDUCTIVITY, VOL. 23, NO. 3,JUNE 2013, P. 5200704.

[19]   S. Mine, M. Xu, S. Buresh, W. Stautner, C. Immer, E. T. Laskaris, K. Amm and G. Grasso, "Second Test Coil for the Development of a Compact 3 T MgB_2 Magnet", IEEE TRANSACTIONS ON APPLIED SUPERCONDUCTIVITY, VOL. 23, NO. 3, JUNE 2013, 4601404.

[20]   F. Sætre, I. Hiltunen, M. Runde, N. Magnusson, J. Järvelä, J. Bjerkli and E. Engebrethsen, "Winding, cooling and initial testing of a 10 H superconducting MgB_2 coil for an induction heater", Supercond. Sci. Technol. 24 (2011) 035010.

[21]   S.S. Kalsi, "Applications of high temperature superconductors to electric power equipment", ISBN 978-1-118-11009-6, John Wiley & Sons (2011).

[22]   B. Maples, M. Hand and W. Musial, "Comparative Assessment of Direct Drive High Temperature Superconducting Generators in Multi-Megawatt Class Wind Turbines", National Renewable Energy Laboratory, Technical Report NREL/TP-5000-49086 (2010).

[23]   H. Karmaker, E. Chen, W. Chen and G. Gao ," Stator Design Concepts for an 8 MW Direct Drive Superconducting Wind Generator", 2012 XXth International Conference on Electrical Machines (ICEM), p. 769 (2012). 10.1109/ICEIMach.2012.6349962

[24]   B. B. Jensen, N. Mijatovic, and A. B. Abrahamsen, "Reducing Conductor Usage in Superconducting Machines by Multiple Power Supplies", IEEE TRANSACTIONS ON APPLIED SUPERCONDUCTIVITY, VOL. 23, NO. 5, OCTOBER 2013, p. 5202708.

[25]   V. Selvamanickam , "Research activities in U.S. on coated conductors", presentation at Coated Conductors for Applications, Heildelberg, Germany, November 13 - 16, 2012. Link: http://www.superpower-inc.com/system/files/2012_1114+CCA2012_Selva_overview.pdf. Slide 10 is showing that 65 km of a 12 mm wide Superpower tape for a 10 MW wind generator is expected to decrease to 16.25 km by 2015. Slide 17 is showing that American Superconductors are expecting the usage of their tape to decrease from 225 kg/MW now and to less than 45 kg/MW in some years from now.

(INNWIND.EU, WP3 internal report, First assessment of performance indicators of SC and PDD generators*)*

CHAPTER 5 MAGNETIC PSEUDO DIRECT DRIVE GENERATORS

5.1 Introduction

The objective of this chapter is to document the performance indicators of two Pseudo Direct Drive (PDD®) designs for the INNWIND reference turbine rated at 10MW and 20MW respectively.

The designs reported represent the first design iteration and it is expected that the design will be revised as further information is made available throughout the project. This information may include:

- Size and mass restrictions
- Efficiency targets
- Cost sensitivities
- Turbine architecture developments
- Design improvements indicated by the development of the advanced modelling techniques

This chapter will detail the machine designs and performance indicators and will also document the research undertaken thus far in the development of the advanced modelling techniques and initial output from these

5.2 Description of the generator topology

PDD technology

Currently, for the purposes of this study, wind turbine drive systems can be broadly categorised as geared drive or direct drive. It is argued, that for large offshore applications the adoption of a geared drive system will lead to a failure rate that when coupled with the service schedule and logistical difficulties will give offshore wind turbine systems that are commercially unviable

To achieve the very high torques at low speeds in direct drive systems, brushless permanent magnet motors are typically used due to their superior torque density and torque-speed characteristics.

However, due to limits on magnetic, electrical and thermal stresses, even when employing high energy rare-earth permanent magnets, the continuous torque output per-unit-volume/mass is limited. The resulting generator required for direct drive is then prohibitively large and the cubic scaling law will dictate that this type of system is not feasible for the large offshore wind turbines considered.

The PDD employs a magnetic gear stage, and the purpose of this is twofold. Firstly the size of the generator is minimised by virtue of the torque converter which is analogous to a mechanical gear in this respect and secondly the (mechanical) gearbox system with the very high "consequence of failure" is removed from the system.

A PDD is a full magnetic and mechanical integration of an electrical generator and magnetic gear. The resulting electrical machine, which is shown in Figure 5.1.1 below, has been called the Pseudo-Direct Drive (because it has the characteristics of a direct-drive machine, although it uses a magnetic gear to achieve its very high torque-densities).

The PDD consists of three components:
- Outer stator, comprising a conventional lamination stack with copper windings, and stationary outer magnets
- Inner permanent-magnet array rotating at high-speed with no external mechanical connection
- Intermediate annular component, the modulating rotor, with ferro-magnetic pole-pieces, rotating at low-speed and connected to the input shaft of the generator.
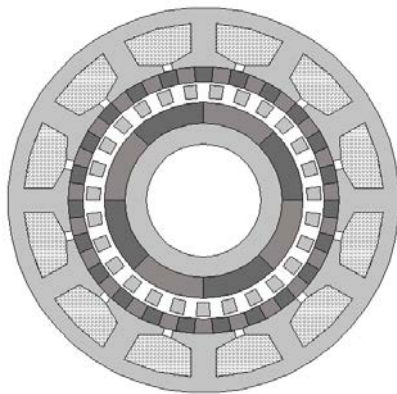
Fig 5.1.1. Pseudo-Direct Drive (PDD)   Fig 5.1.2. Components forming the PM generator
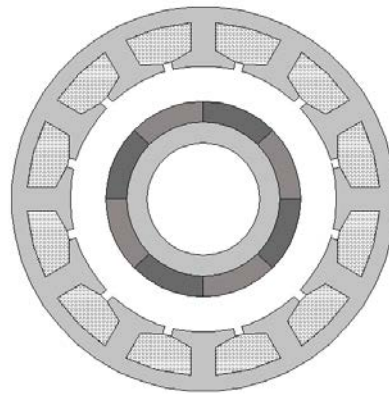
The principal of operation of the PDD can be understood by considering the operation of the different sub-components within it; i.e. the magnetic gear and the electrical machine. The components it shares with the magnetic gear are evident from Figure 5.1.1, which also shows the elements of the device which contribute to its operation as an electrical machine; i.e. the outer lamination stack with the copper windings and the inner permanent magnet rotor. Thus the inner rotor contributes to the operation of both the electrical machine and the magnet gear, and, as a result, the PDD uses less magnet material than would be used by a combination of a magnetic gear and separate electrical machine. Further, the PDD is controlled in an identical manner to a conventional direct-drive PM machine, through the use of existing full-rated power converter technology.

Specific advantages of the PDD technology are:

- Ultra-compact and lightweight motor/generator technology
- High power factor (typically > 0.9 at rated load)
- Standard COTS converters can be used

- Significantly reduced maintenance
- Extended operating lifetime
- Noise and vibration reduction – and significantly reduced degradation in noise and vibration performance over time
- High efficiency at rated and part load – loss mechanisms are well-understood, and mitigation strategies are common to existing electric motor design
- Passive and safe overload protection through torque shear – this can be precisely predicted and allows de-rating of other drive-train components
- Elimination of wear and wear related failure modes
- Elimination of gear lubricants and the need for complex filtration and regular oil checks
- Minimized Unbalanced Magnetic Pull (UMP) - significantly reducing the radial forces and thus stresses on the shafts and bearings that exist in mechanical systems

Generator topology

The design evolution at Magnomatics was completed in two phases.

1) Initially a concept phase was undertaken. This was completed by using a first order design tool developed at Magnomatics (as shown in figure 5.2.3) which is used to give indicative design details such as the diameter of the machine, the gear ratio and other basic operational and performance factors. The output from this tool was complemented by discussions held with project partners to align the machine design with the specific requirements of the turbines and to ensure that the design data would be presented in a format to allow the competing technologies to be compared.

2) Secondly the initial machine design concepts were translated into a finite element model of the machine. This model was implemented in a parametric format which allows a large degree of finite element based what-if studies to be undertaken. This modelling approach allowed a large number of machines to be analysed to a very high degree of fidelity to inform the design decisions on the trade-offs and sensitivities in the design and figure 5.2.4 shows a sample finite element model output. In this respect the designs presented in this chapter represent a single point output from this study, when the design of the entire turbine system matures it will be possible to re-evaluate the PDD generator design to give a more appropriate solution. Figure 5.2.5 shows sample optimisation data from this type of study where the total magnet mass (as an indicator of material costs in the generator) is plotted against the overall length of the (fixed diameter) generator. (Each individual dot in figure 5.2.5 represents output data from a unique finite element model.) This important trade-off shows the sensitivity of the requirement to minimise the volume of the generator and can be used to demonstrate the cost implications of this technical goal. The cost of the magnet material is assumed to be €50/kg; the volatility in heavy Rare Earth material will be mitigated by using low coercivity grades of material.
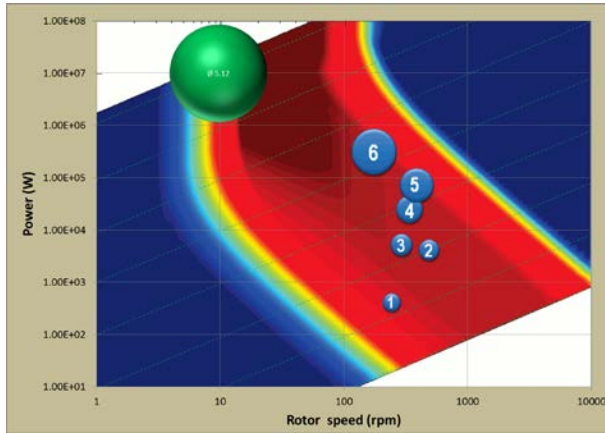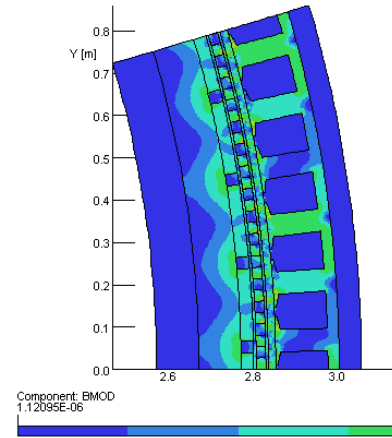
Figure 5.2.3. Initial applicability of 10MW turbine

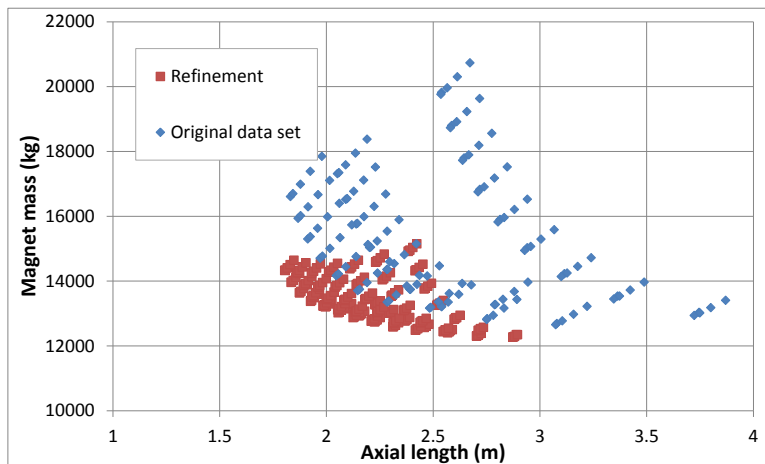Figure 5.2.4. Sample flux density plot for a section of a 10MW PDD design

Figure 5.2.5. Sample optimization data for the 10MW specification

5.3   Conclusion: performance indicators

Design details of 10MW PDD wind turbine generator			
Rated power [MW]	10	Remanent flux density of PMs [T]	1.25
Rated speed of inner rotor [rpm]	72.4	Relative recoil permeability of PMs	1.05
Rated speed of outer rotor [rpm]	9.65	Number of slots per pole per phase	1
Gear ratio	7.5:1	Mechanical air gap length [mm]	6
Electromagnetic torque [MNm]	10.5	Maximum air gap flux density [T]	0.522
Electrical freq. at rated speed [Hz]	55	Electrical steel mass [kg]	28400
Stator current density [A/mm2]	0.51	Stator slot filling factor	0.35
Outer diameter [mm]	6000	Copper mass [kg]	9110
Air gap diameter [mm]	5602	Magnet mass [kg]	12740
Axial length [mm]	2225	Efficiency [%]	98.9
Total generator mass [kg]	156000	Cost [k€]	1160

Table 5.3.1 Design details and Performance Indictors for 10MW generator

Design details of 20MW PDD wind turbine generator			
Rated power [MW]	20	Remanent flux density of PMs [T]	1.25
Rated speed of inner rotor [rpm]	44.33	Relative recoil permeability of PMs	1.05
Rated speed of outer rotor [rpm]	6.82	Number of slots per pole per phase	1
Gear ratio	6.5:1	Mechanical air gap length [mm]	11
Electromagnetic torque [MNm]	10.5	Maximum air gap flux density [T]	0.40
Electrical freq. at rated speed [Hz]	49	Electrical steel mass [kg]	58400
Stator current density [A/mm2]	0.51	Stator slot filling factor	0.35
Outer diameter [mm]	11000	Copper mass [kg]	27000
Air gap diameter [mm]	10500	Magnet mass [kg]	35620
Axial length [mm]	1980	Efficiency [%]	98.7
Total generator mass [kg]	TBD	Cost [k€]	TBD

Table 5.3.2 Design details and Performance Indictors for 20MW generator

5.4 Analytical design and optimisation tool

Analytical models of the prediction of the flux density distributions in the airspaces of the magnetic gear element of the PDD and the resulting transmitted torques have been developed, figure 5.4.1. The models have been extensively validated using magnetostatic finite element analysis, as can be seen in Figure 5.4.2, which compares the analytically and finite element predicted radial components of the flux density in the airgaps of the magnetic gear element of the PDD. It can be seen, that very good agreement exists. In addition to the flux density waveforms, the transmitted is also compared in Figure 5.4.3, where a very good agreement can again be seen between the analytical and finite element predictions.

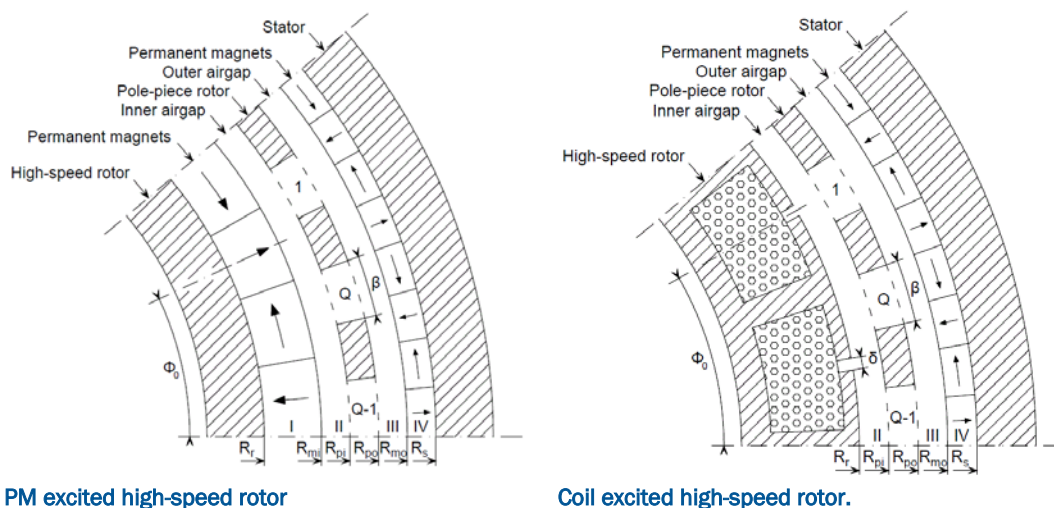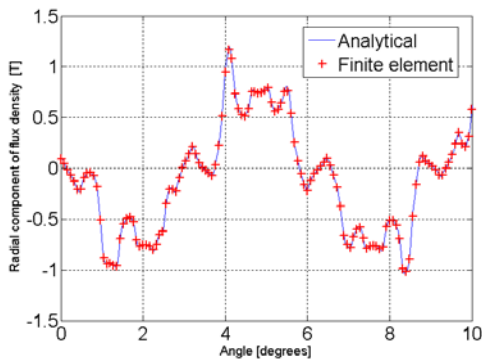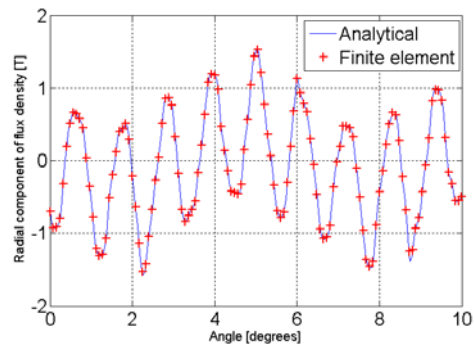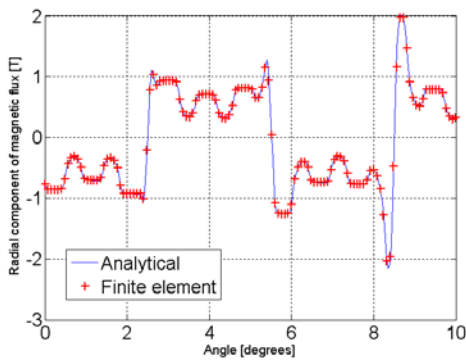PM excited high-speed rotor

Coil excited high-speed rotor.

Figure 5.4.1 Analytical model for the determination of the magnetic field distribution in air spaces of the magnetic gear element of the PDD
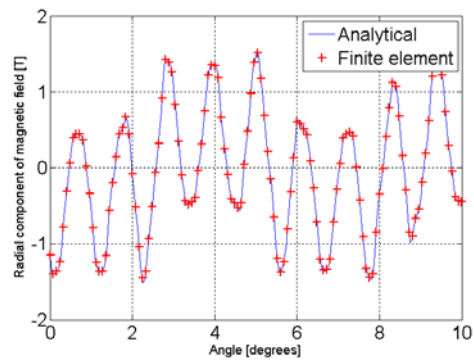
Radial flux density in inner airgap of PM excited high-speed rotor

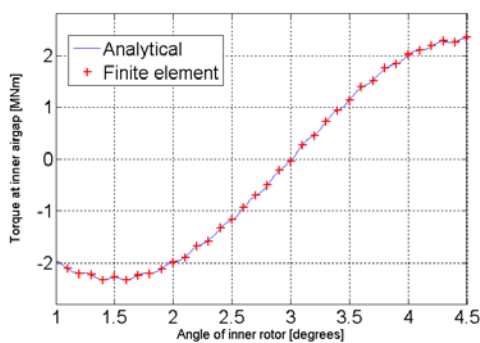Radial flux density in outer airgap of PM excited high-speed rotor

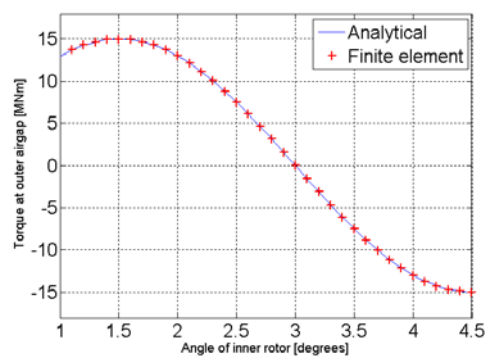Radial flux density in inner airgap of coil excited high-speed rotor

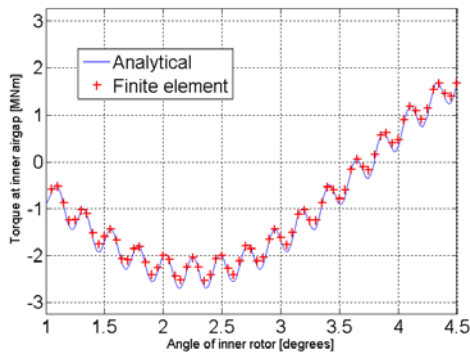Radial flux density in inner airgap of coil excited high-speed rotor

Figure 5.4.2 Radial components of flux density waveforms in the airgaps of the magnetic gear element of the PDD.
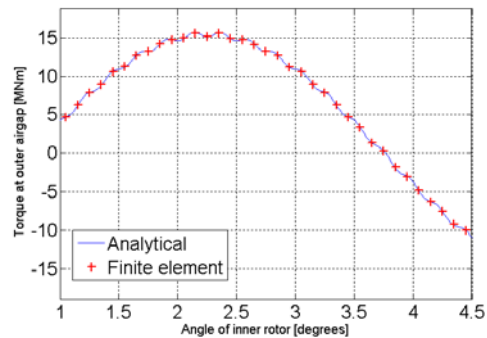

Electromagnetic torque in inner airgap of PM excited high-speed rotor

Electromagnetic torque in outer airgap of PM excited high-speed rotor

(INNWIND.EU, WP3 internal report, First assessment of performance indicators of SC and PDD generators*)*

Electromagnetic torque in inner airgap of coil excited high-speed rotor

Electromagnetic torque in inner airgap of coil excited high-speed rotor

Figure 5.4.3 Electromagnetic torque in the airgaps of the magnetic gear element of the PDD.

The developed models have been used to undertake an initial study on the effects of some of the leading design parameters, such as mass of permanent magnets, airgap diameter etc, on the achievable shear stress in the airgaps. For example, for a 10MW PDD, having the high-speed rotor exited by permanent magnets, figure 5.4.4 shows the variation of the maximum achievable shear stress with the total mass of permanent magnets, for different magnetisation distributions on the high speed rotor, viz. radial or Halbach, and for different supply frequencies at the rated speed. It can be seen that airgap shear stress in excess of 200kPa can be achieved, albeit at the expense of increased mass of the permanent magnets.
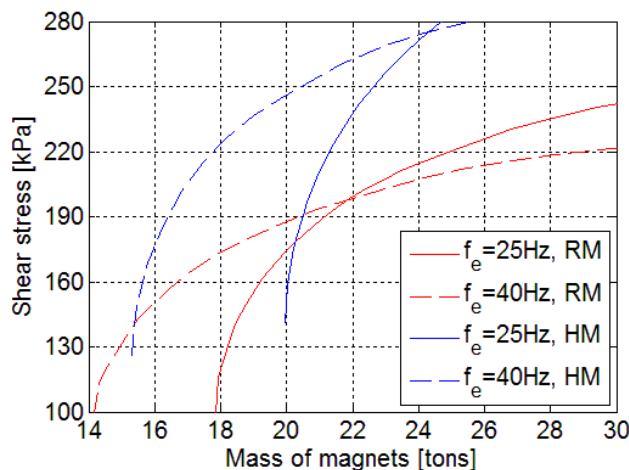

Figure 5.4.4 Variation of the maximum achievable shear stress with the total mass of permanent. (HM: Halbach magnetisation; RM: Radial magnetisation)

For a PDD with a coil excited high-speed rotor, figure 5.4.5, shows the relationship between the achievable stress in the airgaps, the mass of the permanent magnets on the stator and the copper loss in the coil excited rotor. It can be seen that for a 10MW machine, a shear stress in excess of 150kPa can be achieved, with a mass of permanent magnets less than half the mass of the PDD with permanent magnet excited high-speed rotor, and with a copper loss in the high-speed rotor less that 5% of the rated power.
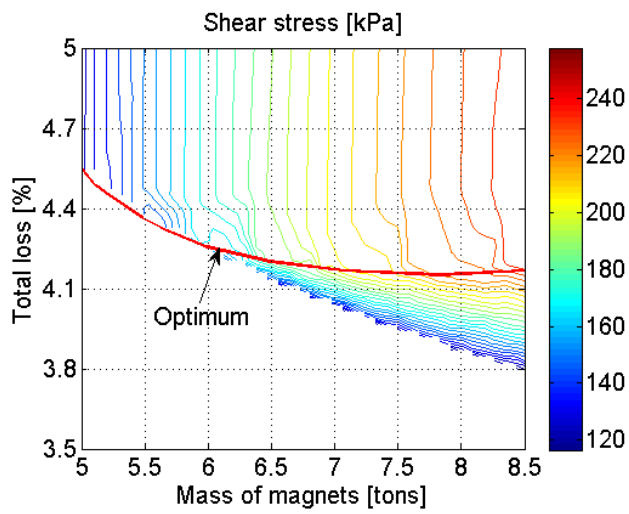
Figure 5.4.5 Relationship between the achievable shear stress, the mass of permanent magnets and the copper losses in the high-speed rotor for a 10MW PDD. (supply frequency 25Hz at rated speed)

CHAPTER 6 POWER ELECTRONICS

6.1 Introduction

The objective of this chapter is to evaluate the performance indicator of the different power electronic converters for the 10 MW and 20 MW wind turbine based on superconducting direct-drive generator (SCDDG) and the magnetic pseudo direct drive generator (PDDG), respectively. The size, efficiency, and the current total harmonics distortion (THD) of the power electronics converters will be assessed.

In this chapter, the possible power converter topologies for wind energy systems are introduced. Three power converters are discussed. One is with the back-to-back voltage source converter (VSC). One is with the diode rectifier, DC/DC converter, and grid side VSC. The other one is with an AC/AC converter.

6.2 Description of the power electronics

Power converters are widely used in wind energy conversion system. To date, a variety of power converters are presented for the variable-speed wind turbine system [1, 2]. Fig. 6-1 illustrates three practical wind energy conversion systems using different power converter configurations. Fig. 6-1(a) shows a wind energy conversion system based on a back-to-back converter configuration with two VSCs. Fig. 6-1(b) shows a wind turbine system based on a low-cost diode rectifier, a DC/DC converter, and a grid side VSC. Fig. 6-1(c) shows the wind turbine system with an AC/AC power electronic converter.

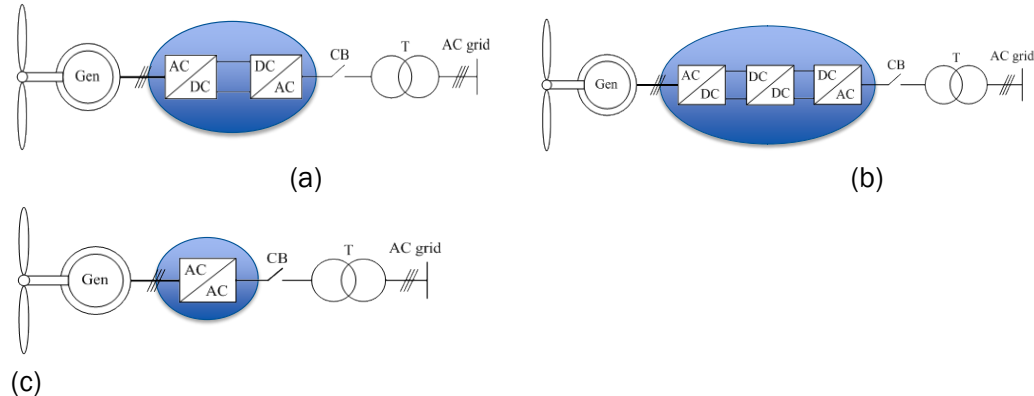(a)   (b)

(c)

Fig. 6-1.   Three typical wind energy conversion system based on (a) Back-to-back converters. (b) Diode rectifier, DC/DC converter, and DC/AC converter. (c) AC/AC converter.

6.3 WECS based on back-to-back converters

Fig. 6-2(a) shows the block diagram of a wind energy conversion system based on two-level VSCs, which has been widely used in wind power industry. The two-level VSC is composed of six switches, and each switch takes the dc-link voltage.

Fig. 6-2(b) shows the block diagram of a wind energy conversion system based on three-level neutral point clamped (NPC) converters. The three-level NPC converter is composed with 12 switches, and each switch takes only half of the dc-link voltage. The three-level NPC converter is widely used for medium voltage applictions. In comparison with two-level VSC, the three-level NPC converter has lower dv/dt and smaller THD in its ac output voltages under the same switching frequency.

Fig. 6-2(c) shows the block diagram of a wind energy conversion system based on a configuration with parallel converters, where a few converters are connected in parallel for one wind turbine. The rating of each converter can be a fraction of the power rating of the wind turbine. In addition, the paralleled converter system may also improve the system efficiency and reliability. However, the circulating current derived from the parallel configuration may affect the system performance, and some measures should be taken to suppress the circulating current.

Fig. 6-2(d) shows the block diagram of a wind energy conversion system based on a modular multilevel converter (MMC). The MMC becomes attractive in recent year for high power and high voltage applications. The MMC consists of a number of series-connected submodule (SM) converters, which can used for high voltage level and produce small THD in its ac output voltage. Each SM can be built with a small voltage rating, and the low voltage-level power semiconductor can then be used for the high voltage and high power system. while the series-connected arm inductor in each arm can limit the current and protect the system during short-circuit faults.
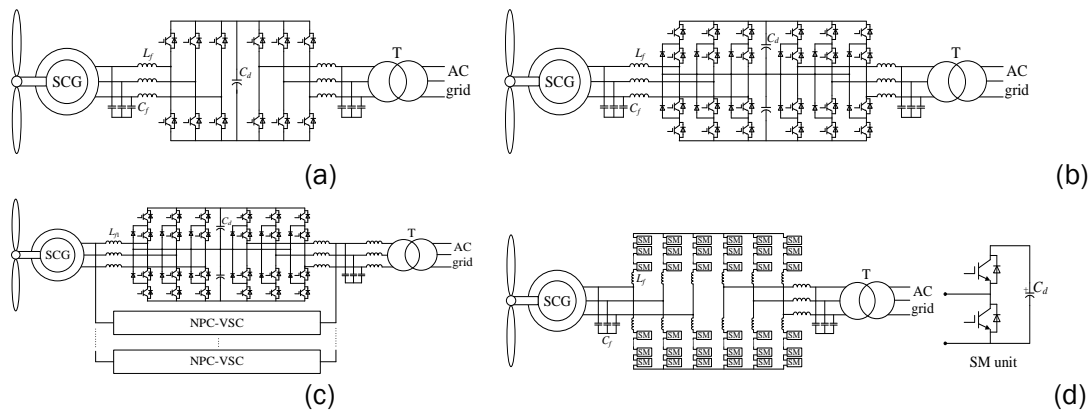

(a)

(b)

(c)

(d)

Fig. 6-2. Wind energy conversion system based on (a) 2-level VSCs. (b) 3-level NPC converters. (c) Parallel NPC converters. (d) MMCs.

6.3.1 Performance indicator of back-to-back power electronics converters

Tables I and II shows the performance indicator of the back-to-back power converters for 10 MW and 20 MW wind turbine based on SCG and PDDG, respectively. The nominal electricity frequencies of the SCG and PDDG are just around 5 Hz and 25 Hz, respectively. The line-to-line voltage of the 10 and 20 MW wind turbine is 3.3 and 6.6 kV, respectively, the dc-link voltage of the back-to-back converter may be selected as 5.4 and 10.8 kV, respectively. Recently, the appearance of the IGCT makes the capacities of three-level NPC converter reach up to approximately 6~9 MW just with one power semiconductor for each switch in Fig. 6-2(b). In parallel NPC converter system, 2 three-level NPC converters are in parallel configuration for 10 MW wind turbine, and 3 parallel three-level NPC converters are used for 20 MW wind turbine. In the MMCs configuration, 2 and 3 SMs are respectively used in each arm for 10 and 20 MW wind turbine, and can produce 5- and 7-level voltage
.

According to the output capacity and voltage ratings of the power converters, as well as available commercial IGBT and diode modules in market, the 1700V/1800A IGBT (5SNA1800E170100) and1700V/1800A fast recovery diode (FRD) (1700V/1800A RM1800HE-34S) are chosen here to make a number of comparisons for building the different power converters, as shown in Tables I and II. The high voltage rating can be realized by series-connection of several power semiconductors. In Tables I and II, the total

used inductance and capacitance for the different converters are listed. In addition, the generator current THD with the different power converters at the rated power of the wind turbine is shown in Tables I and II, where the switching frequencies are all 500 Hz. The efficiencies of the power converters in 10 MW and 20 MW wind turbine based on SCDDG and PDDG are shown in Fig. 6-3 and Fig. 6-4, respectively.

Table I. 10 MW power electronic converters

Converter type	Total inductor (mH)	Total installed capacitor (F)	IGBT number	Clamped diode number	Switch power (MW)	Generator current THD (%)
2-L converter	3.6	0.24	144	No	440	3.5 (SCG)
						9 (PDDG)
3-L NPC converter	1.8	0.24	144	72	440	1.1 (SCG)
						6.4 (PDDG)
2×Parallel converter	6	0.24	144	72	440	0.7 (SCG)
						2 (PDDG)
MMC (2SMs/arm)	3.6	1.8 (SCG)	144	No	440	0.7 (SCG)
		0.5 (PDDG)				1.4 (PDDG)

Table II. 20 MW power electronic converters

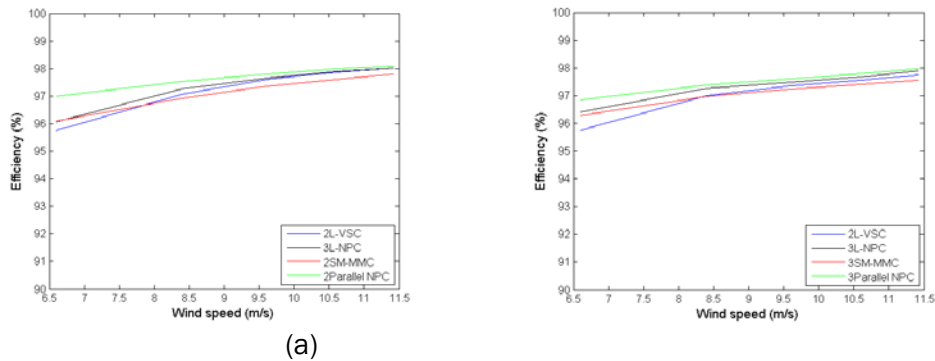| Converter type	Installed inductor (mH)	Installed capacitor	IGBT number	Clamped diode number	Switch power (MW)	Generator current THD (%)
2-L converter	3.6	0.12	288	No	881	4 (SCG)
						12 (PDDG)
3-L NPC converter	1.8	0.12	288	144	881	1.2 (SCG)
						6.8 (PDDG)
3×Parallel converter	4.2	0.12	432	216	1322	0.9 (SCG)
						2.1 (PDDG)
MMC (3SMs/arm)	4.8	2.2 (SCG)	288	No	881	0.7 (SCG)
		0.7 (PDDG)				0.7 (PDDG)

(a)   (b)

Fig. 6-3. Power converters efficiency for SCDDG-based wind turbine. (a) 10 MW wind turbine system. (b) 20 MW wind turbine system.
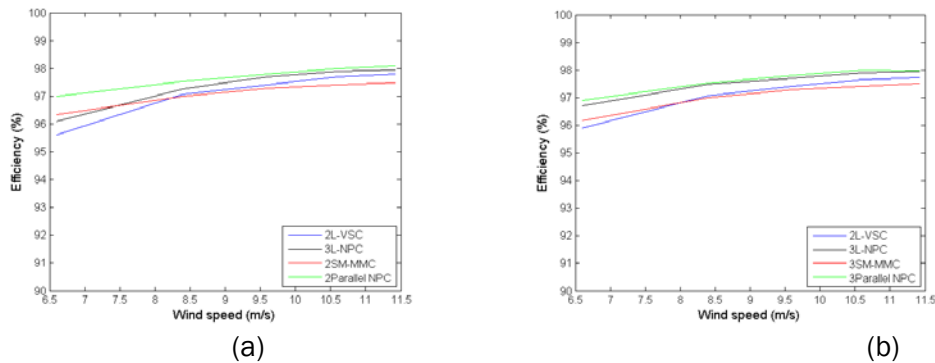

(a)   (b)

Fig. 6-4. Power converters efficiency for PDDG-based wind turbine. (a) 10 MW wind turbine system. (b) 20 MW wind turbine system.

6.3.2 Summary of back-to-back VSC configurations

In this chapter, the 10 MW and 20 MW back-to-back VSC is applied for the SCDDG- and PDDG-based wind turbine system. The possible power converter configurations including two-level VSC, three-level NPC VSC, parallel NPC converter, and MMC are compared in the view of power semiconductor, harmonics, and efficiency. In the two-level, three-level, and parallel NPC converters, the series-connection configuration of several power semiconductors may be required. The small-voltage module configuration of each submodule in MMCs enables one power semiconductor for each switch in the medium-voltage MW-level wind turbine system. Among these converters, the two-level VSC produces a highest THD in the generator current. The three-level NPC converter and parallel NPC converter configurations have high efficiency. However, the circulating current may exist in the parallel configuration and some methods should be taken to suppress it. The MMC can produce the lowest THD of the generator current.

6.4 Modular multilevel AC/AC converters

In this section, the Hexverter, the Modular Multilevel Matrix converter and their performance indicators are investigated. There are some common benefits of the direct AC/AC converters. As with all modular multilevel topologies, high voltage and high power is achievable with serial connected modules built up with standard devices. By adding additional modules in each branch, a high redundancy is easily accomplished. Every change in a single module output voltage causes a change in the branch output voltage.

Thus, for the same number of changes in the branch output voltage per time (effective branch switching frequency), the module switching frequency decreases with an increasing module number. Furthermore a low output voltage THD results from the increased number of modules. A common disadvantage is a high branch energy variation with similar or same system frequencies on both sides of the converters.

As performance indicators for a comparison between modular multilevel converters, the total installed capacity, total installed inductance, efficiency, number of modules and switching power of installed semiconductors are used. The switching power indicates the needed chip size but thermal design has to be considered in further investigations. All factors act as cost indicators. The total installed capacity and inductance, as well as the number of modules, are indicators for the size and weight of the converter.

For the numerical calculation of the performance indicators, the following assumptions were made: The maximum dc-link voltage per module is 900 V, the minimum dc-link voltage per module is 720 V, the allowed dc-link voltage variation during normal operation is 108 V, the system voltages are U_1=3.3 kV, U_2=3.3 kV for the 10 MW generator and U_1=6.6 kV, U_2=6.6 kV for the 20 MW generator, the grid-frequency is 50 Hz, the nominal generator frequencies are 5 Hz respectively 25 Hz, the power factor range is from 0.95 leading to 0.95 lagging, the allowed branch current ripple is 5% of the maximum branch current, and the effective branch switching frequency is 5 kHz. For the calculation of the efficiency, a 5SNA 1800E170100 IGBT was chosen.

6.4.1 Hexverter

The so called Hexverter-topology [3, 4, 5] belongs to the group of modular multilevel direct converters. In Fig. 6-5, the structure can be seen. It directly links two three phase systems with different frequencies. Therefore each phase of one system is connected with two phases of the other system. This connection is realised via modular multilevel branches which consist of several H-bridge modules and a branch inductor. For simplified system and control analysis, all H-bridge modules in one branch can be considered as a controlled voltage source. In series with the inductor, the whole branch acts like a controlled current source, as long as the summed dc-link voltages are sufficient. Hence it is possible to control the three line currents of each system and an additional circulating current through all branches. Besides, the neutral point voltage between the systems is controllable. With this circulating current and neutral point voltage, a branch energy control, which is essential for proper operation, can be realised. More detailed information on topology, and on branch energy control in particular, can be found in [3], [4] and [5]. The results of the performance indicator calculation are listed in Table III.
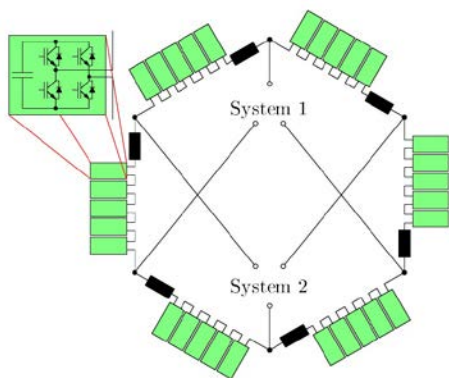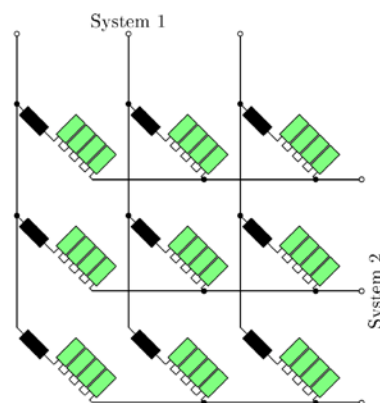

Fig. 6-5 Hexverter topology.

Fig. 6-6 Modular Multilevel Matrix Converter.

6.4.2 Modular Multilevel Matrix Converter

Another modular multilevel direct converter is the Modular Multilevel Matrix Converter (MMMC) [6, 7, 8, 9], which can be seen in Fig. 6-6. Each phase of a system is connected with all three phases of the second system. This connection is realized with H-bridge modular multilevel branches, similar to the branches used for the Hexverter. Branch energy is controlled with the four independent circulating currents. The usage of the neutral point voltage is possible but not necessary. Details on system behavior and control are described in [6], [7], [8] and [9].

The results of the performance indicator calculation can be found in Table III. These indicators are evaluated without using special circulating current control strategies like the instantaneous power mode from [8] and [9]. Their goal is a reduction of branch energy variation, which would lead to a lower total installed capacity especially for 5 Hz nominal frequency. A disadvantage of these methods is an increase of the maximum branch current. The quantitative effect of these methods remains to be analyzed.

Table III. Performance indicators for Hexverter and MMMC

Topology	Hexverter				MMMC			
Maximum power in MW	10	10	20	20	10	10	20	20
Nominal generator frequency in Hz	5	25	5	25	5	25	5	25
Nominal generator voltage in kV	3.3	3.3	6.6	6.6	3.3	3.3	6.6	6.6
Maximum branch voltage in kV	5.93	5.93	11.86	11.86	5.39	5.39	10.78	10.78
Maximum branch current in kA	3.52	3.52	3.52	3.52	1.69	1.69	1.69	1.69
Total installed capacity in F	15.4	3.7	30.9	7.5	5.1	1.6	10.1	3.3
Total installed inductance in mH	0.68	0.68	0.36	0.36	2.4	2.4	1.3	1.3
Switching Power in MW	501	501	1001	1001	328	328	657	657
Efficiency (nominal operation, Qgrid=0 VAr)	97.6%	97.6%	98.0%	98.0%	98.1%	98.1%	98.4%	98.4%
Efficiency (average, uniformly	97.1%	97.1%	97.7%	97.7%	97.7%	97.7%	98.1%	98.1%

distributed wind speed, Qgrid=0 VAr)								
Number of modules	54	54	102	102	72	72	135	135

6.5 Diode Rectifier – DC/DC Converter – Grid VSC Inverter

6.5.1 General analysis of power quality

Initially, the rectifier system was simulated at rated power for a range of different generator per-unit reactance, in order to determine the effects of the reactance on the power quality and generator losses. The boost converter switching was not simulated, but instead a DC-link operating at either a constant voltage or constant current was used, reflecting the different ways that such a system could be controlled, with a PI controller setting the DC voltage or current to obtain the desired power output.

The generator currents are shown in Fig. 6-7 for voltage- and current-source. A lower reactance leads to a significantly more distorted waveform for voltage-source, with the waveform becoming more sinusoidal with higher reactances. For the current-source arrangement, a higher reactance leads to a longer commutation time for the diodes, which causes the current to lag, increasing the reactive power and hence the current for a given real power transfer.
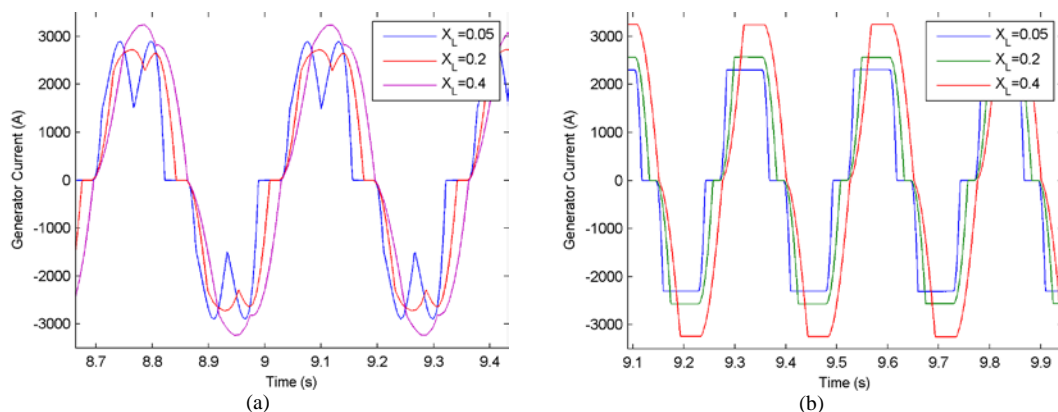

Fig. 6-7 Generator current with different reactances (a) Voltage-source, (b) Current-source.

The passive rectifier is not able to provide reactive power support to the generator, which must be provided by the generator itself, so the generator reactance places an upper limit on the real power output. It was found that the rated power of the generator could only be achieved if the per-unit reactance was below 0.45 for the voltage-source DC-link, and 0.4 for the current-source. The variation in current THD with generator reactance for the current- and voltage-source DC-link are shown in Fig. 6-8. A current-source link gives a better THD at lower reactances while a voltage-source link is better at high reactances.

The inability to provide reactive power support to the generator means that the generator terminal voltage must be significantly lower than with a 4-quadrant converter to draw rated power, leading to a higher current. This, combined with the current distortion, leads to higher generator losses compared with connection via a 4-quadrant converter. Generator RMS currents, which determine the resistive losses, were found from simulation for the different reactances with a voltage-source DC-link and calculated for a generator connected to a 4-quadrant converter with sinusoidal current. These were used to calculate the difference in losses between the different systems, which is shown in Fig. 6-9. At low reactances, losses are slightly higher for the diode-rectifier system, due to the current distortion giving higher current peaks, while at higher reactances the losses are significantly higher due to the lower terminal voltage.
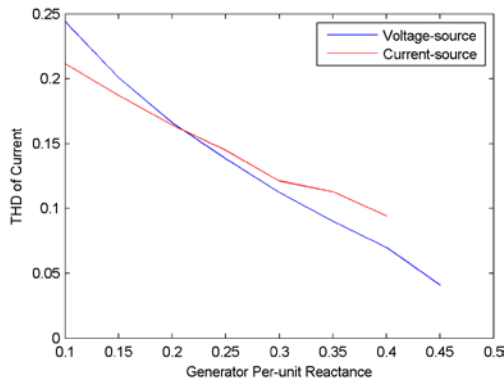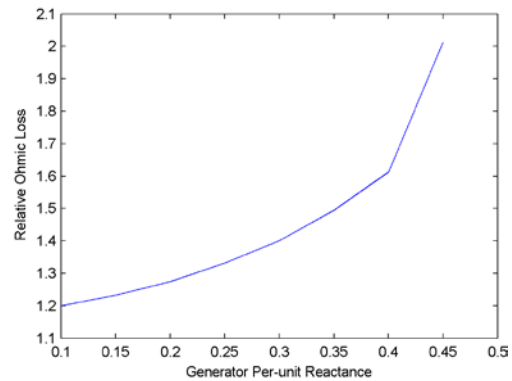
Fig. 6-8 Current THD vs. generator reactance. Fig. 6-9 Generator losses relative to 4-Quadrant converter.

6.5.2 Performance indicators for the AC-DC DC-DC converter

6.5.2.1 Power Semiconductor Quantities

For the selected generator inductance for the superconducting generator of 0.2, a generator current of around 2000A RMS is obtained at rated wind speed. This requires two parallel IGBTs or diodes of the selected type. To achieve the required voltage rating 7 series devices are required for the 10MW converter and 13 for the 20MW. This gives the semiconductor quantities shown in Table IV, in which a 2-level inverter is used for the grid connection.

Table IV Converter component counts

Turbine Rating	Line-line voltage (kV)	Line current (kA RMS)	DC-link voltage	Quantity –rectifier		Quantity-inverter	
				IGBT	Diode	IGBT	Diode
10MW	3.3	1.99	5700	14	98	84	0
20MW	6.6	2.00	11400	26	182	156	0

6.5.2.2 Losses and power quality

Conduction and switching losses were calculated based on simulation, at wind speeds between the cut-in and rated wind speeds, and used to find the converter efficiency. A voltage-source DC-link was used as the current-source model had issues with voltage spikes around the rectifier commutation which affected the control system.

A breakdown of the efficiency of the different stages of the converter is shown in figure 6-10 for the 10MW turbine, at wind speeds up to the rated speed. The 20MW turbine shows an almost identical result. A comparison between the converter efficiencies for the 10MW and 20MW turbines is shown in figure 6-11. The slightly higher lower efficiency for the 10MW turbine is due to a lower switch voltage utilisation with 7 series devices compared with 13 for the 20MW. Obviously 6.5 series devices is not possible, but would lead to identical efficiencies for both turbines.
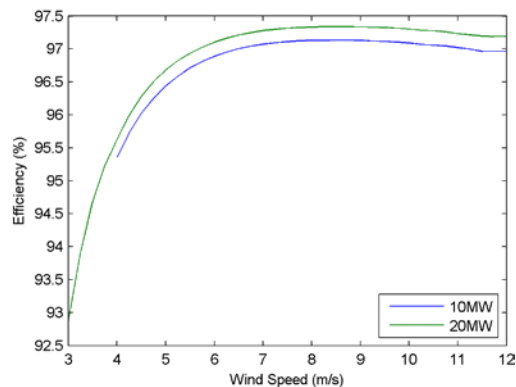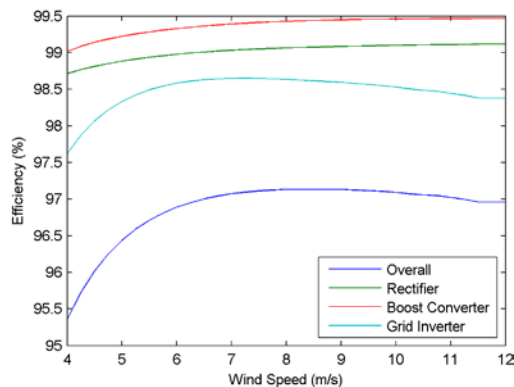
Fig. 6-10 Efficiency of different converter stages, 10MW turbine. Fig. 6-11 Comparison of 10MW and 20MW turbine converter efficiencies.

The THD of the current was calculated at different wind speeds and is shown in　　　Fig. -12 for the 10MW turbine, with the 20MW turbine being almost identical. THD is extremely high at low wind speeds, where the generator currents are low, and the generator current for the 10MW turbine operating at 4m/s wind is shown in　　　　Fig. .
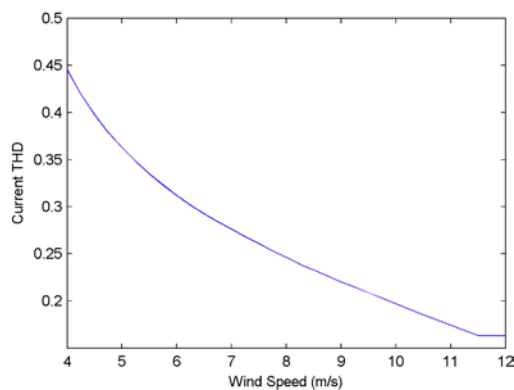

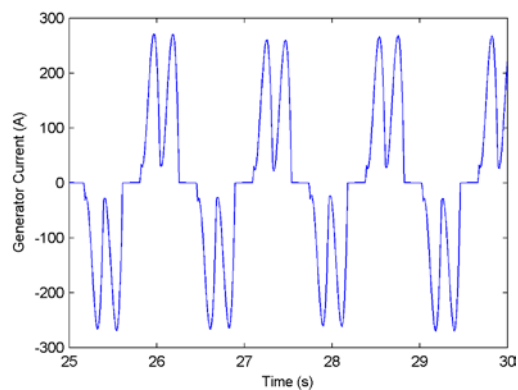
Fig. 6-12 Variation of current THD with wind speed. Fig. 6-13 Current distortion at 4m/s wind speed.

6.5.3 Summary of Diode Rectifier – DC/DC Converter – Grid VSC Inverter System

Using a passive rectifier with a boost converter has some advantages over a 4-quadrant converter, such as a slightly higher efficiency and lower IGBT count. However this is likely to be outweighed by a number of disadvantages:

- The generator per-unit reactance cannot be higher than 0.45, and at high reactances the generator losses will be significantly higher than if it is connected to a 4-quadrant converter. Capacitors can be connected across the generator terminals to allow operation with higher generator reactances, but this would lead to even higher generator losses.
- The generator current is extremely distorted, particularly with low generator reactances. The distortion is at harmonics of the generator fundamental frequency, so they will vary with turbine speed and thus be difficult to filter using a tuned filter.

Reactances for the Superconducting and Pseudo-Magnetic Direct Drive generators are not known, but are likely to be around 0.1-0.2 for the SC generator based on other SC designs, and greater than 0.5 for the PMDD, based on other direct drive designs.

Based on these reactances, the SC generator will be subjected to a highly-distorted current, at a low frequency, which will lead to significant losses in the rotor. The low frequency of the distortion means that it will not be possible to shield the rotor from magnetic fields at that frequency, unlike the high-

frequency distortion with other converter designs. The reactance of the PMDD generator will almost certainly be too high for use with this converter without extra capacitors on the generator terminals.

A possible option may be to use an active filter, based on IGBTs, to correct the current distortion. This may offer some advantages, but may result in a similar device count and efficiency to the 4-Quadrant converter.

6.6 References

[1]   Chen, Z. " An introduction of power electronic technology ", in *Direct-Drive Wind and Marine Energy Systems, Edited by Markus Mueller,* Woodhead Publishing Ltd. 2013.

[2]   Chen, Z. " Power electronic converter systems for direct drive renewable energy applications", in *Direct-Drive Wind and Marine Energy Systems, Edited by Markus Mueller,* Woodhead Publishing Ltd. 2013.

[3]   Baruschka, L.; Mertens, A., "A new 3-phase AC/AC modular multilevel converter with six branches in hexagonal configuration," *Energy Conversion Congress and Exposition (ECCE), 2011 IEEE*, vol., no., pp.4005,4012, 17-22 Sept. 2011 doi: 10.1109/ECCE.2011.6064314

[4]   Baruschka, L.; Mertens, A., "A new 3-phase direct modular multilevel converter," *Power Electronics and Applications (EPE 2011), Proceedings of the 2011-14th European Conference on* , vol., no., pp.1,10, Aug. 30 2011-Sept. 1 2011

[5]   Baruschka, L.; Mertens, A., "A New Three-Phase AC/AC Modular Multilevel Converter With Six Branches in Hexagonal Configuration," *Industry Applications, IEEE Transactions on* , vol.49, no.3, pp.1400,1410, May-June 2013

[6]   Kammerer, F.; Kolb, J.; Braun, M., "Fully decoupled current control and energy balancing of the Modular Multilevel Matrix Converter," *Power Electronics and Motion Control Conference (EPE/PEMC), 2012 15th International*, vol., no., pp.LS2a.3-1,LS2a.3-8, 4-6 Sept. 2012

[7]   Kammerer, F.; Kolb, J.; Braun, M., "A novel cascaded vector control scheme for the Modular Multilevel Matrix Converter," *IECON 2011 - 37th Annual Conference on IEEE Industrial Electronics Society* , vol., no., pp.1097,1102, 7-10 Nov. 2011

[8]   Korn, A.J.; Winkelnkemper, M.; Steimer, P.; Kolar, J.W., "Direct modular multi-level converter for gearless low-speed drives," *Power Electronics and Applications (EPE 2011), Proceedings of the 2011-14th European Conference on*, vol., no., pp.1,7, Aug. 30 2011-Sept. 1 2011

[9]   Kawamura, W.; Akagi, H., "Control of the modular multilevel cascade converter based on triple-star bridge-cells (MMCC-TSBC) for motor drives," *Energy Conversion Congress and Exposition (ECCE), 2012 IEEE*, vol., no., pp.3506,3513, 15-20 Sept. 2012

CHAPTER 7 COMPARISON

7.1   Introduction

The objective of this chapter is to integrate the performance indicators estimated in the previous chapters for a superconducting generator system and for a pseudo direct drive generator system. Then the performance indicators of these two generator systems are compared with those of a scaled-up reference permanent-magnet direct-drive generator system of 10 and 20 MW.

7.2   System and comparison

In this section, a nacelle, a generator and a power electronic converter are evaluated in terms of performance indicators. There are two proposed systems:
1) Superconducting direct-drive generator system (SCDD)
2) Pseudo direct-drive generator system (PDD)

For SCDD, three superconductors (LTS, HTS and MgB$_2$) give three types of SCDD generators. All of the three are assessed in terms of performance indicators (size, mass and cost). PDD has only one type in this assessment. A reference permanent-magnet direct-drive generator system (PMDD) scaled up from lower power levels is shown to make a comparison with SCDD and PDD.

7.2.1 PMDD generator basis

Shrestha [1] has presented scaling functions for electromagnetic material mass and structural mass of PMDD generators with respect to power level. The parameters of the reference generators in [1] are close to a single-bearing 2 MW Harakosan Z72 and a double-bearing 2 MW Enercon E82.

Since the King-pin nacelle design in Chapter 3 does not employ the single bearing concept, we use the results from the reference generator close to Enercon E82. This model is electrically excited but its structural model can be used for a PMDD generator. The electromagnetic model is obtained from [2] which gives optimized parameters of a 10 MW PMDD generator for the minimal cost. The 10 MW electromagnetic model is scaled up to 20 MW by increasing the torque while decreasing the speed.

The electromagnetic or active mass consists of electromagnetic iron, armature winding copper and permanent magnets. The structural mass consists of stator arm, rotor arm, stator cylinder and rotor cylinder. The generator mass means the sum of active and structural masses.

The active mass and its cost are derived from the optimization results [2] and the structural mass and its cost are obtained and calculated based on [1]. The prices of the materials used in these calculations are:
-    Copper: 15 €/kg
-    Ferromagnetic iron: 3 €/kg
-    Permanent magnet: 50 €/kg

7.2.2 Comparison

The performance indicators of SCDD and PDD are summarized from Chapter 4 and Chapter 5 respectively and those of PMDD are obtained from Section 7.2.1. There are four SCDD designs involved with three different superconductors employed. One PDD design from Chapter 5 and one PMDD contrast are involved in this comparison.

The performance indicators are compared between SCDD, PDD and PMDD for 10 MW shown in Table 7-1 and for 20 MW shown in Table 7-2. The generator size is indicated in outer diameter and axial length. The generator mass consists of active mass and structural mass. The generator cost consists of active mass cost and structural mass cost. The nacelle mass and its cost only takes into account the main bearings and the structural steel. The efficiencies of generator and converter are the values at the rated power. The converter mass and the converter cost are currently unable to be predicted due to the complexity of various possible power electronic components.

Table 7-1: Comparison of performance indicators between SCDDs, PDD and PMDD for 10 MW

Generator type	SCDD				PDD	PMDD
	LTS	MgB2	HTS			
	GE [3]	DTU	AmSC [4]	Jensen 2G		
Outer diameter [m]	4.83	5.8	5	5.5	6.0	10.1
Axial length [m]	1.88	3.1	3.3	1.5	2.225	1.8
Generator mass [ton]	145	TBD[a] (53, active mass)	150 – 180	TBD (69, active mass)	156	285 (62.8 active mass)
Active materials cost [k€]	-	2263 (840, potentially[b])	-	8740	-	650,[c]
Generator cost [k€]	1644	TBD	2380	TBD	1160	1317
Nacelle mass[d] [ton]	200 – 300					400 - 500
Nacelle cost [k€]	TBD					TBD
Active materials cost/capacity [[€/kW]	-	226.3 (84)	-	874	-	65
Gen cost/capacity [[€/kW]	164.4	TBD	238	TBD	116	131.7
Generator efficiency	95%	TBD	96%	97.8%	98.9%	97%
Converter efficiency	97%					97%

Table 7-2: Comparison of performance indicators between SCDDs, PDD and PMDD for 20 MW

Generator type	SCDD				PDD	PMDD
	LTS	MgB2	HTS			
	GE	DTU	AmSC	Jensen 2G		
Outer diameter [m]	4.83	TBD	5	5.5	11	14.1
Axial length [m]	5.32	TBD	9.9	4.24	1.98	2.52
Generator mass [ton]	410	TBD	450 – 540	TBD (207, active mass)	TBD	700 (139.5 active mass)
Active materials cost [k€]	-	TBD	-	26220	TBD	1896
Generator cost [k€]	3706	TBD	7140	TBD	TBD	3578
Nacelle mass [ton]	560-850					1100 - 1450
Nacelle cost [k€]	TBD					TBD
Gen cost/capacity [[€/kW]	185.3	TBD	357	1311	TBD	94.8 (178.9)
Generator efficiency	TBD	TBD	TBD	TBD	98.7%	97%
Converter efficiency	97.3%					97%

[a] To be decided yet

[b] The price of MgB$_2$ will potentially drop and the generator price will consequently go down.

[c] The structural steel price is variable. Here 3€/kg is used as the structural price.

[d] The nacelle mass does not include the mass of drive train and converter but is only the mass of nacelle frames and structures.

Although for 20 MW there are many performance indicators to be decided in future, the pros and cons of compared generator systems according to the first assessment can be now seen for both 10 and 20 MW.

In this comparison, we can observe the following from PDD and SCDD generator systems:

1. PDD performs very well in all size, mass, nacelle requirement, cost and efficiency. The usage of permanent magnets and the shear stress is able to be optimized further.

2. Within the superconducting generator systems, LTS is all good except relatively lower efficiency due to the large demand of cooling power. The cost of HTS generators is considerable because the current price of YBCO superconductors is rather high. It is expected that the price of YBCO superconductors will drop to an acceptable price level from the year 2015. In Fig. 4.7, the gap between "Jensen 2G" and "UH 2G now" designs and the "20% of 1.5€/W" line is where to be explored and minimized. However the efficiency of HTS generators is better than that of LTS ones. All the SCDD generators are of much smaller size compared with PMDD generators although the cost of SCDD generators (especially HTS) is a big issue, which must be highlighted. The nacelle can be designed to be relatively light with SCDD and PDD generators while significantly heavy with PMDD generators at 10 and 20 MW.

(INNWIND.EU, WP3 internal report, First assessment of performance indicators of SC and PDD generators)

7.3   Conclusion and recommendation

This is a fist assessment which is aiming at showing the possible advantages and disadvantages of proposed superconducting generator and magnetic pseudo direct-drive generator systems for 10 and 20 MW wind turbines in terms of size, mass and cost. Some of the assessment is based on actual design details while the other is derived from conceptual designs and scaling functions. This assessment provides useful information on the potential of proposed generator systems that are probably able to address the problems of size, weight and cost for 10 and 20 MW wind turbines.

7.3.1 Conclusion

As the proposed candidates to challenge permanent-magnet direct-drive generator systems, SCDD and PDD are better in size and weight than PMDD systems. PDD is very promising because its performance indicators are all very excellent in the first assessment. SCDD has different types according to which type of superconductor is used. In general, all SCDD generators in this first assessment have smaller size and mass compared to PMDD ones while the cost is relatively high especially when HTS is used. Therefore a lot of work is needed in future for SCDD in order to defeat PMDD in cost. The efficiency drop due to cooling power remains as an issue to be investigated especially for the LTS generator.

7.3.2 Future work

In this first assessment, some performance indicators are not yet found, such as the structural mass of some SCDD generators, the mass and cost of power electronic converters and the eventual cost of energy. For 10 MW, the mechanical design of SCDD and PDD generator structures has not been completed yet and therefore some performance indicators, such as the generator mass and consequently the generator cost, are not presented or rough estimations and need improving and updating in future work.

For 20 MW, the majority of performance indicators are estimated based on, say, scaling functions or scaling-up assumptions. There will be much work to do on the accurate assessment of all the performance indicators for 20 MW.

It has been seen that the cost of HTS SCDD using YBCO superconductors is rather high. Therefore it is quite necessary to explore how to reduce this cost and make HTS SCDD generator systems feasible in cost.

The future work can be broken down into the following tasks:

1) Obtain feedback from work package 1 on the generator KPI obtained. Is there an economical advantage of providing a lighter generator?
2) Determine electrical machine models to be provided to the power electronics task.
3) Obtain the wind speed distribution of the INNWIND.EU offshore site as input for evaluating the annual energy production.
4) Combine generator, power electronic and bearing efficiency to calculate annual energy production

(INNWIND.EU, WP3 internal report, First assessment of performance indicators of SC and PDD generators*)*

5) Evaluate the cost of energy at the INNWIND.EU offshore site of the different generator systems.

References

[1] G. Shrestha, "Structural flexibility of large direct drive generators for wind turbines", PhD thesis, Delft University of Technology, 2013.

[2] Hui Li, Z. Chen, H. Polinder, "Optimization of multibrid permanent-magnet wind generator systems", IEEE Transactions on Energy Conversion, vol. 24, pp. 82-92, 2009.

[3] R. Fair el. al., "Superconductivity for large scale wind turbines", DOE report DE-EE0005143 (2012).

[4] B. Maples, M Hand and W. Musial, "Comparative assessment of Direct Drive High Temperature Superconducting Generators in Multi-Megawatt Class Wind Turbines", National Renewable Energy Laboratory report, NREL/TP-5000-49086 (2010).

(INNWIND.EU, WP3 internal report, First assessment of performance indicators of SC and PDD generators*)*